2018-09-14

Modeling of Non-Equilibrium Interphase Mass Transfer during Solvent-Aided Thermal Recovery Processes

Al-Gawfi, Abdullah

UNIVERSITY OF CALGARY

Modeling of Non-Equilibrium Interphase Mass Transfer during Solvent-Aided Thermal Recovery Processes

by

Abdullah Al-Gawfi

A THESIS

SUBMITTED TO THE FACULTY OF GRADUATE STUDIES

IN PARTIAL FULFILMENT OF THE REQUIREMENTS FOR THE

DEGREE OF MASTER OF SCIENCE

GRADUATE PROGRAM IN CHEMICAL AND PETROLEUM ENGINEERING

CALGARY, ALBERTA

SEPTEMBER, 2018

Abstract

As most of the heavy oil reserves in the world are too viscous to be exploited conventionally, enhanced oil recovery (EOR) methods are applied mainly through utilizing heat or dilution. Two thermal recovery methods stand out to be the most viable and commercially practical for exploiting extra-heavy and highly viscous oil reservoirs are Steam-Assisted Gravity Drainage (SAGD), and Cyclic Steam Stimulation (CSS) processes. Both processes apply heat to the reservoir using steam to reduce the viscosity of the bitumen rendering it mobile. Despite the commercial success of these thermal recovery processes, solvent-aided thermal recovery processes recently gained increased industrial interest for their potential to achieve higher energy efficiency, reduced environmental impact, and increased economic viability. In solvent-aided thermal processes, solvent is co-injected with steam to further aid in reducing bitumen viscosity through mass and heat transfer and diffusion of solvent into bitumen.

Several field trials of solvent-based recovery processes have been carried out and field results were mixed or inconclusive, and that can be attributed to the lack of knowledge of the physics and inter-related mechanisms involved with interphase-mass transfer and solvent dissolution into bitumen. The first part of this thesis aims to address the mechanisms of solvent dissolution into bitumen due to solvent diffusion and defines the key parameter of diffusive dominant interphase-mass transfer coefficient for several solvent/bitumen binary mixtures. The results show that the diffusion of lighter solvents into bitumen is lower than heavier solvents particularly at low temperatures. Also, it was found that the diffusion dominant interphase mass transfer coefficient is relatively higher for lighter solvents such as methane, ethane, and propane. Therefore, modelling of the non-

equilibrium interphase mass transfer phenomena is relatively more important for lighter solvents for designing and implementing a successful solvent-aided thermal recovery process.

One of the most important mechanisms involved in solvent-aided thermal recovery processes is interphase-mass transfer phenomena which involves a variation of a system property due to a non-equilibrium state. However, in current reservoir simulation models a local equilibrium is assumed such that a simulation grid block is at instantaneous equilibrium. In reality, local equilibrium assumption often fails at larger scales or in situations where flow velocities are large compared to that of mass or heat transfer. In the second part of this thesis, solvent-aided gravity drainage of bitumen was simulated with propane as a solvent using CMG-STARS. The effect of non-equilibrium mass transfer was included in the model to simulate the process using a kinetic approach. The results show that the assumption of the local instantaneous equilibrium result in 3% to 6% lower oil recovery for the typical field scale simulation models. This difference in oil recovery can be mitigated fairly through the inclusion of the non-equilibrium interphase mass transfer. Correlations for the non-equilibrium interphase mass transfer coefficients for propane/bitumen mixture were developed which can be used as guidelines for modelling the non-equilibrium interphase mass transfer for field scale simulations of solvent-based EOR processes.

Acknowledgements

My two years of graduate studies at University of Calgary has been rewarding and fulfilling, and I am grateful for those who made this possible. I would like to express my utmost gratitude and appreciation to my supervisor Dr. Hassan Hassanzadeh for providing me with the opportunity to be part of the SHARP research group, and for his mentorship, guidance, and constant support during my MSc studies. My thanks go to my co-supervisor Dr. Jalal Abedi for his support and encouragement.

I am also thankful to the members of my thesis committee, Dr. Maen Husein and Dr. Hemanta Kumar Sarma, for dedicating their time and efforts to read my thesis and providing their valuable feedback and comments. Finally, special thanks go to CMG and particularly Dr. Ehsan Ranjbar and Dr. Hossein Nourozieh for their technical feedback and support on the simulation aspect of this thesis.

I wish to express my appreciation for the financial support of Natural Sciences and Engineering Research Council of Canada Industrial Research Chair (NSERC-IRC) program and all member companies of SHARP Research Consortium: BP Canada Energy Group ULC, Brion Energy, Cenovus Energy, Computer Modelling Group Ltd., ConocoPhillips Canada, Devon Canada Co, Foundation CMG, Husky Energy, Imperial Oil Limited, Japan Canada Oil Sands Limited, Nexen Energy ULC, N-Solv Co., PennWest Energy, Statoil Canada Ltd., Suncor Energy, and Total E&P Canada.

To

My parents, Ahmed and Fatimah

and

my beloved wife, Ehsrak

Table of Contents

List of Tables

List of Figures and Illustrations

List of Symbols, Abbreviations and Nomenclature

List of Abbreviations

AARD	Absolute Average Relative Deviation
CMG	Computer Modelling Group
CSI	Cyclic Solvent Injection
CSS	Cyclic Steam Stimulation
DNAPL	Dense Non-Aqueous-Phase Liquids
EOR	Enhanced Oil Recovery
ESEIEH	Enhanced Solvent Extraction Incorporating Electromagnetic Heating
ES-SAGD	Expanding Solvent Steam Assisted Gravity Drainage
IEA	International Energy Agency
NCG	Non-Condensable Gas
PRESS	Predicted Residual Errors Sum of Squares
SAGD	Steam Assisted Gravity Drainage
SAP	Solvent Aided Process
SA-SAGD	Solvent-Aided Steam Assisted Gravity Drainage
SCO	Synthetic Crude Oil
SHARP	Solvent Heat Assisted Recovery Processes

SOR	Steam Oil Ratio
SVX	Solvent Vapor Extraction
UTF	Underground Test Facility
VAPEX	Vapor Extraction
VIF	Variance Inflation Factor

List of Symbols

$[A/L]$	characteristic area / characteristic length
a_{lg}	specific interfacial area separating gas and liquid phases
C_s	solubility limit
C_β^K	concentration of component *K* in phase *B*
D_{ik}	diffusion of component *i* in phase *k*
D_{AB}^{∞}	infinite dilution diffusion coefficient
d^k	diffusion length of component *k*
Ea	activation energy
E_i	measure of the degree of non-equilibrium with respect to component *i*
F	formation resistivity factor
H	column height of the liquid phase
j_l^k	micro-scale diffusive mass flux of component *k* in liquid phase

k	effective interphase mass transfer coefficient
M_B	molecular weight for bitumen
N_{ik}	moles of component i in phase k
P	pressure
q_{ik}	molar injection/production rate
$Q^K_{\alpha\to\beta}$	rate of interphase mass transfer of component K from phase a to phase B
R	universal gas constant
Sh	Sherwood number
S_k	saturation of phase k
T	temperature
T_{ik}	transmissibility of component i in phase k
T_c	critical temperature
V_c	critical volume
y_{ik}	molar composition of phase k
Z_c	critical compressibility factor
ρ	density
ε	energy parameter

σ	size parameter
$\mu_{i,L}$	chemical potential of the component *i*
Ψ_B	association factor
ρ_k	molar density of phase *k*
Φ	potential for flow
$\partial\omega/\partial x$	concentration gradient of the diffusing component in the *x*-direction
$\left(\rho D_{AB}\right)^o$	density-diffusivity product at low pressure
τ_i	interphase transfer term of component *i*
ω	mass fraction
X_α^k	micro-scale mass fraction of component *k* in phase
V_A	molar volume of the diffusing solvent at its normal boiling point
v_i^o	partial molar volume of component
ρ_r	reduced density
μ_B	viscosity of bitumen in cP

Chapter One: **Introduction**

1.1 Background

As the demand for energy continues to increase, alternative energy sources such as bioenergy, hydropower and renewable energy will not be sufficient. According to the International Energy Agency, crude oil is considered to be the largest contributor to the total world primary energy demand, and will continue to remain so until 2014 (Canadian Association of Petroleum Producers, 2017). Due to the global economy growth increase to a rate of 3.4% per year and continuous increase in world population, total energy demand is forecasted to increase about 30% from today till 2040 (IEA, 2017).

Canada ranks in the top ten producing countries in the world and the largest exporter of oil to the United States. However, the challenge we face in Canada and around the world is not simply producing enough energy to meet the world increasing demand, but to reduce the environmental impact and greenhouse gas (GHG) emissions when developing energy resources. As Canada has the third largest reserves of crude oil, nearly 170 billion barrels of recoverable oil, 165 billion of which are located in the oil sands, Canada's energy future depends on the oil sands industry.

1.1.1 Oil Sands Technologies

Commercially, there are two main methods currently used to extract oil sands: open pit mining operations and in-situ thermal technologies. Open pit mining is employed when oil sands deposits are closer to surface (<75m). In this method, the oil sands ore is excavated and transported to

separation units where it is mixed with hot water and solvents to separate the bitumen from the clay and sand. However, for in-situ thermal technologies, when bitumen is too deep to be accessible by open-pit mining, wells are being drilled to access the reservoir through which steam is injected in order to liquify the bitumen and reduce its viscosity. Once bitumen is mobile, it is produced to surface by either natural or artificial lifting mechanisms.

1.1.2 Steam Assisted Gravity Drainage

Steam Assisted Gravity Drainage (SAGD) is an in-situ technology in which a pair of horizontal wells, one located 5 m above the other, is drilled. The injector well (top) used to inject steam to ground to heat up the heavy oil and reduce its viscosity. Once heavy oil is mobile enough, it drains by gravity force to the producing well (bottom), the emulsion is then pumped to surface by either gas lifting mechanism or artificial lifting techniques such as electrical submersible pumps (see Figure 1.1 below). The importance of SAGD technology comes from the fact that most of the oil sands that is too deep to be accessible by open pit mining is also quite shallow for high pressure steam injection technologies such as Cyclic Steam Stimulation (CSS) that has been used for decades. By January 2017, SAGD technology accounted for 81% of the total in-situ oil sands production in Alberta.

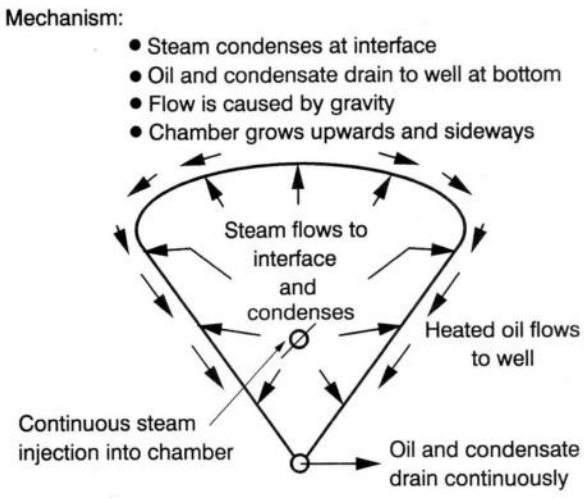

Figure 1.1: Steam Assisted Gravity Drainage (Butler, 1991).

Currently around 55% of the oil sands is being extracted with in-situ technologies. However, nearly 80% of the oil sands reserves is only recoverable using in-situ thermal recovery processes (International Energy Agency, 2015). Alberta oil sands producers aim is to develop new technologies that will improve the performance of SAGD projects and make them more competitive with other oil plays in terms of operational costs, environmental footprint, and GHG emotions. Such initiatives are vital to the oil sands industry given the unstable low oil prices, the booming US shale plays, the increasingly stringent environmental regulations, and social pressure to reduce GHG emissions.

Both in-situ processes: SAGD and CSS require the injection of steam into the reservoir to reduce bitumen's viscosity from typically ~1000,000 cP to less than 10 cP in order to mobilize the bitumen and pump it to surface. However, there are multiple challenges facing current in-situ processes including high supply cost due to high initial capital and operational costs compared to the

conventional oil and gas developments; high energy intensity due to the nature of the oil sands reservoir characteristics which makes bitumen extraction highly energy intensive; high GHG emissions due to its energy intensity; substantial water treatment; water consumption and footprint as in-situ processes typically require around three barrels of water to produce one barrel of oil (Nduagu *et al.*, 2017). Figure 1.2 shows the primary challenges of the oil sands industry. As shown, production costs and GHG emission intensity of the oil sands production represented by the Synthetic Crude Oil (Canada SCO) and diluted bitumen (Canada dilbit) are the highest compared to the rest of the world conventional and unconventional crude oils (Nduagu *et al.*, 2017). It is forecasted that GHG emissions from in-situ operations will rise as high as 300% by 2030 (Acedemies, 2015). Therefore, it is vital for the continuing growth of the oil sands industry to lower the production costs, energy intensity and GHG emissions to equal or lesser values than that of other unconventional oil and gas plays.

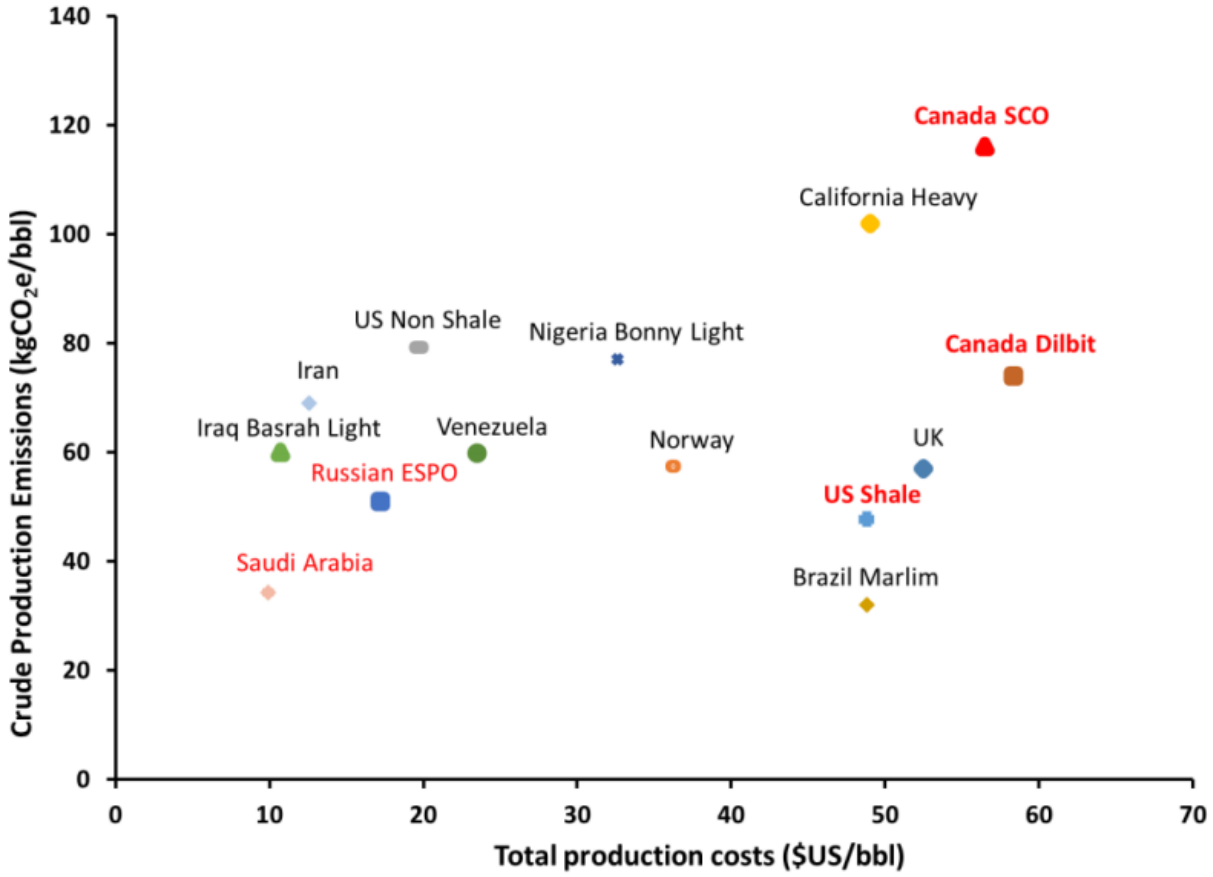

Figure 1.2: Production costs and greenhouse gas emissions of world crude oils (Nduagu et al., 2017).

As 80% of the recoverable oil sands is only extractable through in-situ technologies, in-situ operations will account for much of the new growth in production. Therefore, new advances and innovative technologies in current in-situ operations are needed in order to face the current challenges of unstable low oil price environment, the increasingly stringent environmental regulations, and social pressure to reduce GHG emissions. Operators have been experimenting on new and innovative technologies to reduce energy intensity of in-situ operations by reducing natural gas use and water consumption. These innovations include co-injection of solvents (SA-

SAGD), using alternative sources of thermal energy such as electromagnetic energy (ESEIEH), pure solvents injection (Nsolv), and downhole equipment modifications such as the use of steam splitters and flow control devices.

1.1.3 Solvent-Assisted Recovery Processes

SAGD with solvent co-injection was proposed and developed by (Nasr and Isaacs, 2002). The fundamental mechanism of the process is that solvent condenses with steam around cold formation interface of the steam chamber causing oil dilution and viscosity reduction. SAGD with solvent co-injection processes can be operated in a thermodynamic window for it to be effective and provides the maximum efficiency productivity. Figure 1.3 shows a diagram in which a spectrum for the operation window was indicated for different injected solvents (Hassanzadeh and Harding, (2016)). It was postulated that the phase change of the injected solvent need to be the same as steam along the vapor/bitumen interface (Sheng, 2013).

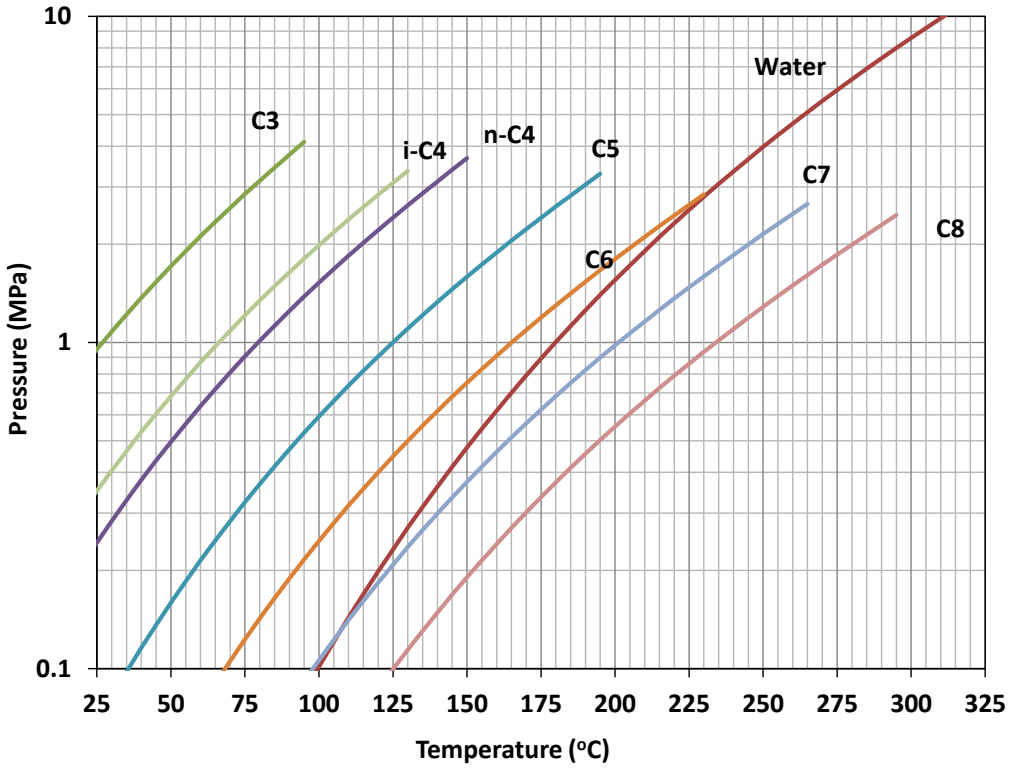

Figure 1.3: PT diagram of steam solvent spectrum (Hassanzadeh and Harding, 2016).

SAGD with solvent co-injection technologies are considered among the most promising technologies and is currently being piloted by several operators. It is expected that energy intensity reduction would be in the range of 10-30% on a per barrel basis and it could reduce GHG emission by 15-35% (Acedemies, 2015). Figure 1.4 shows expected reduction of supply costs and GHG emissions when using solvent based technologies when compared to a typical SAGD project. In the case of pure solvent injection technology (Nsolv), there is an expected 75% reduction in energy intensity and 75 to 80% reduction in direct fuel-derived emissions. In the case of solvent-assisted processes (SAP, ES-SAGD), there is a forecasted reduction in steam-oil-ratio (SOR) of 33-36%, 35% reduction in natural gas consumption, and 15-20% emissions reduction relative to the SAGD base case (Israel, 2017).

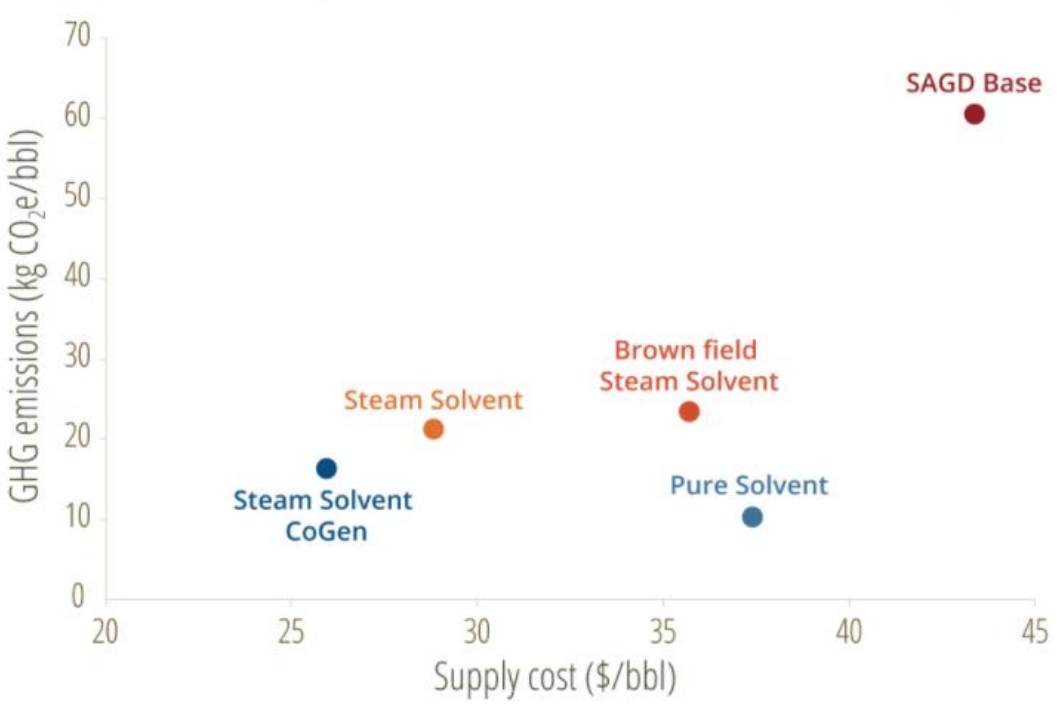

Figure 1.4: Cost and carbon emissions per barrel for different types of oil sands extraction technologies (Israel, 2017).

1.2 Motivations and Objectives

Despite being one of the most promising technologies, solvent-assisted processes are quite complex due to the inherent complexities of the associated mechanisms of heat and mass transfer coupled with complex phase behaviour involved in the processes. As steam delivers its latent heat to the reservoir and condenses at the boundary of the steam chamber, solvent vapor pressure increases near the interface increasing its solubility into bitumen. Both bitumen viscosity and density are decreased by the combined effect of temperature increase and solvent dissolution into the oil (Faradonbeh, 2013). In the latter mechanism, mass transfer parameters become very important to understand the process. Diffusion coefficient, interphase mass transfer coefficient,

and solubility are the basic mass transfer parameters in understanding the dissolution of vapor solvents into heavy oils. The first two parameters express the rate of dissolution, and the latter one shows the maximum amount of solvent dissolution into heavy oil. Therefore, thorough understanding and knowledge of solvent mass transfer mechanism and its impact in modelling the process is necessary for proper design and implementation of a successful solvent-assisted thermal recovery processes.

One of the most basic assumptions when modelling multiphase flow in porous media is the assumption of local thermodynamic equilibrium within an averaging volume. It is assumed that concentration of species in contact are reached instantaneous equilibrium everywhere in the averaged volume. Such assumption may be acceptable in the cases of fast mass transfer processes. However, local thermodynamic equilibrium assumption will give erroneous results in the cases of slow mass transfer processes where the characteristic time of mass transfer is small compared to flow velocities of the system (Niessner and Hassanizadeh, 2011).

Since interphase mass transfer process is inherently a pore-scale process as it takes place across fluid-fluid interfaces (Niessner and Hassanizadeh, 2011), local thermodynamic equilibrium assumption may be valid when modelling the process at small scale grid sizes. Therefore, the motivation of this study is to get a better understanding and proper modelling of solvent-assisted recovery processes at the macro-scale level (reservoir simulation grid block scale) while capturing the physics of the interphase mass transfer mechanism through the exclusion of the local thermodynamic equilibrium assumption in the simulation model. The main objective of this thesis is to perform a numerical study of solvent-assisted recovery process using high resolution

numerical simulations to capture the physics of interphase mass transfer phenomena. Secondary objectives are:

- Determining diffusion dominant interphase mass transfer coefficients for different solvent/bitumen mixtures at different pressures and temperatures
- Modelling non-equilibrium mass transfer of vapor solvents and quantifying its impact on oil recovery
- Finding correlations for the non-equilibrium interphase mass transfer phenomena that as a guideline can be applied at macro-scale level for the use and applications of field scale simulation models

1.3 Outline of Study

- Chapter Two will present a literature review about non-equilibrium interphase mass transfer in multiphase flow in porous media, and the different approaches investigated by researchers to capture the physics of non-equilibrium mass transfer.
- In Chapter Three, a description of the physical model used in the numerical simulation and the respective mathematical formulations are presented. The purpose of the mathematical formulations is to find interphase mass transfer coefficients analytically for later comparisons with numerical simulations. The analytical solution found will be applied on several solvent/bitumen mixtures to estimate the interphase mass transfer coefficients at different pressure to and temperature conditions. The solvents applied are C_1 to C_5 and the bitumen samples used are JACOS, MacKay River and Surmont Bitumen.

- In Chapter Four, a full description of the fluid model generation and methodology used will be presented. The experimental data used to generate the fluid model is from SHARP experimental Report for Surmont bitumen/Propane mixture. Modelling of fluid density, viscosity and k-values will be explained thoroughly, and the obtained results will be compared with experimental data for validation purposes.
- In Chapter Five, mechanistic studies will be carried out using commercial thermal reservoir simulator (STARS) to identify the impact of non-equilibrium interphase mass transfer on oil recovery and determine correlations for non-equilibrium interphase mass transfer coefficients for the use of field scale simulation models. Primarily, cumulative oil drainage will be used as the objective function to scale non-equilibrium interphase mass transfer coefficients. To start, simple 2D simulation models with fine grid sized blocks will be developed and analyzed. Then, simulation models will be gradually up-scaled to field scale levels to obtain the scaling relations.
- Chapter Six will present a thorough summary of the findings of each chapter of this thesis, conclusions, and recommendations for future research

Chapter Two: **Literature Review**

2.1 Introduction

Multiphase flow in porous media is encountered in numerous applications such as enhanced oil recovery (EOR), remediation of dense non-aqueous-phase liquids (DNAPLs), carbon storage, drying of porous media, and fuel cell technology. A common fundamental process in all these applications is non-equilibrium interphase mass transfer. However, perhaps one of the most basic assumptions of modelling multiphase flow in porous media is the assumption of the local thermodynamic equilibrium. It is assumed that instantaneous equilibrium is reached within an averaging volume. Such an assumption may be valid for cases of fast mass transfer processes. However, in the cases of slow mass transfer processes or when a heat source is present in the porous medium, this assumption is questionable (Nuske, Joekar-Niasar and Helmig, 2014). Also, equilibrium assumption may be valid at small scale or pore-scale levels. However, at larger scales (field scale) it often fails (Niessner and Hassanizadeh, 2009b).

Given the importance of the non-equilibrium interphase mass transfer in multiphase flow in porous media, several approaches were investigated to capture the physics of the non-equilibrium mass transfer. In subsequent sections, a summary of the different approaches used are presented.

2.2 Classical Kinetic Approach to Capture the Non-equilibrium

The study of the non-equilibrium mass transfer is not new in the literature and several researchers have worked on this subject. Niessner and Hassanizadeh (2011) investigated and described the

physics of interphase mass transfer processes and presented a complete set of balance equations that can be used to model the non-equilibrium mass transfer on a macro scale. Mayer *et al.* (2005) expressed the non-equilibrium mass transfer as a first-order kinetic mass transfer between fluid phases in a porous medium as:

$$Q^K_{\alpha\to\beta} = k^K_{\alpha\to\beta} a_{\alpha\beta}(C^K_{\beta,s} - C^K_{\beta}), \qquad \textbf{(2.1)}$$

where $Q^K_{\alpha\to\beta}$ $[M/L^3t]$ is the rate of interphase mass transfer of component *K* from phase α to phase β, $k^K_{\alpha\to\beta}$ $[L/t]$ is the interphase mass transfer coefficient, $a_{\alpha\beta}$ $[1/L]$ is the specific interfacial area separating phases α and β, $C^K_{\beta,s}$ $[M/L^3]$ is the solubility limit of component *K* in phase β, and C^K_{β} $[M/L^3]$ is the concentration of component K in phase β. Hunt, Sitar and Udell (1988) was the first to apply this model to estimate the non-aqueous phase liquids (NAPLs) dissolution rates.

Due to the complexities exerted by the heterogeneity of the porous media, it is difficult to estimate the specific interfacial area parameter $a_{\alpha\beta}$. Therefore, several authors lump interphase mass transfer coefficient $k^K_{\alpha\to\beta}$ and the specific interfacial area $a_{\alpha\beta}$ parameters into a single parameter *k*, effective interphase mass transfer coefficient, (Miller, Poirier-McNeil and Mayer, 1990; Powers, Abriola and Weber, 1992; Imhoff, Jaffe and Pinder, 1993; H. Zhang and F.W. Schwartz, 2000; Nambi and Powers, 2003), which yields to a simplified notation:

$$Q = k(C_s - C), \qquad \textbf{(2.2)}$$

where C_s is the solubility limit, and C is the actual concentration and k is the effective interphase mass transfer coefficient.

(Nghiem and Sammon, 1997) modeled the non-equilibrium mass transfer using a compositional simulator in which the oil and gas approach thermodynamic equilibrium through a rate process. As thermodynamic equilibrium prevails at the oil/gas interface, diffusion process drives the oil and gas composition towards these equilibrium values. To model the non-equilibrium phenomena, they accounted for the component flow equations in the oil and gas phases separately. These equations are:

$$\Delta T_{io} y_{io} \Delta\Phi_o - \tau_i + q_{io} - \frac{V}{\Delta t}(N_{io}^{n+1} - N_{io}^{n}) = 0, \qquad \textbf{(2.3)}$$

$$\Delta T_{ig} y_{ig} \Delta\Phi_g - \tau_i + q_{ig} - \frac{V}{\Delta t}(N_{ig}^{n+1} - N_{ig}^{n}) = 0\ , \qquad i=1,\ldots..,\ n_c \qquad \textbf{(2.4)}$$

where T_{ik} [mol/Pa.s] is the transmissibility of component *i* in phase *k*, y_{ik} is mole fraction of component *i* in phase *k*, Φ [Pa] is potential for flow, q_{ik} [mol/s] is molar injection/production rate , V [m^3] is grid block volume, N_{ik} is moles of component *i* in phase *k* per grid block volume [mol/m^3], and τ_i [mol/s] is the interphase transfer term of component *i* per grid block volume. The transfer term τ_i was expressed as:

$$\tau_{ik} = \pm[A/L]\frac{\rho_k}{S_k}\frac{D_{ik}}{F}\left(y_{ik} - y_{ik}^{*}\right), \qquad \textbf{(2.5)}$$

where $[A/L]$ [m^2/m] is characteristic area / characteristic length, ρ_k [mol/m^3] is molar density of phase *k*, S_k is saturation of phase *k*, D_{ik} [m^2/s] is diffusion of component *i* in phase *k*, *F* is formation

resistivity factor, and y_{ik} is molar composition of phase *k*. The results of their simulations of a gas injection displacement process in a core showed that non-equilibrium cases lie between equilibrium cases and no-mixing cases. Figure 2.1 below shows their results:

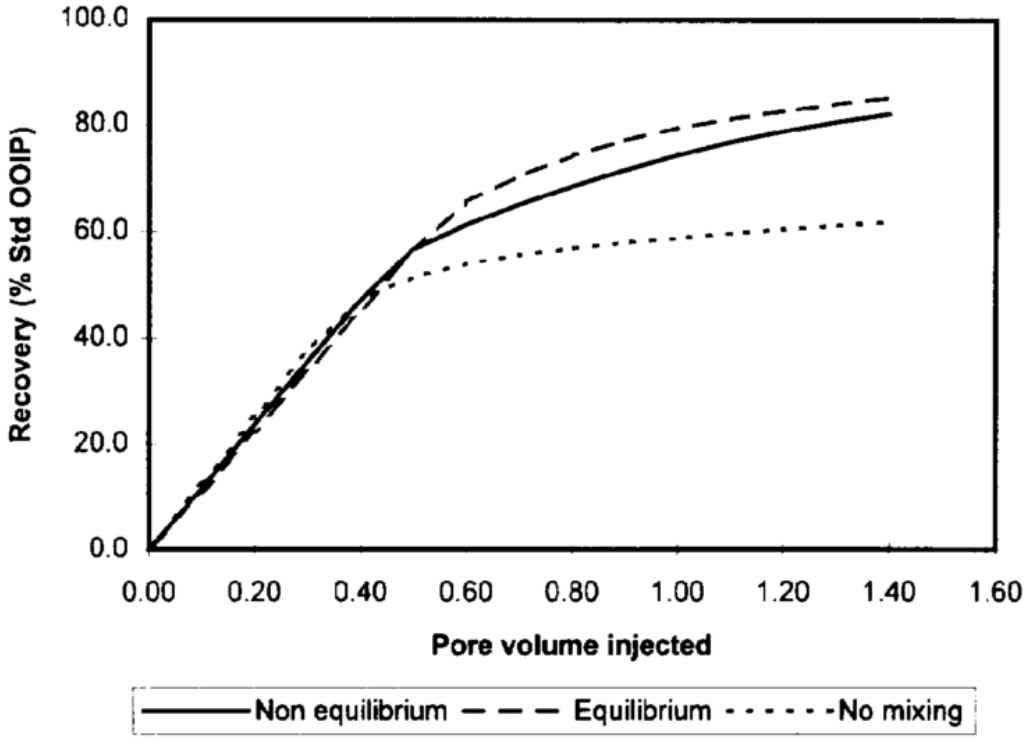

Figure 2.1: Comparison of recovery for non-equilibrium, equilibrium, and no-mixing runs (Nghiem and Sammon, 1997).

Indrupskiy and Lobanova (2015) and Lu, Ji and Liu (2011) modeled non-equilibrium mass transfer using component mass transfer rate, which is proportional to the difference of the component chemical potentials in the phases, i.e.

$$\tau_{i,L\to V} = C(\mu_{i,L} - \mu_{i,V}), \quad \textbf{(2.6)}$$

where, $\mu_{i,L}$ and $\mu_{i,V}$ are the chemical potentials of the component *i* in the liquid and vapor phases, respectively, and *C* is a function of reservoir characteristics and dynamic flow properties. Through their analysis, they showed that the necessity for non-equilibrium phase behaviour depends on simulation scale.

Wu *et al.* (1998) assessed the effect of the non-equilibrium mass transfer on the productivity of a single well producing from a gas condensate field. Their model incorporated the non-equilibrium mass transfer term on a compositional simulator and they used the model of Wilkins et al. (1995): $ja_0 = k_0(C_s - C)$. Their simulation results reveal that the non-equilibrium mass transfer lead to a reduction in the condensate saturation in the near wellbore region and therefore slower reduction in well productivity. Figure 2.2 shows that oil saturation reduces in the case of the non-equilibrium compared to equilibrium cases near wellbore.

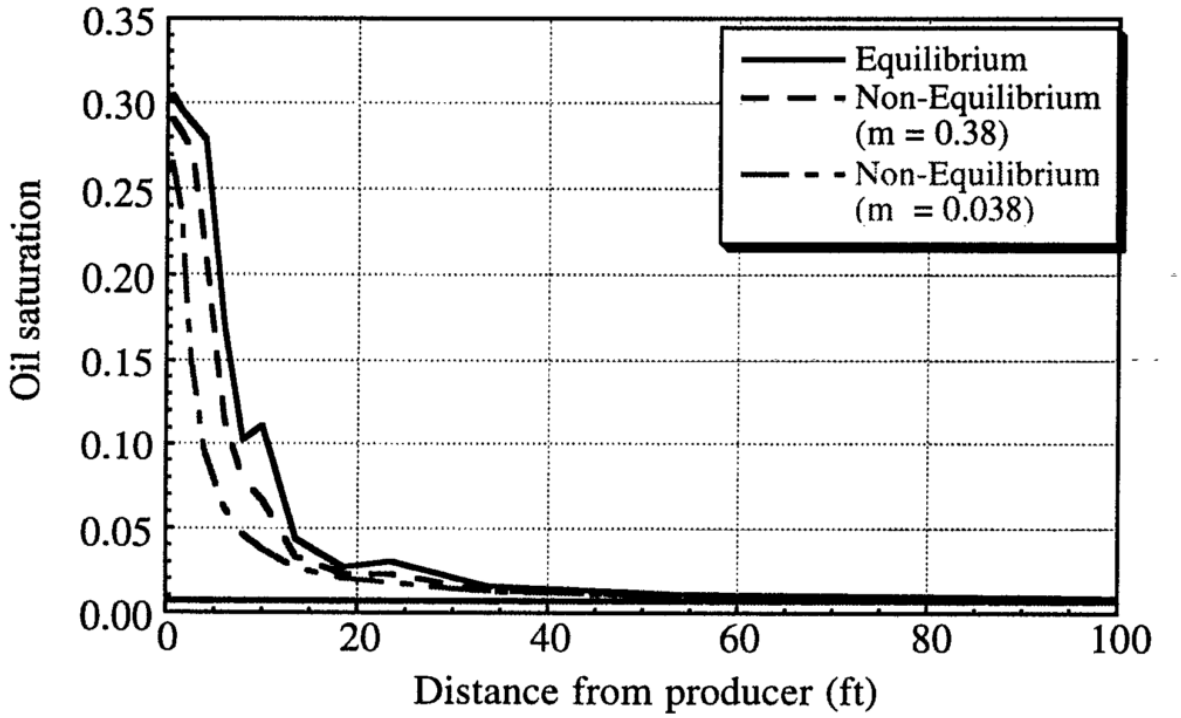

Figure 2.2: Effect of non-equilibrium mass transfer on oil saturation (Wu *et al.*, 1998).

Chang and Ivory (2013) developed numerical simulation models of the Cyclic Solvent Injection (CSI) process which incorporate non-equilibrium rate equations representing the delay in solvent reaching equilibrium concentration as it dissolves or exsolves in the oil in response to changes in the pressure and/or gas-phase composition. Their formulations are described by:

$$\frac{\partial N_{i,L}}{\partial t} = k_i N_o^{n1} (x_{i,g}^* - x_{i,L})^{n1} N_g^{n2} y_{i,g}, \qquad \textbf{(2.7)}$$

where, k_i is rate constant for solvent dissolution, N_g is the moles of the gas phase, $N_{i,L}$ is the moles of solvent in the oleic phase, N_o is the moles of the oil phase, n_1 and n_2 are exponent constants. They concluded that the assumption of instant equilibrium results in a 23% reduction in oil production compared to the non-equilibrium cases. Figure 2.3 below shows their results of

equilibrium versus non-equilibrium cases in terms of cumulative oil and cumulative gas productions. They explained that instant equilibrium assumption results into a faster gas exsolution when pressure is decreased during production and lower reservoir pressure due to the elimination of bubble creation and foamy oil drive, which result in lower oil productions and higher gas production in general.

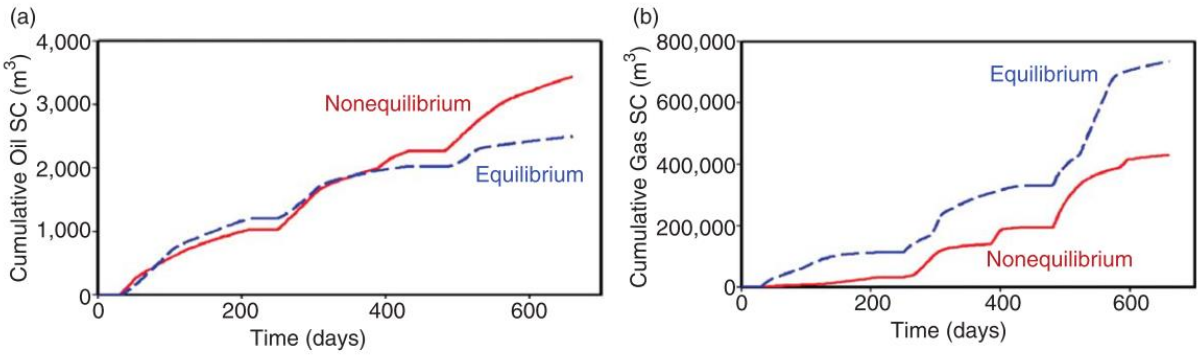

Figure 2.3: Impact of equilibrium versus nonequilibrium on (a) oil production and (b) gas injection (one-quarter well basis) (Chang and Ivory, 2013).

Soh et al. (2018) conducted experimental and numerical studies of pure methane, methane/propane mixture, and CO_2 as CSI in heavy oil. In their numerical simulation study, they modeled the non-equilibrium behaviour using two reaction terms. The first reaction illustrates the clustering of dissolved gas bubbles to be trapped in pore space, and the second reaction explains the development of free gas phase. Both reactions are defined in the numerical simulation using Arrhenius equation:

$$R = Ae^{\frac{-Ea}{RT}} \prod C^n, \qquad \textbf{(2.8)}$$

where, R is the reaction rate, A is a pre-exponential factor, Ea is activation energy, R is the universal gas constant, T is temperature, and C is the component concentration. They concluded that methane-propane mixture reduces the foaminess effect of pure methane solvent which turns the process close to instantaneous equilibrium. Therefore, using equilibrium assumption when simulating methane-propane mixture as a solvent when simulating CSI process is suitable.

Jia et al. (2013) conducted numerical simulation to model solvent vapor extraction process (SVX) incorporating non-equilibrium solvent solubility phenomenon. They used a time-dependent mass transfer term of the solvent vapor dissolving into oil phase using a chemical reaction term. The chemical reaction controls how quickly the solvent vapor converts to solvent liquid and dissolves into oil phase. The reaction equation is incorporated into CMG's STARS software.

$$\frac{\partial c}{\partial t} = \frac{r_a(\phi S_{mix} \frac{n_{Total}}{V_{Mix}} \frac{n_{Oil}}{V_{Total}})^a}{(1 + A\frac{n_{Solvent}}{n_{Total}})^b}. \qquad \textbf{(2.9)}$$

Their study showed that simulations conducted using non-equilibrium method resulted into more realistic relative permeability curves that closely resembles curves obtained from classical core displacement curves. Also, the dissolved solvent concentrations and diluted oil viscosity curves are more realistic. In addition, the concluded that numerical dispersion effect for larger grid block sizes can be compensated by tuning the reaction rate frequency factor, r_a. They found a correlation for the frequency factor, r_a, as a function of grid blocks size shown in Figure 2.4. However, it is noted from Figure 2.4 that their extrapolation of the frequency factor correlation with grid block

size is far from definitive and beyond the range of the simulated data. Therefore, the correlation may give erroneous results for the reaction frequency factors at coarse grid blocks.

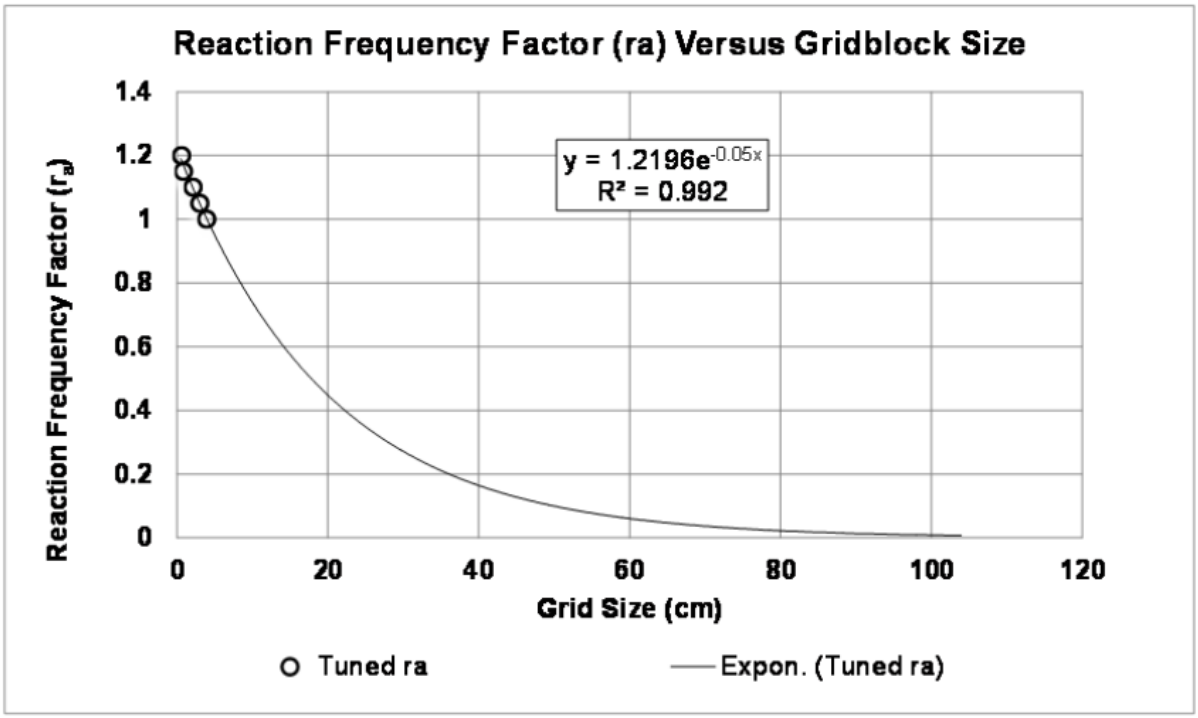

Figure 2.4: Reaction frequency factor versus grid block size correlation

(Jia et al., 2013).

Nourozieh et al. (2015) conducted numerical simulations using CMG's STARS to model non-condensable gas injection for a hybrid SAGD process. They incorporated in their simulation rate-dependent dissolution and ex-solution of solution gas using chemical reactions. Since the evolved solution gas doesn't instantaneously dissolve and exsolve from bitumen, the phase equilibrium calculations are assumed to have these rate-dependent dissolution and ex-solution terms. They noted that by incorporating rate-dependent dissolution and ex-solution terms for the NCG co-injection with steam, a slight improvement in oil production with reduction in SOR was observed.

Also, they concluded that real field behaviour was captured, and steam chamber conformance was not affected by initial solution gas amount when using the non-equilibrium dissolution and ex-solution reaction terms.

Peng (1992) proposed a correlation to model non-equilibrium mass transfer through the use of a partition coefficient to modify the equilibrium k-values as given by:

$$K_i^* = K_i(1-E_i), \qquad \textbf{(2.10)}$$

where E_i is a measure of the degree of non-equilibrium of the system with respect to component *i*.

Figure 2.5 shows the results of their first experiment. The model consists of 49.8% n-C_4 and 50.2% n-C_{10} and methane was used as the injection gas. The results show that the equilibrium model shows slightly more optimistic results compared to both experimental and non-equilibrium cases.

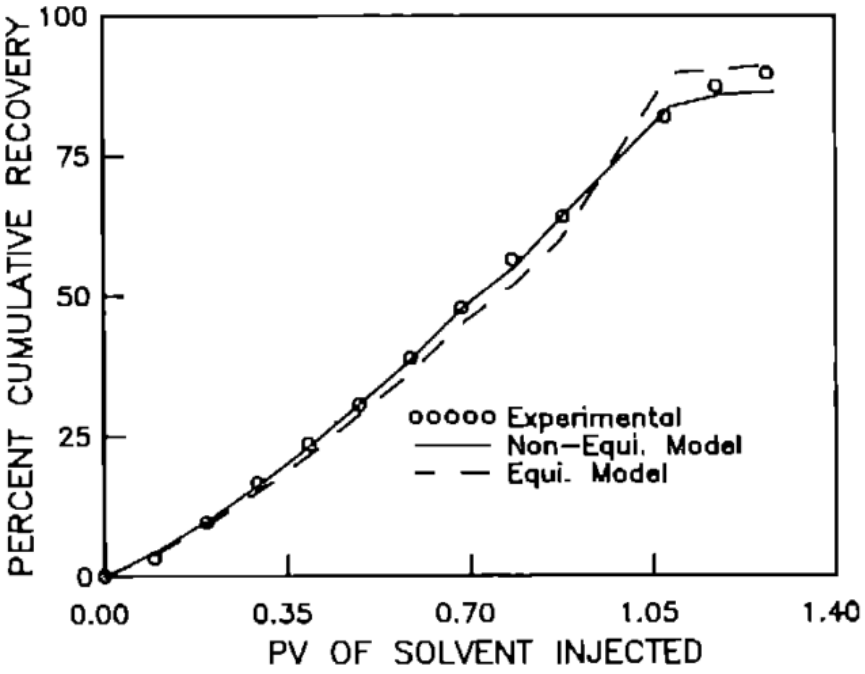

Figure 2.5: Recovery curve for experimental, non-equilibrium, and equilibrium runs (Peng, 1992).

Niessner and Hassanizadeh (2011) presented an interfacial-area-based model in which they included interfaces explicitly in their formulations to describe kinetic interphase mass and energy transfer in a thermodynamically-based approach. The set of balance equations are described by six mass conservation equations and three momentum balance equations. The resulting number of mass equations is for each component of each phase (total is four equations: two components and two phases) and the fluid-fluid interface for the two components (2 equations). In their formulations, they included a micro-scale diffusive flux through which kinetic interphase mass transfer is captured. For illustration purposes, one mass conservation equation is shown below:

$$\frac{\partial(\phi S_l \rho_l \bar{X}_l^k)}{\partial t} + \nabla.(\phi S_l \rho_l \bar{X}_l^k \bar{v}_l) - \nabla.(\phi S_l \bar{j}_l^k) = \rho_l Q_l^k + \frac{1}{V}\int_{A_{lg}} [\rho_l X_l^k (v_{lg} - v_l) + j_l^k].n_{lg} dA, \qquad \textbf{(2.11)}$$

where j_l^k is the micro-scale diffusive mass flux of component *k* in liquid phase. They further proceeded to apply Fick's law to relate the micro-scale diffusive flux j_l^k to the local concentration gradient resulting in the following formulation:

$$j_\alpha^k . n_{\mathrm{lg}} = \pm \frac{\rho_\alpha D^k}{d^k} a_{\mathrm{lg}} \left(X_{\alpha,s}^k - X_\alpha^k \right), \qquad \textbf{(2.12)}$$

where D^k is the micro-scale Fickian diffusion coefficient for component *k*, d^k is the diffusion length of component k, $X_{\alpha,s}^k$ is the solubility limit of component k in phase α, X_α^k is the micro-scale mass fraction of component k in phase α, and a_{lg} is the specific interfacial area separating gas and liquid phases.

Bayestehparvin *et al*. (2017) tried to model the non-equilibrium mass transfer using a time-dependent partition coefficient. They concluded that the equilibrium assumption is not valid in solvent assisted SAGD processes. Also, they concluded that solvent co-injection with non-equilibrium assumption can have negative impact on oil recovery as solvent stays in the vapor phase longer and doesn't dissolve into oil readily at early times compared to instantaneous equilibrium assumption. Figure 2.6 shows the results of their simulations. It shows that cumulative oil of the ES-SAGD process is lower in the case of non-equilibrium assumption compared to both classical SAGD and ES-SAGD with equilibrium assumption.

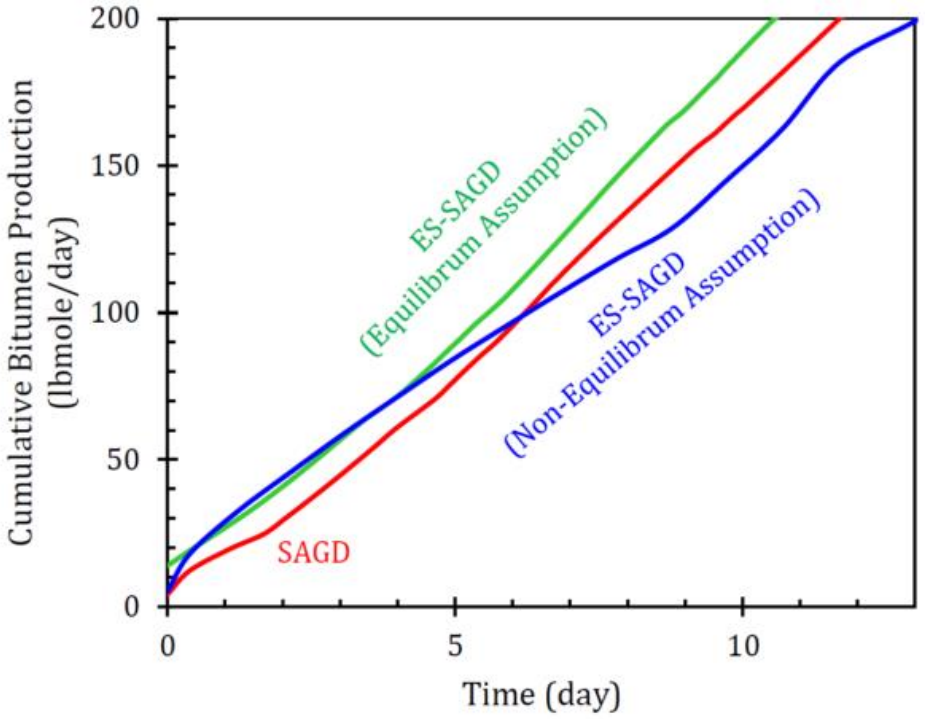

Figure 2.6: Oil production steam gravity drainage processes. Red, blue, and green lines are SAGD, ES-SAGD (non-equilibrium assumption), and ES-SAGD (equilibrium assumption) (Bayestehparvin et al. 2017).

Chapter Three: **Pure Diffusive Interphase Mass Transfer Coefficient**

3.1 Introduction

Interphase mass transfer is a fundamental process in multiphase flow as it is encountered in numerous applications. Therefore, a good understanding of the process is necessary for proper design and implementation of the application. However, the complexity lies in the proper determination of diffusion parameters, especially for multicomponent mixtures and/or non-ideal liquid mixtures such as bitumen/ heavy oil. Another challenge is that there are several mechanisms and forces affecting the interphase mass transport: diffusive mixing, convective mixing, dispersion, adsorption, etc. Therefore, a proper mathematical model is required to characterize the process of interphase mass transfer. When the dominant mass transfer mechanism is pure diffusion an analytical treatment is possible subject to some simplifying assumptions. However, when other processes are involved, the analytical treatment is not possible. In this chapter, a description of the model used in the determination of the interphase mass transfer coefficient is presented.

3.2 Mass Transfer by Diffusion

Diffusive mass transfer was first developed by Fick in 1855. Fick's first law stipulates that mass transfer rate of a component is proportional to the concentration gradient.

$$j = -\rho D \frac{\partial \omega}{\partial x}, \qquad \textbf{(3.1)}$$

where j is the rate of mass transfer, ω is the mass fraction, ρ is density, and D is the diffusion coefficient of the diffusing component with units of $[L^2/t]$. Assuming density remains constant throughout the mass transfer process for dilute mixtures one can write:

$$j = -D\frac{\partial C}{\partial x}, \qquad \textbf{(3.2)}$$

where C is the concentration of the diffusing component. Fick's second law describes the proportionality of the rate of change of concentration with second derivative of concentration gradient.

$$\frac{\partial C}{\partial t} = D\frac{\partial^2 C}{\partial x^2}. \qquad \textbf{(3.3)}$$

3.3 Physical Model

When a gaseous solvent is brought into contact with bitumen, as depicted in Figure 3.1, it diffuses into the liquid phase as described by Fick's law. Equilibrium concentrations are established instantaneously at the gas-liquid interface. As gas is further dissolving into liquid until an equilibrium concentration, $C_{\alpha,eq}$ is established throughout the system.

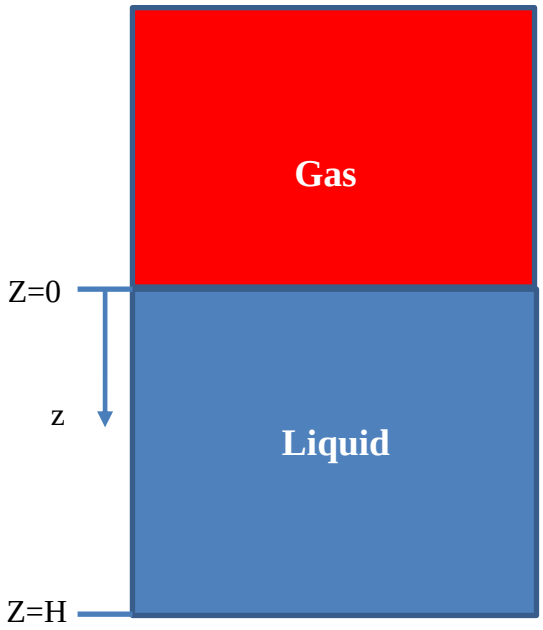

Figure 3.1: Mass transfer by diffusion - model representation.

Before proceeding with the mathematical formulations, it is importance to mention that it is assumed that heavy oil is non-volatile component and therefore only gas is diffusing into the heavy oil. Also, swelling of heavy oil is assumed negligible and this assumption is reasonable based on the work of (Sheikha et al. 2005). Their results show that ignoring swelling of bitumen when estimating diffusion coefficients for CH_4, CO_2, and N_2 resulted in an error of 5.2% to 9.3%. In addition, it is assumed that the diffusion coefficient is constant, and the system is at isothermal condition.

3.4 Initial and Boundary Conditions

The initial and boundary conditions will be considered for one-dimensional diffusive mixing problem. The initial and boundary conditions for the diffusive mixing process of the physical system depicted above are:

$$C(z, t=0) = 0,$$

$$C(z=0, t) = C^{*},$$

$$\left.\frac{\partial C}{\partial z}\right|_{z=H} = 0,$$

where C is the concentration of the diffusing component, z is the space coordinate, H is the column height of the liquid phase.

3.5 Analytical Solution for the Diffusive Mixing Problem

The analytical solution for the diffusion equation (3.2) with the above initial and boundary conditions is obtained by using the method of separation of variables, (Hassanzadeh, et al., 2005):

$$C(z,t) = 1 - \frac{4}{\pi}\sum_{n=0}^{\infty}\left(\frac{1}{2n+1}\right)\sin\left[\left(\frac{2n+1}{2H}\pi\right)z\right]\exp\left[-\left(\frac{2n+1}{2H}\pi\right)^{2} Dt\right]. \qquad \textbf{(3.4)}$$

Also, the average concentration can be found at an average depth of the liquid column:

$$\bar{C}(t) = 1 - \frac{8}{\pi^{2}}\sum_{n=0}^{\infty}\left(\frac{1}{2n+1}\right)^{2}\exp\left[-\left(\frac{2n+1}{2H}\pi\right)^{2} Dt\right]. \qquad \textbf{(3.5)}$$

Converting equations (3.4) and (3.5) to dimensionless forms using the following dimensionless numbers:

$$t_D = \frac{Dt}{H^2}, \tag{3.6}$$

$$z_D = \frac{z}{H}\ , \tag{3.7}$$

$$C_D = \frac{C}{C^*}, \tag{3.8}$$

results in the following equations:

$$C_D(z_D, t_D) = 1 - \frac{4}{\pi}\sum_{n=0}^{\infty}\left(\frac{1}{2n+1}\right)\sin\left[\left(\frac{2n+1}{2}\pi\right)z_D\right]\exp\left[-\left(\frac{2n+1}{2}\pi\right)^2 t_D\right]. \tag{3.9}$$

$$\bar{C}_D(t_D) = 1 - \frac{8}{\pi^2}\sum_{n=0}^{\infty}\left(\frac{1}{2n+1}\right)^2\exp\left[-\left(\frac{2n+1}{2}\pi\right)^2 t_D\right]. \tag{3.10}$$

In order to find the mass transfer coefficient from the above analytical solution of the diffusive mixing problem, we know that mass transfer coefficient is commonly expressed in terms of the mass transport flux and concentration gradient:

$$j = k\left(C^* - C(z,t)\right). \tag{3.11}$$

Therefore, using Fick's first law, equation (3.2), in combination with the above equation, mass transfer coefficient can be expressed as:

$$k = \frac{-D\dfrac{\partial C}{\partial z}(z=0)}{\left(C^* - C(z,t)\right)}\ . \tag{3.12}$$

In dimensionless form:

$$k = -\frac{D}{H\left(1-C_D\right)}\frac{\partial C_D(z_D=0)}{\partial z_D}. \qquad \textbf{(3.13)}$$

It is worth noting that Sherwood number is commonly expressed as:

$$Sh = \frac{kH}{D}.$$

Therefore, we can relate Sherwood number to the analytical solution of the diffusive mixing problem as the following:

$$Sh = \frac{kH}{D} = \frac{1}{\left(1-C_D\right)}\frac{\partial C_D(z_D=0)}{\partial z_D}. \qquad \textbf{(3.14)}$$

The typical time dependent Sherwood number is shown in Figure 3.2 where the pseudo steady state condition reaches a value of $\pi^2/4$.

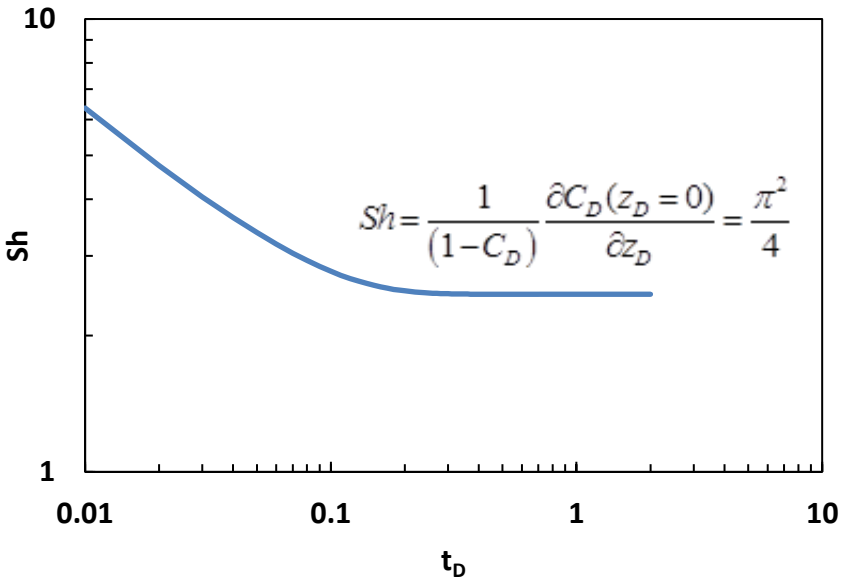

Figure 3.2: Sherwood number versus dimensionless time.

3.6 Interphase Mass Transfer Coefficients for Solvent/Bitumen Systems

An analytical solution for the diffusive interphase mass transfer process was presented in the previous section which can be used for multiphase binary mixtures. In this section the analytical solution will be applied on solvent/bitumen mixtures to estimate the interphase mass transfer coefficients at different pressure and temperature. The solvents studied are C_1 to C_5 and the bitumen samples used are JACOS, MacKay River and Surmont. As noted from equation (3.13), all parameters are in dimensionless form except for H [m] and D [m^2/s]. H is the column height of the liquid phase and is a property of the physical model which can be set to any arbitrary value for the analytical solution. To unify the solution of the analytical and numerical models that will be discussed in subsequent chapters, the value for H was set to 1m. D is the molecular diffusion coefficient of the diffusing solvent into liquid.

Analytical determination of the interphase mass transfer coefficients requires prior knowledge of the corresponding molecular diffusion coefficients. However, experimental molecular diffusion coefficients are scarce for solvent/bitumen systems at different temperature and pressure conditions. Therefore, well-known correlations developed for prediction of molecular diffusion coefficient for binary systems will be used to determine the molecular diffusion coefficients. Nevertheless, the quality of the estimated non-equilibrium interphase mass transfer coefficients will strongly depend on the accuracy of the estimated molecular diffusion coefficients.

3.7 Estimation of Molecular Diffusion Coefficient

Knowledge of diffusion coefficients of multiphase systems in petroleum engineering is crucial for proper design of solvent-aided EOR processes. In a binary system, if there is a concentration gradient of a specific component in the binary system, then it will diffuse in the direction of decreasing concentration, and this process is governed by Fick's first law:

$$j = -D\rho\frac{\partial\omega}{\partial x}, \qquad \textbf{(3.15)}$$

where j is the mass flux of the diffusing component in the x-direction, $\partial\omega/\partial x$ is the concentration gradient of the diffusing component in the x-direction and D is the diffusion coefficient. From thermodynamic equilibrium aspect, the main driving force of diffusion is chemical potential $\partial\mu/\partial x$ which is function of T, P, and concentration. Therefore, for systems with uniform T and P, the chemical potential gradient is only a function of concentration (Riazi, 2001).

There are several correlations proposed for estimation of the molecular diffusion coefficients. However, it is worth mentioning that such empirical correlations are mainly accurate for the range of data, temperature, and pressure conditions used for their developments. For the prediction of diffusivity of liquids, Wilke and Chang developed a relation to estimate the molecular diffusion coefficient at infinite dilution:

$$D_{AB}^{\infty} = 7.4\times10^{-8}\frac{\left(\Psi_B M_B\right)^{1/2} T}{\mu_B V_A^{0.6}}, \qquad \textbf{(3.16)}$$

where D_{AB}^{∞} is the infinite dilution diffusion coefficient [cm^2/s], Ψ_B is called the association factor and its value is 1 for most hydrocarbon solvents, M_B [g/mol] is the molecular weight for bitumen in this case, T is for temperature in Kelvin, μ_B is the viscosity of bitumen in cP, and V_A is the molar volume of the diffusing solvent at its normal boiling point [cm^3/mol]. It is estimated that the average error of this correlation for some 250 systems is about 10% (Riazi, 2001).

Another empirical correlation to estimate the molecular diffusion coefficient for liquids at infinite dilution is proposed by Hayduk and Minhas in 1982. For normal paraffin solutions, they proposed the following correlation:

$$D_{AB}^{\infty} = 13.3\times10^{-8}\frac{T^{1.47}\mu_B^{10.2/V_A-0.791}}{V_A^{0.71}}, \qquad \textbf{(3.17)}$$

where the parameters and units are the same as equation (4-1). Hayduk and Minhas (1982) correlation was developed on solvents ranging from C_5 to C_{32} diffusing in normal paraffins encompassing C_5 to C_{16}. An average error of 3.4% was reported (Poling et al., 2001). Figure 3.3 below is a comparison of the two empirical correlations discussed above. It shows the infinite dilution diffusivity of pentane/bitumen mixture as a function of bitumen viscosity.

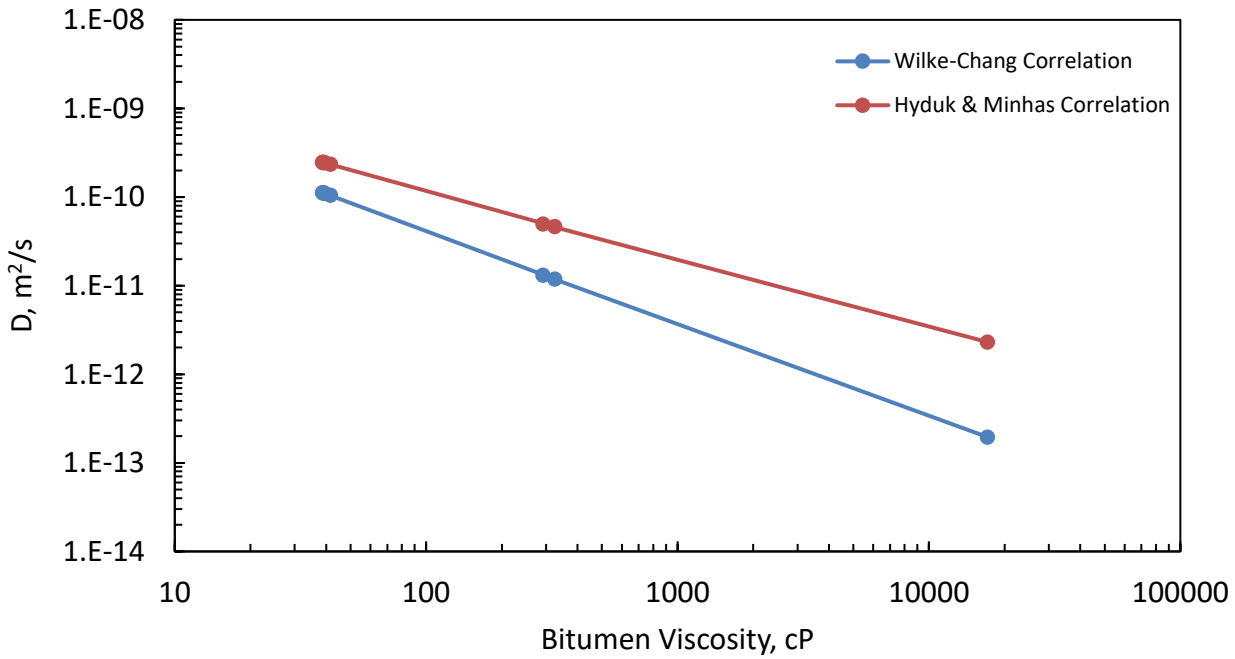

Figure 3.3: Infinite dilution diffusion for pentane/bitumen system – comparison.

The two empirical correlations presented above are mainly for liquid systems at low pressures. Therefore, generalized correlations to estimate diffusion coefficients for gases and liquids at high pressures were sought after. The most well-known generalized correlation to estimate diffusion coefficient for liquids and gases at high pressures is Sigmund's relation. Sigmund measured binary

diffusion coefficient for C_1, C_2, C_3, n-C_4, and N_2 at different pressures and temperatures and solvent mole fractions. He correlated density-diffusivity product to the reduced density.

$$\frac{\left(\rho D_{AB}\right)}{\left(\rho D_{AB}\right)^{o}} = 0.99589 + 0.096016\rho_r - 0.22035\rho_r^2 + 0.032874\rho_r^3, \quad \textbf{(3.18)}$$

where $\left(\rho D_{AB}\right)^{o}$ is the density-diffusivity product at low pressure, and ρ_r is the reduced density of the diffusing component. $\left(\rho D_{AB}\right)^{o}$ can be calculated using Chapman-Enskog equation and Stiel and Thodos relations:

$$\left(\rho D_{AB}\right)^{o} = \frac{2.2648\times10^{-5}T^{0.5}}{\sigma_{AB}^2\Omega_{AB}}\left(\frac{1}{M_A}+\frac{1}{M_B}\right)^{0.5}, \quad \textbf{(3.19)}$$

$$\sigma_{AB} = \frac{\sigma_A + \sigma_B}{2}, \quad \textbf{(3.20)}$$

$$\sigma_i = 0.1866V_c^{1/3}Z_c^{-6/5}, \quad \textbf{(3.21)}$$

$$\Omega_{AB} = \frac{1.06036}{\left(T_{AB}^{*}\right)^{0.1561}} + 0.193\exp\left(-0.47635T_{AB}^{*}\right) + ... \quad \textbf{(3.22)}$$
$$1.76474\exp\left(-3.89411T_{AB}^{*}\right) + 1.03587\exp\left(-1.52996T_{AB}^{*}\right),$$

$$T_{AB}^{*} = \frac{T}{\varepsilon_{AB}}, \quad \textbf{(3.23)}$$

$$\varepsilon_{AB} = \left(\varepsilon_A\varepsilon_B\right)^{1/2}, \quad \textbf{(3.24)}$$

$$\varepsilon_i = 65.3T_cZ_c^{18/5}, \quad \textbf{(3.25)}$$

where $(\rho D_{AB})^o$ is in [mol/cm.s]. ε and σ are energy and size parameters. V_c, T_c, Z_c are the critical constants for each component. Sigmund's correlation main advantage is that it can be used for both liquids and gases and that is why it is widely used in reservoir and petroleum engineering calculations and readily available in most of the commercial reservoir simulation software such as CMG and Eclipse.

Another generalized correlation developed to estimate diffusion coefficient for dense fluids is Riazi's Correlation (Riazi and Whitson, 1993). Riazi correlated the diffusivity-density product to viscosity deviation from ideal gas.

$$\frac{(\rho D_{AB})}{(\rho D_{AB})^o} = 1.07\left(\frac{\mu}{\mu^o}\right)^{b+cP_r}, \quad \textbf{(3.26)}$$

$$b = -0.27 - 0.38\omega, \quad \textbf{(3.27)}$$

$$c = -0.05 + 0.1\omega, \quad \textbf{(3.28)}$$

$$P_r = P / P_c, \quad \textbf{(3.29)}$$

$$T_c = \chi_A T_{c,A} + \chi_B T_{c,B}, \quad \textbf{(3.30)}$$

$$P_c = \chi_A P_{c,A} + \chi_B P_{c,B}, \quad \textbf{(3.31)}$$

$$\omega = \chi_A \omega_A + \chi_B \omega_B, \quad \textbf{(3.32)}$$

where $(\rho D_{AB})^{o}$ is determined from the equation (3.19) presented above. The remaining notations are similar to equation (3.18) to (3.20). The author claims that this correlation gives around 9% average error when evaluated against 17 diffusivity data points that were not used in the development of his correlation. Also when comparing Riazi's correlation with Wilke-Chang correlation (3.16) to estimate infinite dilution diffusion coefficient, the results were comparable (Riazi, 2001). The plot below shows a comparison of Sigmund correlation and Riazi's correlation for Propane/Bitumen system at different temperatures and pressures.

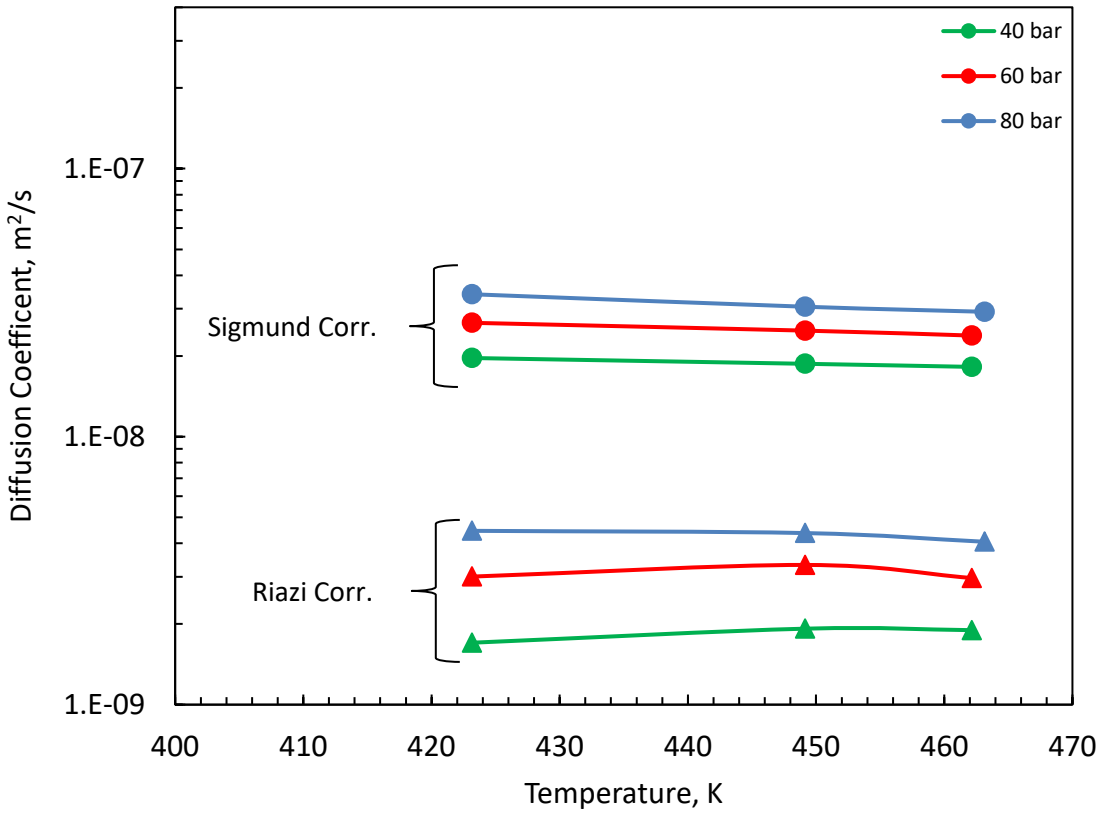

Figure 3.4: Diffusion coefficients for propane/bitumen system - Sigmund versus Riazi's correlation.

As noted from Figure 3.4 above, Sigmund's correlation tends to generally overpredicts the diffusions coefficients compared to Riazi's correlation. Tables 3.1 to 3.4 summarize the results obtained for the estimation of diffusion coefficients for methane/bitumen, ethane/bitumen, and propane/bitumen mixtures using Riazi and Sigmund methods. The properties of the solvents/bitumen mixtures (viscosities, densities, critical properties, solubilities, etc.) used in the calculation of the diffusion coefficients are obtained from SHARP experimental data (Nourozieh, 2013, Zirrahi *et al.*, 2017; Azinfar *et al.*, 2018).

Table 3.1: Estimated diffusion coefficients for methane/bitumen mixture.

P (bar)	T (K)	D_{AB} (m^2/s), Sigmund	D_{AB} (m^2/s), Riazi
11	323.15	7.4E-09	8.8E-12
11	373.15	1.1E-08	1.2E-10
11	423.15	1.5E-08	4.8E-10
21	323.15	8.2E-09	1.9E-11
21	373.15	1.2E-08	1.9E-10
21	423.15	1.6E-08	6.8E-10
21	463.15	1.9E-08	1.3E-09
41	323.15	9.3E-09	4.7E-11
41	373.15	1.3E-08	3.7E-10
60	324.15	1.1E-08	9.2E-11
60	373.15	1.4E-08	5.6E-10
60	423.15	1.9E-08	1.5E-09
60	463.15	2.2E-08	2.7E-09
81	325.15	1.2E-08	1.4E-10
81	373.15	1.5E-08	7.4E-10
81	423.15	2.0E-08	1.9E-09

81	462.15	2.4E-08	3.3E-09

Table 3.2: Estimated diffusion coefficients for ethane/bitumen mixture.

P (bar)	T (K)	D_{AB} (m^2/s), Sigmund	D_{AB} (m^2/s), Riazi
10	324.15	7.2E-09	3.1E-11
10	374.15	8.3E-09	1.2E-10
10	423.15	1.1E-08	3.5E-10
20	324.15	1.0E-08	1.1E-10
20	373.15	1.0E-08	2.3E-10
20	423.15	1.2E-08	5.6E-10
20	462.15	1.4E-08	1.0E-09
40	324.15	1.8E-08	4.9E-10
40	374.15	1.5E-08	5.7E-10
40	422.15	1.6E-08	1.0E-09
60	324.15	2.4E-08	1.1E-09
60	374.15	1.9E-08	1.1E-09
60	423.15	2.0E-08	1.7E-09
81	324.15	2.8E-08	1.4E-09
81	374.15	2.4E-08	1.5E-09
81	423.15	2.3E-08	2.2E-09

Table 3.3: Estimated diffusion coefficients for propane/bitumen mixture.

P (bar)	T (K)	D_{AB} (m^2/s), Sigmund	D_{AB} (m^2/s), Riazi
14	423.15	9.4E-09	3.7E-10
14	447.15	1.1E-08	7.0E-10
14	462.15	1.1E-08	7.0E-10
20	373.15	1.4E-08	6.5E-10
20	423.15	1.3E-08	7.1E-10
20	448.15	1.3E-08	1.0E-09
40	373.15	3.1E-08	4.2E-09
40	423.15	2.0E-08	1.7E-09
40	449.15	1.9E-08	1.9E-09
40	462.15	1.8E-08	1.9E-09
60	423.15	2.7E-08	3.0E-09
60	449.15	2.5E-08	3.3E-09
60	462.15	2.4E-08	3.0E-09
80	423.15	3.4E-08	4.5E-09
80	449.15	3.1E-08	4.4E-09
80	463.15	2.9E-08	4.1E-09

Table 3.4: Estimated diffusion coefficients for butane/bitumen mixture.

P (bar)	T (K)	D_{AB} (m^2/s), Sigmund	D_{AB} (m^2/s), Riazi
8	373.15	1.2E-08	5.6E-10
10	423.15	9.8E-09	5.5E-10
12	373.15	2.0E-08	1.9E-09
14	461.15	1.1E-08	9.3E-10
20	423.15	1.5E-08	1.5E-09
24	461.15	1.6E-08	1.9E-09
30	423.15	2.2E-08	2.8E-09
32	461.15	2.0E-08	3.0E-09
39	463.15	2.4E-08	3.6E-09
59	463.15	3.7E-08	5.4E-09

Figure 3.5 shows an example of the estimated molecular diffusion coefficients for four different solvents/bitumen mixtures at 20 bar. It shows that the diffusion of lighter solvents into bitumen is lower than heavier solvents at low temperatures. However, lighter solvents diffusivity into bitumen increases rapidly at higher temperatures. In contrast, heavier solvents diffusivities are less sensitive to temperature changes compared to the lighter solvents.

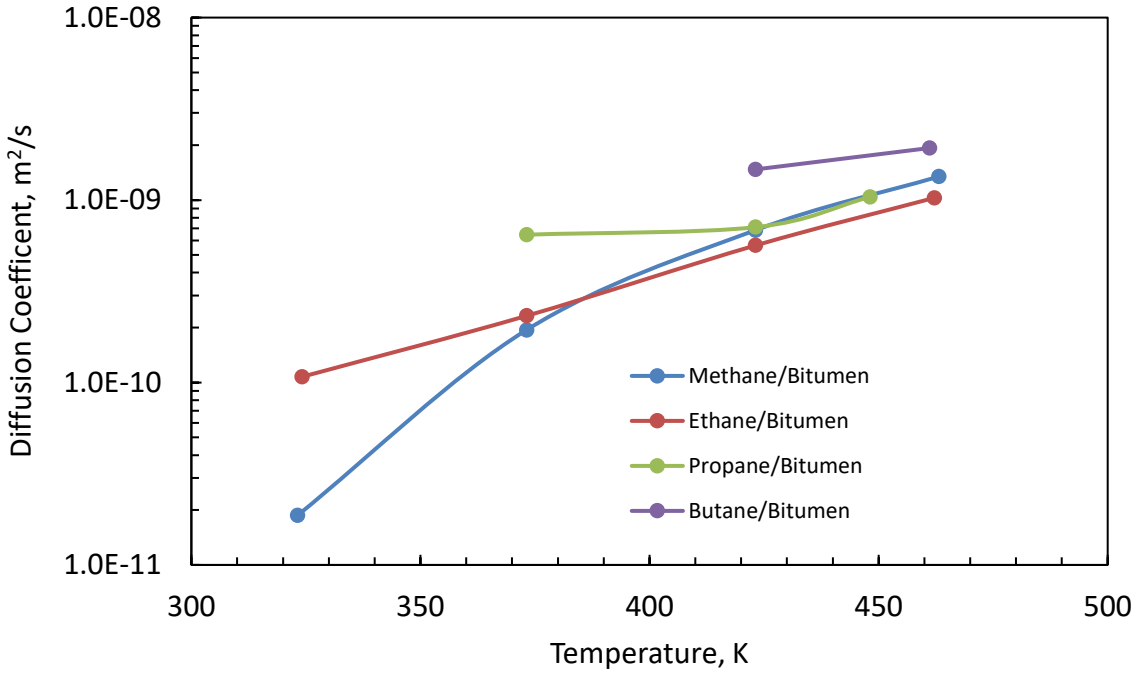

Figure 3.5: Estimated diffusion coefficients for different solvents/bitumen mixtures at 20 bar.

3.8 Estimation of Interphase Mass Transfer Coefficient

Having considered all parameters in equation (3.13), the interphase mass transfer coefficient can now be estimated. However, in order to find the interphase mass transfer coefficient at the pseudo steady state condition, infinite dilution diffusion coefficient will be used instead. Hyduk and Minhas correlation therefore will be applied to estimate the infinite dilution diffusion coefficient and used in the calculation of the interphase mass transfer coefficients. Tables 3.5 to 3.15 summarize the results of the estimated the interphase mass transfer coefficients for three bitumen samples (Surmont, MacKay River, and JACOS). The solvents used are C_1 to C_5. All experimental data and properties of the solvents/bitumen mixtures used in the estimation of the interphase mass

transfer coefficients are obtained from SHARP experiments, which have been reported elsewhere (Nourozieh, 2013, Zirrahi *et al.*, 2017; Azinfar *et al.*, 2018).

Table 3.5: JACOS Bitumen/Ethane (V/L) mixture.

Temperature, K	Pressure, MPa	D_{AB}, m^2/s	Bitumen Viscosity, cP	k, m/s
324.15	2.1	1.55E-11	8772.5050	3.82E-11
324.15	4.1	1.48E-11	9540.6050	3.66E-11
322.15	6.1	1.41E-11	10308.7050	3.49E-11
323.15	8.1	1.37E-11	11076.8050	3.38E-11
373.15	2	1.73E-10	228.6792	4.28E-10
373.15	4.1	1.68E-10	244.5439	4.13E-10
373.15	6.1	1.63E-10	259.6531	4.01E-10
373.15	8.1	1.58E-10	274.7623	3.90E-10
423.15	2.2	7.03E-10	30.7773	1.74E-09
423.15	4.1	6.74E-10	33.2675	1.66E-09
423.15	6.2	6.45E-10	36.0197	1.59E-09
423.15	8.2	6.21E-10	38.6409	1.53E-09

Table 3.6: Surmont Bitumen/Methane (V/L) mixture.

Temperature, K	Pressure, MPa	D_{AB}, m^2/s	Bitumen Viscosity, cP	k, m/s
323.15	1.1	3.11E-11	16326.3890	7.68E-11
323.15	2.1	3.11E-11	16590.3790	7.67E-11
323.15	4.1	3.10E-11	17118.3590	7.66E-11
324.15	6.1	3.11E-11	17646.3390	7.67E-11
325.15	8.1	3.12E-11	18174.3190	7.69E-11
373.15	1.1	3.11E-10	297.1482	7.68E-10
373.15	2.1	3.08E-10	306.5647	7.59E-10
373.15	4.1	3.01E-10	325.3977	7.43E-10
373.15	6.1	2.95E-10	344.2307	7.28E-10
373.15	8.1	2.90E-10	363.0637	7.15E-10
423.15	1.1	1.08E-09	38.9365	2.67E-09
423.15	2.2	1.07E-09	39.9670	2.64E-09
423.15	6	1.04E-09	43.5268	2.56E-09
423.15	8.1	1.02E-09	45.4941	2.52E-09
463.15	1.4	1.83E-09	18.4156	4.51E-09
463.15	2.1	1.82E-09	18.6424	4.49E-09
463.15	6	1.78E-09	19.9060	4.39E-09
462.15	8	1.76E-09	20.5540	4.33E-09

Table 3.7: Surmont Bitumen/Ethane (V/L) mixture.

Temperature, K	Pressure, MPa	DAB, m2/s	Bitumen Viscosity, cP	k, m/s
323.15	1.1	1.05E-11	16326.3890	2.60E-11
323.15	2.1	1.05E-11	16590.3790	2.58E-11
323.15	4.1	1.04E-11	17118.3590	2.56E-11
324.15	6.1	1.03E-11	17646.3390	2.54E-11
325.15	8.1	1.03E-11	18174.3190	2.53E-11
373.15	1.1	1.48E-10	297.1482	3.64E-10
373.15	2.1	1.45E-10	306.5647	3.58E-10
373.15	4.1	1.41E-10	325.3977	3.48E-10
373.15	6.1	1.37E-10	344.2307	3.38E-10
373.15	8.1	1.33E-10	363.0637	3.29E-10
423.15	1.1	6.08E-10	38.9365	1.50E-09
423.15	2.2	6.00E-10	39.9670	1.48E-09
423.15	6	5.75E-10	43.5268	1.42E-09
423.15	8.1	5.63E-10	45.4941	1.39E-09
463.15	1.4	1.09E-09	18.4156	2.70E-09
463.15	2.1	1.09E-09	18.6424	2.68E-09
463.15	6	1.05E-09	19.9060	2.60E-09
462.15	8	1.04E-09	20.5540	2.55E-09

Table 3.8: JACOS Bitumen/Methane (V/L) mixture.

Temperature, K	Pressure, MPa	D_{AB}, m^2/s	Bitumen Viscosity, cP	k, m/s
324.15	2.2	4.35E-11	8810.9100	1.07E-10
324.15	4.1	4.22E-11	9540.6050	1.04E-10
324.15	6.1	4.11E-11	10308.7050	1.01E-10
324.15	8.2	4.01E-11	11115.2100	9.89E-11
373.15	2	3.58E-10	228.6792	8.84E-10
373.15	4	3.50E-10	243.7884	8.63E-10
373.15	6	3.42E-10	258.8976	8.44E-10
373.15	8	3.35E-10	274.0068	8.27E-10

Table 3.9: MacKay Bitumen/Ethane (V/L) mixture.

Temperature, K	Pressure, MPa	D_{AB}, m^2/s	Bitumen Viscosity, cP	k, m/s
423.15	1.1	7.23E-10	29.3095	1.78E-09
423.15	2	7.16E-10	29.8932	1.77E-09
423.15	4.1	7.00E-10	31.2553	1.73E-09
424.15	6	6.89E-10	32.4876	1.70E-09
423.15	8.1	6.73E-10	33.8497	1.66E-09
463.15	1.4	1.22E-09	15.3137	3.02E-09
462.15	2.1	1.22E-09	15.4090	3.00E-09
463.15	4.1	1.21E-09	15.6814	2.99E-09
463.15	6	1.21E-09	15.9402	2.98E-09
463.15	8.1	1.20E-09	16.2262	2.96E-09

Table 3.10: Surmont Bitumen/Propane (V/L) mixture.

Temperature, K	Pressure, MPa	D_{AB}, m^2/s	Bitumen Viscosity, cP	k, m/s
373.15	2	8.71E-11	305.7200	2.15E-10
373.15	4	8.42E-11	324.6500	2.08E-10
423.15	1.2	4.03E-10	39.0624	9.95E-10
423.15	2.1	3.98E-10	39.9297	9.83E-10
423.15	4	3.89E-10	41.7607	9.59E-10
423.15	6	3.79E-10	43.6881	9.35E-10
423.15	8.1	3.69E-10	45.7118	9.12E-10
447.15	1.5	6.88E-10	19.6166	1.70E-09
448.15	2.2	6.84E-10	19.9229	1.69E-09
449.15	4.2	6.70E-10	20.7983	1.65E-09
449.15	6.1	6.56E-10	21.6300	1.62E-09
449.15	8.1	6.41E-10	22.5054	1.58E-09
462.15	1.4	7.53E-10	18.4156	1.86E-09
462.15	4	7.35E-10	19.2580	1.81E-09
462.15	6	7.22E-10	19.9060	1.78E-09
463.15	8	7.12E-10	20.5540	1.76E-09

Table 3.11: Surmont Bitumen/Butane mixture.

Temperature, K	Pressure, MPa	D_{AB}, m^2/s	Bitumen Viscosity, cP	k, m/s
323.15	2.1	3.26E-12	16590.3790	8.05E-12
323.15	8	3.13E-12	18147.9200	7.73E-12
374.15	2.1	6.23E-11	306.5647	1.54E-10
374.15	4	6.03E-11	324.4560	1.49E-10
374.15	5.1	5.91E-11	334.8142	1.46E-10
374.15	8	5.65E-11	362.1220	1.39E-10
423.15	4	2.94E-10	41.6532	7.26E-10
423.15	8.1	2.80E-10	45.4941	6.90E-10

Table 3.12: Surmont Bitumen/Propane (L/L) Mixture.

Temperature, K	Pressure, MPa	D_{AB}, m^2/s	Bitumen Viscosity, cP	k, m/s
323.15	2.1	5.13E-12	16590.3800	1.27E-11
323.15	5	5.04E-12	17355.9500	1.24E-11
323.15	8.1	4.94E-12	18174.3200	1.22E-11
373.15	6	8.15E-11	343.8142	2.01E-10
373.15	8	7.92E-11	362.1220	1.95E-10

Table 3.13: JACOS Bitumen/Propane (L/L) mixture.

Temperature, K	Pressure, MPa	D_{AB}, m^2/s	Bitumen Viscosity, cP	k, m/s
323.15	2.1	7.79E-12	8772.5050	1.92E-11
323.15	6.1	7.11E-12	10308.7100	1.75E-11
348.15	6.1	3.44E-11	1100.0000	8.48E-11
373.15	2.1	1.05E-10	229.4300	2.59E-10
373.15	4	1.02E-10	243.7884	2.51E-10
373.15	6.1	9.80E-11	259.6531	2.42E-10

Table 3.14: Surmont Bitumen/Butane (L/L) mixture.

Temperature, K	Pressure, MPa	D_{AB}, m^2/s	Bitumen Viscosity, cP	k, m/s
373.15	0.8	6.36E-11	294.3230	1.57E-10
373.15	1.2	6.31E-11	298.0890	1.56E-10
423.15	1	3.07E-10	38.8400	7.57E-10
423.15	2	3.02E-10	39.7790	7.46E-10
423.15	3	2.98E-10	40.7164	7.36E-10
461.15	1.4	5.81E-10	18.4156	1.43E-09
461.15	2.4	5.75E-10	18.7396	1.42E-09
461.15	3.2	5.71E-10	18.9988	1.41E-09
463.15	3.9	5.71E-10	19.2256	1.41E-09
463.15	5.9	5.60E-10	19.8736	1.38E-09

Table 3.15: Surmont bitumen/pentane (L/L) mixture.

Temperature, K	Pressure, MPa	D_{AB}, m^2/s	Bitumen Viscosity, cP	k, m/s
323.15	4	2.31E-12	17091.9600	5.70E-12
373.15	0.5	4.97E-11	291.4980	1.23E-10
373.15	4	4.65E-11	324.4560	1.15E-10
422.15	0.8	2.47E-10	38.6554	6.10E-10
422.15	1	2.47E-10	38.8428	6.09E-10
422.15	1.1	2.46E-10	38.9365	6.08E-10
422.15	1.4	2.45E-10	39.2175	6.05E-10
422.15	1.5	2.45E-10	39.3112	6.04E-10
422.15	4	2.36E-10	41.6532	5.84E-10

It is imperative to note that the analytical solution of the interphase mass transfer coefficient is for pure diffusion. Therefore, the values obtained are the low limiting values for mass transfer. When considering other mechanisms influencing mass transfer such as convective mixing and adverse mobility and density distribution, the mass transfer coefficient values will be much higher as will be shown in subsequent chapters.

Figure 3.6 illustrates the impact of solvent type on interphase mass transfer. The dotted lines are for gaseous solvents and solid lines are for liquid solvents. As can be observed from the figure, lighter solvents have relatively higher mass transfer coefficient compared to the heavier solvents. Therefore, for solvent-aided enhanced oil recovery processes such as ES-SAGD, SAP, and Vapex, proper modelling and inclusion of the interphase mass transfer phenomena is relatively more

important for gaseous solvents compared to heavier/liquid solvents. The results show that for a light solvent such as methane, mass transfer coefficient can be expressed as $k = 2\times10^{-8}\mu_B^{-0.593}$, and for a heavier solvent such as pentane it can be expressed as $k = 1\times10^{-8}\mu_B^{-0.771}$. Also, another observation that can be deduced from Figure 3.6 is that when heat is involved, interphase mass transfer across different phases is higher and thus more important to be properly modelled when designing solvent-aided thermal recovery processes regardless of the solvent type used in the process. Nuske et al. (2014) observed the same and mentioned in their paper that the assumption of local thermodynamic equilibrium is questionable when a heat source is present in the porous medium.

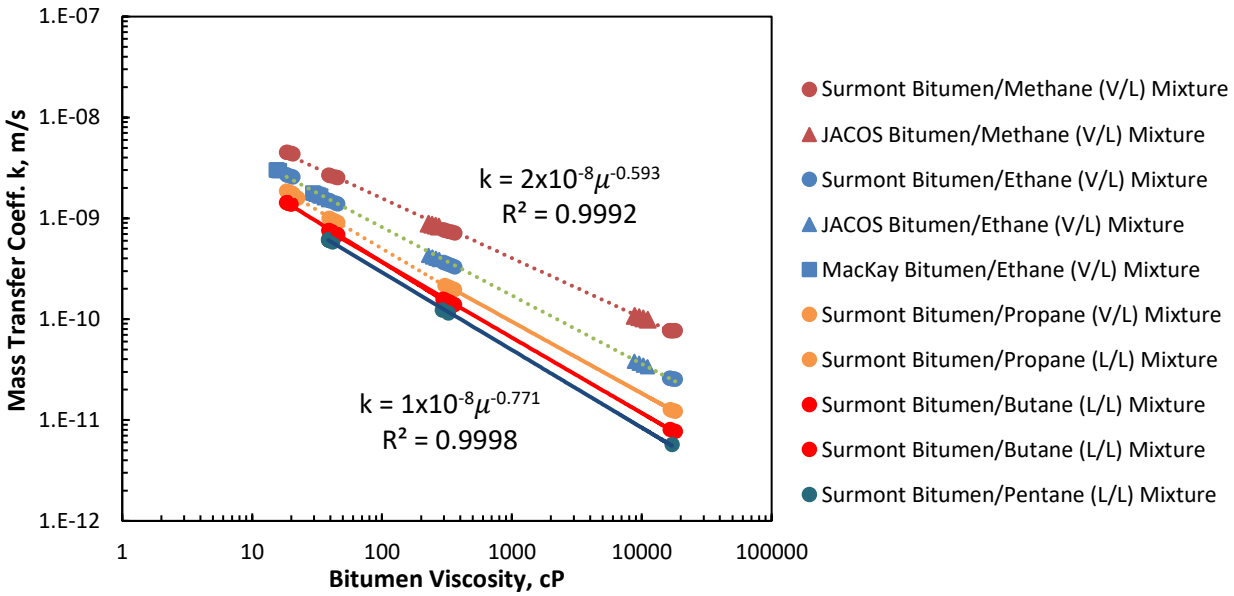

Figure 3.6: Estimated mass transfer coefficients for several solvent/bitumen mixtures.

3.9 Summary

The analytical solution for 1D diffusive mixing process was developed and used to determine the interphase mass transfer coefficient for several solvent/bitumen systems at different pressure and temperature settings. In this chapter, several empirical correlations for the estimation of molecular diffusion coefficient were reviewed. The estimated molecular diffusion coefficients for several solvent/bitumen mixtures were summarized. It was found that the diffusion of lighter solvents into bitumen is lower than heavier solvents at low temperatures. However, lighter solvents diffusivity into bitumen increases rapidly at higher temperatures. After estimating molecular diffusion coefficients, interphase mass transfer coefficients were calculated and presented in Tables 3.5 to 3.15 for different solvent/bitumen mixtures using infinite dilution diffusion coefficients estimated by Hyduk and Minhas correlation. Interphase mass transfer coefficient was shown to be relatively higher for lighter solvents such as methane, ethane, and propane and specially when a heat source is present. Therefore, proper modelling of non-equilibrium interphase mass transfer phenomena is relatively more important for gaseous solvents when designing and implementing a successful solvent-aided thermal recovery process.

Chapter Four: **Modelling of Thermophysical Properties for the Propane/Bitumen Mixture**

4.1 Introduction

In this chapter, a full description of the fluid model generation and methodology will be presented. The experimental data used to generate the fluid model is from SHARP experimental Report for Surmont bitumen/Propane mixture (Nourozieh, 2013, Zirrahi *et al.*, 2017; Azinfar *et al.*, 2018). Modelling of fluid density, viscosity and k-values will be explained thoroughly, and obtained results will be compared with experimental data for validation purposes.

4.2 Density of Bitumen/Propane Mixture

To model the density of raw bitumen, the correlation presented in Zirrahi et al. (2017) is used.

$$\rho = \rho_o \exp(\alpha P), \tag{4.1}$$

where $\rho_o = \alpha_1 + \alpha_2 T + \alpha_3 T^2$, and $\alpha = \alpha_4 \exp(\alpha_5 T)$. T and P represent temperature and pressure in K and MPa, respectively, and α_1-α_5 are constants. To find the pseudo liquid density of propane in the oleic phase, the following equation was used:

$$\rho = \rho_0 \exp(\alpha P), \tag{4.2}$$

where, $\rho_o = b_1 + b_2 T + b_3 T^2$, and $\alpha = b_4 + b_5 T$ where ρ is density in kg/m^3, T is temperature in K and P is pressure in MPa, respectively, and b_1-b_5 are constants.

The mixture density is found by using the mole-fraction-based mixing rule:

$$\rho_m = \sum_{i=1}^{n} x_i \rho_{ei}, \tag{4.3}$$

where ρ_m is the mixture density, and x_i is the mole fraction, *n* is for number of components, and ρ_{ei} is the pseudo density of the component in the mixture which can be found using equation (4.1) and (4.2) for bitumen and propane, respectively.

The parameters α_1 to α_5 and b_1 to b_5 were found through regression of the experimental data of Surmont bitumen density. The regressed results of the parameters α_1 to α_5 and b_1 to b_5 for Surmont bitumen and the associated AARD % is presented in the Tables 4.1 and 4.2.

For illustration purposes, Figure 4.1 shows a comparison of the calculated densities versus experimental data for two pressure conditions of 1.12 MPa and 10.43 MPa.

Table 4.1: Regressed constants of density correlation eq. (4.1) for Surmont propane/bitumen

α_1	α_2	α_3	α_4	α_5	
(kg/m^3)	**(kg/K m^3)**	**(kg/K^2 m^3)**	**(1/MPa)**	**(1/K)**	**AARD (%)**
1299.651	-1.17221	0.000734	8.99E-05	0.005595	0.0682

Table 4.2: Regressed constants of density correlation eq. (4.2) for Surmont Propane/Bitumen

α_1	α_2	α_3	α_4	α_5	
(kg/m^3)	**(kg/K m^3)**	**(kg/K^2 m^3)**	**(1/MPa)**	**(1/K)**	**AARD (%)**
-2000.57	15.20045	-0.01988	-0.22803	0.000477	0.447665

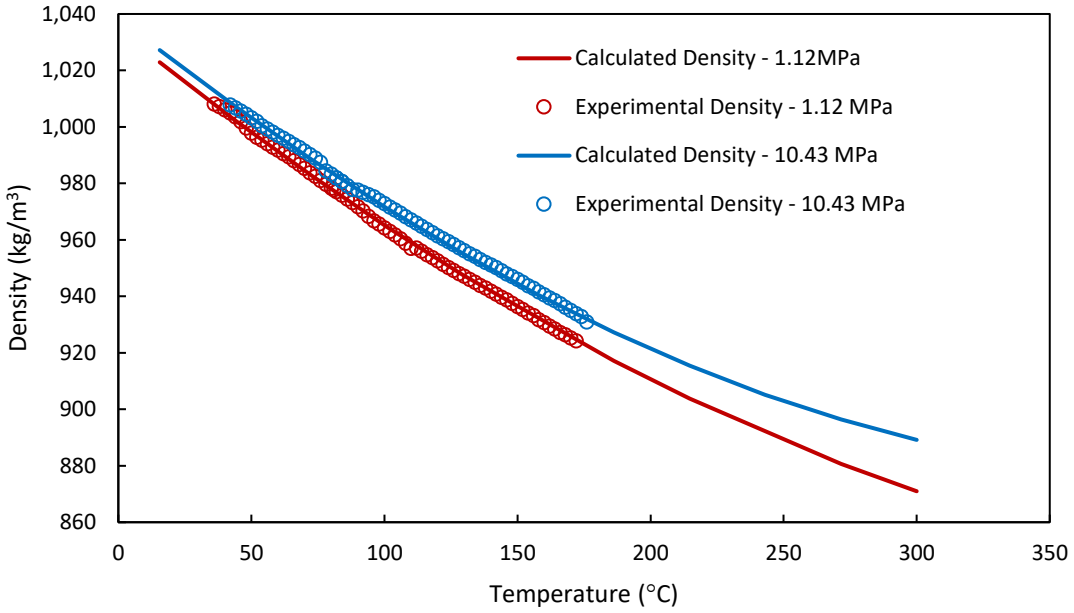

Figure 4.1: Calculated raw bitumen density (eq. (4.1)) versus experimental values for Surmont Bitumen.

Having modeled density of propane/bitumen system, it is possible to estimate the partial mass densities of bitumen and propane at reference temperature and pressure for the use in the simulation model. In our simulation model, the reference temperature and pressure are 15.56 ^{o}C and 101.325 kPa, respectively. Therefore, using equations (4.1) and (4.2) with the tuned constants α_1 to α_5 and b_1 to b_5 the partial mass densities for bitumen and propane are: 1022.424 kg/m^3 and 724.02 kg/m^3, respectively.

To find density of bitumen/propane mixture as a function of pressure and temperature applicable in reservoir simulator CMG STARS (Computer Modelling Group, 2016), the following equation was used:

$$\nu_i = \nu_i^o \exp\left[\begin{array}{l} c_{t1_i}(T - T_{ref}) + c_{t2_i}\dfrac{\left[(T+273.15)^2 - (T_{ref}+273.15)^2\right]}{2} \\ -c_{p_i}(P - P_{ref}) - c_{pt_i}(P - P_{ref})(T - T_{ref}) \end{array}\right], \quad \textbf{(4.4)}$$

where $\nu_i^o = Mw_i / \rho_i$ is the partial molar volume of component *i* found from equations (4.1) and (4.2) for both bitumen and propane, respectively, at reference pressure (101.325 kPa) and temperature (15.6 °C). It is worth noting that ν_i (or ν_i^o) for propane is the pseudo partial molar volume. The mixture molar volume is calculated based on the assumption of no volume change upon mixing using the following mixing rule:

$$\nu_o = \sum_{i=1}^{2} x_i \nu_i \,, \quad \textbf{(4.5)}$$

where x_i is the mole fraction of the components and $\nu_i = 1/\rho_i$ is the component partial volume. The oil phase molar density in kg-mole/m^3 is then obtained by $1/\nu_0$. Regressing experimental data of density for propane/bitumen system to find the constants: $c_{t1_i}, c_{t2_i}, c_{p_i}$, and c_{pt_i} resulted in the following values presented in the Table 4.3.

Table 4.3: Fluid density constants of Equation (4.4) for propane/bitumen fluid model.

	Bitumen Density Constants	**Propane Density Constants**
C_{t1} (1/K)	0.0010524	0.0097915
C_{t2} (1/K^2)	-1.09×10^{-6}	-1.58×10^{-5}
C_p (1/kPa)	3.75×10^{-7}	-2.03×10^{-5}
C_{pt} (1/kPa K)	4.40×10^{-9}	2.02×10^{-7}

It is worth noting that the regressed value for the liquid compressibility for propane results in a negative value, which is not physical. Therefore, this value was modified for the simulation models to be a positive number. The value chosen for propane compressibility is 1×10^{-6}1/kPa as a typical number for liquid hydrocarbons. It is worth noting that changing this value does not affect the density predictions.

4.3 Equilibrium K-Values

The k-values for the simulation model constructed for this study are obtained through regressing the experimental K-value data for the saturated bitumen/propane system using CMG STARS equation:

$$k = \left(\frac{k_1}{P} + k_2 P + k_3 \right) \exp\left(\frac{k_4}{T - k_5} \right), \qquad \textbf{(4.6)}$$

where *P* and *T* are the pressure and temperature of the system in kPa and ^{o}C, respectively. k_1 to k_5 are the k-values constants found through regression of the experimental data. Table 4.4 summarizes the k-values parameters for the Surmont bitumen/propane system, which will be used in the simulation models. Also, the AARD % of the correlated k-values versus experimental counterparts is 5.5%.

Table 4.4: K-values obtained for saturated bitumen/propane system.

k-values	**k_1 (MPa)**	**k_2 (1/MPa)**	**k_3**	**k_4 (K)**	**k_5 (K)**
	3.10E+04	0.000483	-2.267099	-279.601	-49.91377

4.4 Bitumen Viscosity

Bitumen viscosity was modeled using the correlation reported by Mehrotra and Svrcek (1986):

$$\ln\left(\ln(\mu)\right) = \left[b_1 + b_2 \ln(T)\right] + b_3 P, \quad \textbf{(4.7)}$$

where μ is the viscosity of the dead bitumen in cP, P is the gauge pressure in MPa, T is the absolute temperature in K. b_1 to b_3 are the fitting parameters obtained through regressing the experimental viscosity data. The effective viscosity of solvent dissolving in bitumen was determined using the correlation reported by Zirrahi et al. (2017). It is assumed that the effective solvent viscosity in the oleic phase is a function of temperature and pressure of the system.

$$\mu_s = c_1 + c_2 T + c_3 T^2 + (c_4 + c_5 T) P, \quad \textbf{(4.8)}$$

where c_1 to c_5 are fitting parameters which can be found through regressing the experimental viscosity data. T and P are the absolute temperature and pressure in K and MPa, respectively. The mixture viscosity is found through employing a log mixing rule based on mole fractions.

$$\ln \mu_m = x_s \ln \mu_s + x_b \ln \mu_b, \quad \textbf{(4.9)}$$

where the subscripts m, s, and b denote mixture, solvent, and bitumen, respectively. Constants b_1 to b_3 and c_1 to c_5 are the fitting parameters which can be found through regressing the experimental viscosity data of raw bitumen and bitumen/propane mixture. It is worth mentioning that this correlation is only valid for prediction of the mixture viscosity and cannot be used to predict pure solvent viscosity. Also, it is important to note that the temperature and pressure range of validity to accurately predict pseudo liquid viscosity of solvent using (4.8) correlation is: 50 ^{o}C

to 175 ^{o}C and pressure of 101.325 kPa to 4000 kPa, respectively. The results obtained for the fitted parameters of equation (4.7) and (4.8) are shown in Table 4.5.

Table 4.5: Fitting parameters of viscosity correlation given by equation (4.7) and (4.8).

Bitumen Viscosity Correlation Parameters	**b_1**		**b_2**	**b_3**	
	24.10688		-3.77505	0.005782	
Solvent Viscosity Correlation Parameters	**c_1**	**c_2**	**c_3**	**c_4**	**c_5**
	-16.6828	0.148144	-0.00025	-2.09824	0.004773

The AARD % between Correlated viscosity data and experimental viscosity data for a pressure range of 1 MPa to 7 MPa and a temperature range of 60 ^{o}C to 190 ^{o}C is around 10.45%. The plot below shows a comparison of the calculated viscosities versus experimental viscosities for two sets of pressures.

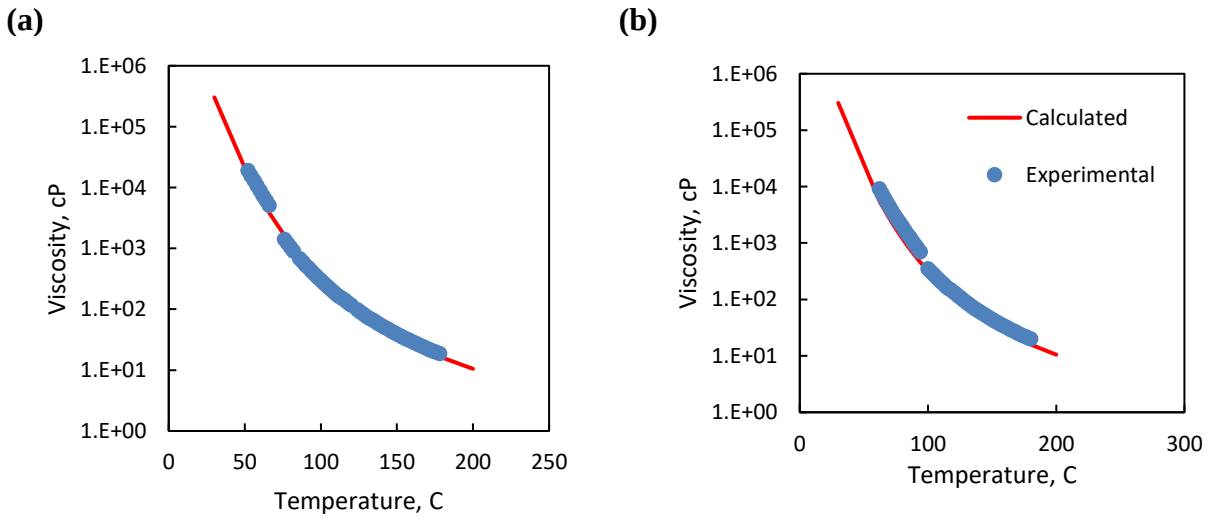

Figure 4.2: Surmont bitumen viscosity – experimental values versus calculated (a) 1.12 MPa, (b) 6.98 MPa).

4.5 Relative Permeability Curves

The relative permeability curves used in the simulation models were taken from the original UTF simulation models presented by Good, Rezk and Felty (1997). Figure 5.3 shows the UTF relative permeability curves.

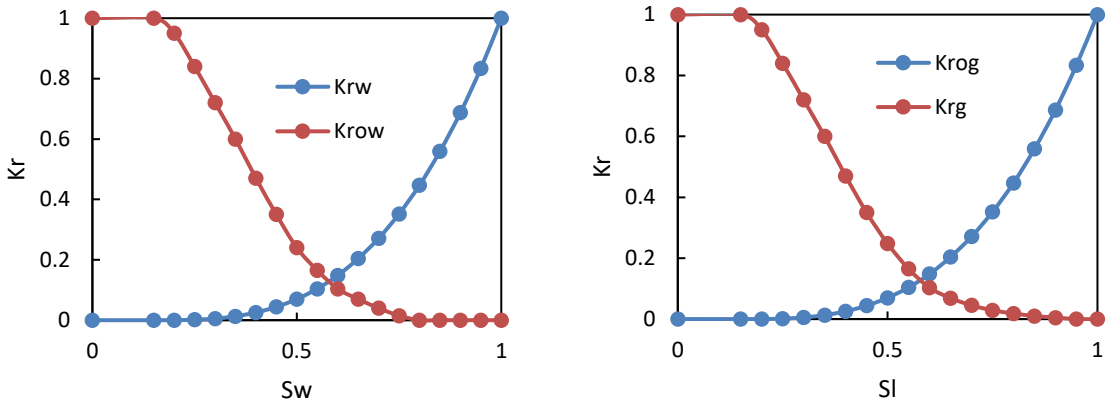

Figure 4.3: UTF relative permeability curves (Good, Rezk and Felty, 1997).

4.6 Summary

In this chapter, fluid model generation, methodology, and results were presented. The results for the thermophysical properties (viscosity, density, k-values) for propane/bitumen mixture were presented and compared to experimental values. The average absolute deviation between the calculated thermophysical properties and their experimental counterparts were found to be: 0.447%, 5.5%, and 10.45% for densities, k-values, and viscosities, respectively.

Chapter Five: **Numerical Modelling of Non-equilibrium Interphase Mass Transfer Phenomena for Propane/Bitumen Mixture**

5.1 Introduction

Transport phenomena involves variation of a system thermophysical properties due to a non-equilibrium state. This variation in the system property causes mass or energy to be transported and redistributed across a representative volume. However, on current reservoir simulation models, local equilibrium is assumed such that a property in a multiphase flow is at equilibrium instantaneously. In reality, local equilibrium assumption often fails at larger scales or in situations where flow velocities are large compared to that of mass or heat transfer (Niessner and Hassanizadeh, 2009). Therefore, non-equilibrium modelling of phase behavior in multiphase systems should be considered. Molecular diffusion, solubility, and interphase mass transfer are the key parameters when it comes to non-equilibrium modelling of phase behavior (Civan and Rasmussen, 2006), (Pacheco Roman and Hejazi, 2016).

In oil sands reservoirs, the bitumen is immobile due to its high viscosity. Therefore, in order to produce it, its viscosity must be reduced either by heat such as steam injection or by dilution using solvents. In the latter mechanism, knowledge of molecular diffusion and interphase-mass transfer coefficients is critical as they control the rate of dissolution of solvents into heavy oil (Etminan et al., 2014). Therefore, the determination of these parameters is necessary for designing a successful solvent-based oil recovery process for heavy oil reservoirs. The diffusion limited case was discussed in the previous chapters.

Analytical estimation of non-equilibrium interphase mass transfer was discussed and presented in the previous chapters. In this chapter, the estimated values for the non-equilibrium interphase mass transfer coefficients using detailed numerical simulations for the propane/bitumen mixture will be determined. The non-equilibrium interphase mass transfer phenomena will be incorporated into multiphase thermal simulation model in order to quantify the impact of non-equilibrium mass transfer and analyze the performance of solvent-aided thermal recovery processes for the propane/bitumen system. The incorporation of the non-equilibrium interphase mass transfer into simulation models will be accomplished using reaction terms. The rate of dissolution and ex-solution of solvent into bitumen will be controlled by rate dependent reaction terms, which are functions of the non-equilibrium mass transfer coefficients, specific interfacial areas separating fluid interfaces and solvent solubility limits. The solubility limits for propane/bitumen system was obtained through the use of SHARP experimental results, which were reported elsewhere (Nourozieh, 2013, Zirrahi *et al.*, 2017; Azinfar *et al.*, 2018).

Mechanistic studies will be carried out using commercial thermal reservoir simulator (STARS) to determine scaling relations for non-equilibrium interphase mass transfer coefficients in order to use them in field scale simulation models. Primarily, cumulative oil drainage will be used as the objective function to scale the non-equilibrium interphase mass transfer coefficients. To start, simple 2D numerical simulation models with fine grid blocks will be developed and analyzed. Then, simulation models will be gradually scaled up to field scaled levels to obtain the scaling relations.

CMG STARS is a three-phase multi-component thermal and steam additive reservoir simulator developed by Computer Modelling Group (CMG) Ltd. The software is a k-valued (KV) based,

advanced process reservoir simulator that was developed to simulate steam flood, steam cycling, steam-with additives, dry and wet combustion, along with many types of chemical additive processes, using a wide range of grid and porosity models in both field and laboratory scale (Computer Modelling Group, 2016). STARS is especially suited for modelling non-isothermal, light and heavy oil recovery processes as well as modelling of chemical reactions, foamy heavy oil production and cold heavy oil production processes.

5.2 Design of Numerical Simulation Models

When a gaseous solvent is brought into contact with bitumen, as depicted in Figure 5.1 (b), it diffuses into the bitumen zone by diffusion as described in Chapter Three. Equilibrium concentrations are established instantaneously at the gas-liquid interface. Subsequently, as the solvent is further dissolving into the bitumen, it diffuses until an equilibrium concentration, $C_{\alpha,eq}$ is established throughout the system. However, in the case of solvent-aided thermal recovery processes such as ES-SAGD, where the process is more complex and dynamic, solvent is co-injected with steam by the injector well. Steam then condenses and transfers its latent heat to the bitumen formation and followed by solvent condensation and diffusion into the bitumen formation. As bitumen formation is exposed to heat and solvent from bottom, this results in reducing its viscosity and consequently increasing its mobility. Diluted bitumen and condensate will then flow downward by adverse density (gravity) effects. Figure 5.1 (a) below explains the process of ES-SAGD and the design of the numerical simulation model performed in this work to capture the physics of solvent-aided thermal recovery processes.

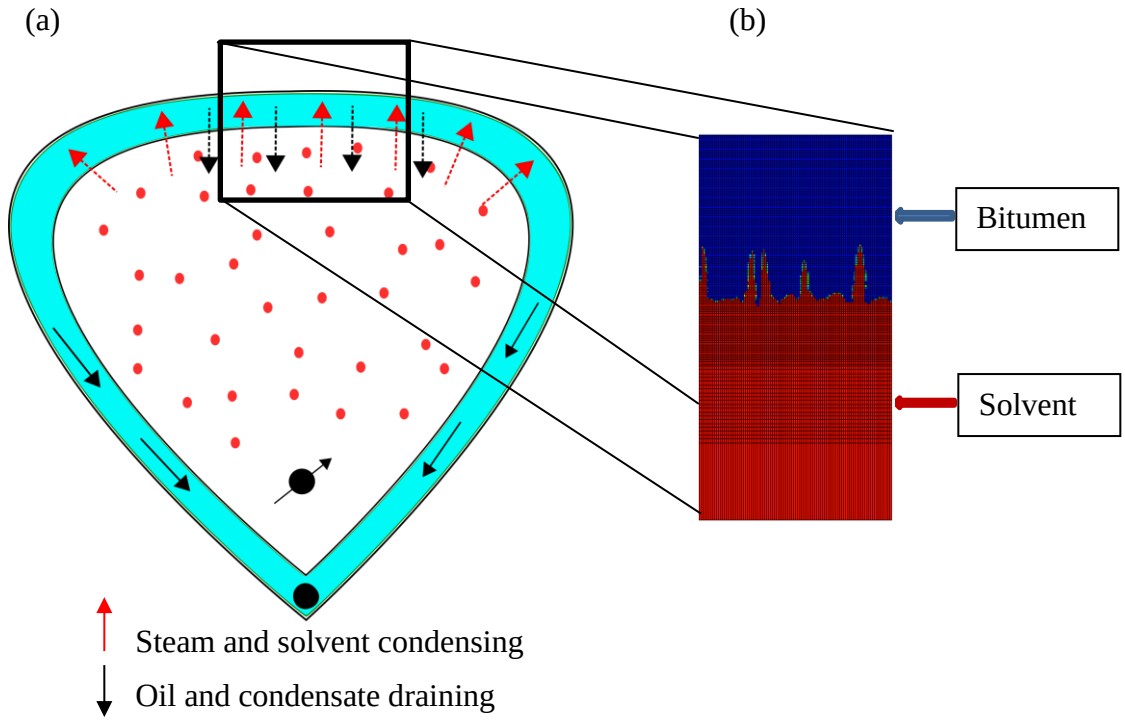

Figure 5.1: (a) Schematic of typical solvent-aided process and (b) numerical simulation geometry of mechanistic model.

In order to understand the impact of non-equilibrium interphase mass transfer on solvent-aided thermal recovery processes, two-dimensional simulation models were constructed as shown in Figure 5.1 (b). To perform mechanistic studies, A 2D 1 m by 2 m numerical model was constructed where the upper half of the model is the bitumen zone and the lower half of the model is the solvent zone. As observed from Figure 5.1 (b), solvent will diffuse into bitumen by diffusion, and the inherent numerical dispersion. As solvent is diffusing into bitumen, bitumen will flow downward due to higher mobility and the adverse density (gravity) effects.

Mechanistic studies will be conducted on the above numerical model where pressure, temperature, and grid size will be varied, and the interphase mass transfer will be calculated from the simulation

resutls. In order to study the impact of the non-equilibrium interphase mass transfer, two main cases will be studied herein.

5.2.1 Equilibrium Case

In equilibrium case, phase distribution of components will reach their respective equilibrium limits in each grid instantly. Typically, phase composition distributions are controlled by k-values and calculated using the vapor-liquid equilibrium flash calculations. The k-value of a component is defined as the ratio of its concentration in gas phase to its concentration in the liquid phase. In CMG for instant, k-value are entered either in tables as function of pressure, temperature, and composition or as a correlation. K-values correlation used in CMG is shown below:

$$K_i(P,T) = \left(\frac{k_{v1_i}}{P} + k_{v2_i} P + k_{v3_i} \right) \exp\left(\frac{k_{v4_i}}{(T - k_{v5_i})} \right), \quad \textbf{(5.1)}$$

where k_{v1} to k_{v5} are the coefficients that can be determined through fitting the experimental data. *T* and *P* are the temperature and pressure of the system in C and kPa, respectively.

5.2.2 Non-Equilibrium Case

In the second set of simulation models, the fluid model used is the same as the equilibrium simulation cases with the difference of adding another component to the fluid model to represent the solvent in the form of free gas phase and solution gas phase. As explained previously, due to the high viscosity of bitumen, the dissolution/exsolution of solvent from bitumen is not instantaneous, and therefore, to simulate the kinetics of the dissolution/exsolution of solvent from bitumen, CMG STARS allows for the definition of different forms of the gaseous solvent. Therefore, for the non-equilibrium cases, propane is defined as solution gas (dissolvable in oil)

and as a free gas. With the addition of the new component, it is now possible to simulate the transformation kinetics of the solvent through the use of reaction described as:

$$\boldsymbol{Solvent_{gas} \xrightarrow{R1} Solvent_{liq}}\,, \qquad \textbf{(5.2)}$$

$$\boldsymbol{Solvent_{liq} \xrightarrow{R2} Solvent_{gas}}\,. \qquad \textbf{(5.3)}$$

The non-equilibrium modelling of mass transfer is generated through the use of rate dependent reaction terms substituting the typical equilibrium k-values method and the flash calculations explained previously. The main function of a reservoir simulator is to solve a set of mass balance equations pertaining to a component in all grid blocks. For the sake of illustrations, lets assume we have a system of two components gaseous solvent and bitumen. In the most general form there is a mass balance equation for each component in each phase when mass transfer is not assumed at instantaneous equilibrium. The equations are (Nghiem and Sammon, 1997):

$$\Delta T_{io} y_{io} \Delta\Phi_o - \tau_i + q_{io} - \frac{V}{\Delta t}(N_{io}^{n+1} - N_{io}^{n}) = 0\,, \qquad i=1,\ldots\ldots,\, n_c \qquad \textbf{(5.4)}$$

$$\Delta T_{ig} y_{ig} \Delta\Phi_g - \tau_i + q_{ig} - \frac{V}{\Delta t}(N_{ig}^{n+1} - N_{ig}^{n}) = 0\,, \qquad i=1,\ldots\ldots,\, n_c \qquad \textbf{(5.5)}$$

where T_{io} and T_{ig} [mol/Pa.s] the transmissibility of component *i* in oil and gas phases, respectively, y_{io} and y_{ig} are the mole fraction of component *i* in oil and gas phases, respectively, Φ_o and Φ_g [Pa] are the flow potentials for both phases, q_{io} and q_{ig} [mol/s] are the molar injection/production rates, V is grid block volume, N_{io} and N_{ig} [mol/m^3] are moles of component *i* per grid block volume in oil and gas phases, respectively, and τ_i [mol/s] is the interphase transfer term of

component *i* per grid block volume. The transfer term τ_i can be expressed as first order Fickian expansion term (Niessner and Hassanizadeh, 2011).

$$\tau_{ik} = \pm \frac{\rho_k D^{ik}}{d^{ik}} a_{\mathrm{lg}} (y_{ik} - y_{ik}^*), \qquad \textbf{(5.6)}$$

where D^{ik} [m^2/s] is the micro-scale Fickian diffusion coefficient for component *i* in phase *k*, ρ_k [mol/m^3] is the molar density of phase *k*, d^k [m] is the diffusion length of component *i*, y_{ik}^* is the solubility limit of component *i* in phase *k*, y_{ik} is the micro-scale mole fraction of component *i* in phase k, and a_{lg} [m^2/m^3] is the specific interfacial area separating gas and liquid phases. In CMG STARS, it is possible to include and model the non-equilibrium interphase mass transfer term τ_{ik} explained above through the use of a rate-based reaction terms. Basically, the term $\frac{D^{ik}}{d^{ik}} a_{\mathrm{lg}}$ in equation (5.6) is lumped into one variable, K^* [1/s], which is called the dissolution/exsolution rate frequency factor. Also, it is worth noting here that the term $\frac{D^{ik}}{d^{ik}}$ in equation (5.6) is the non-equilibrium interphase mass transfer coefficient, k [m/s].

As mentioned earlier, in CMG STARS, it is possible to model non-equilibrium interphase mass transfer using reaction terms. The keyword “RXEQFOR” defines the chemical reaction that deviates from equilibrium previously described by equation (5.1):

$$K_i(P,T) = \left(\frac{k_{v1_i}}{P} + k_{v2_i} P + k_{v3_i} \right) \exp\left(\frac{k_{v4_i}}{(T - k_{v5_i})} \right). \quad \textbf{(5.7)}$$

Assuming bitumen is a non-volatile component, the solubility of a component is defined as the inverse of $K_i(P,T)$. Therefore, by setting k_{v1_i}, k_{v2_i}, k_{v4_i}, and k_{v5_i} to be zero, equation (5.7) becomes:

$$K_i(P,T) = k_{v3_i} = \frac{1}{x_i^*}, \quad \textbf{(5.8)}$$

where x^* is the mole fraction concentration limit of the component in each grid block. Therefore, the reaction term specified by keyword: RXEQFOR is

$$\tau_{ik} = \pm K^* (x_{ik} - x_{ik}^*), \quad \textbf{(5.9)}$$

where K^* is the frequency factor for dissolution or exsolution of the component [1/day], x_{ik} is the mole fraction of the component *i* in phase k in each grid block, and x_{ik}^* is the solubility limit of component i in phase k in each grid block, which is calculated by equation (5.8).

5.3 Methodology of the Numerical Analysis and Mechanistic Studies

The impact of non-equilibrium interphase mass transfer term is most prominent for slow processes, or when heat source is included. However, from a modelling perspective, for fine grid size blocks, the non-equilibrium interphase phenomenon diminishes as the term $(x_{ik} - x_{ik}^*)$ in equation (5.9) will be insignificant. Also, the dissolution/exsolution rate frequency factor approaches zero for very fine grid size blocks. Therefore, theoretically, the assumption of instant equilibrium is valid

when modelling fine grid size blocks. Further to note, it is computationally intensive and time consuming to model field scale cases with fine grid size blocks. Therefore, by including the dissolution/exsolution reaction terms when modelling field scale solvent enhanced oil recovery processes, it is possible to capture the non-equilibrium interphase mass transfer phenomena and study its relative impact on oil recovery for proper design and implementation of solvent-based EOR processes.

To start, several base cases for propane/bitumen system with fine grid size block (1 cm) will be generated at different pressure and temperature conditions using the equilibrium k-values method (instant equilibrium assumption). Then, other cases with the equilibrium k-values will be generated at coarse grid size blocks and compared to their respective base cases to quantify the impact of non-equilibrium mass transfer phenomenon. Subsequently, non-equilibrium cases will be generated using the rate-based reaction terms for dissolution and exsolution of solvent from bitumen. Through tuning the exsolution/dissolution frequency factors for the non-equilibrium cases, a match with their respective base-cases at fine grid size blocks will be achieved. The frequency factors obtained intends to capture the necessary information pertaining to the non-equilibrium mass transfer coefficients. The obtained mass transfer coefficients are used to develop correlations needed to mitigate the impact of non-equilibrium interphase mass transfer when modelling field-scale solvent based EOR processes. The diagram below explains the methodology described herein.

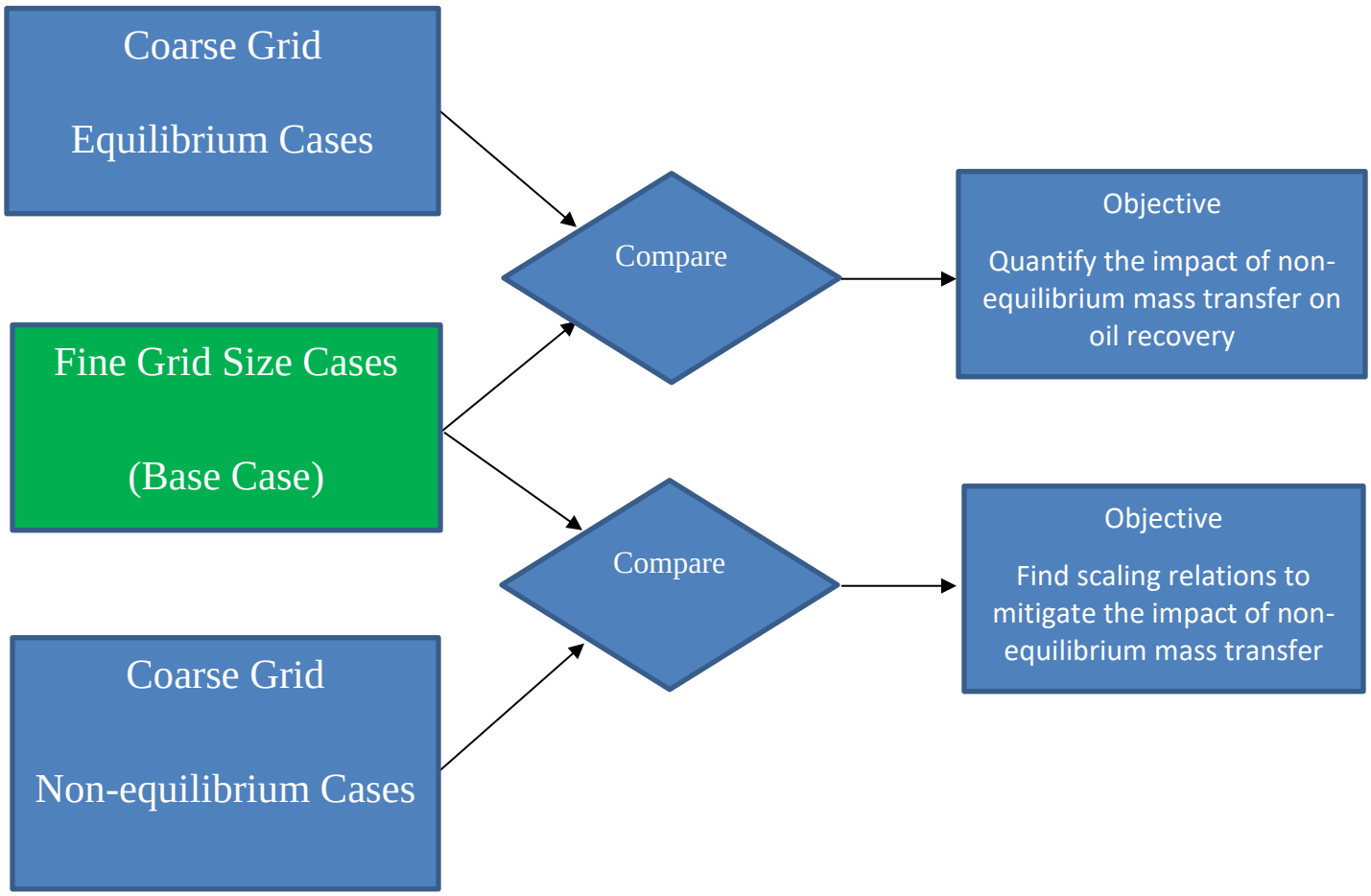

Figure 5.2: Numerical simulations – mechanistic study methodology flowchart.

The base case is basically a 2D vertical cross section of 1 m by 2 m domain where the upper half of the model is the bitumen zone and the lower half of the model is the solvent zone. The grid block size in the bitumen zone is 1 cm in both *x*- and *z*-direction and the total number of grid blocks in the bitumen zone is 10,000. The solvent zone was gridded non-uniformly in the *z*-direction where at the interface the grid block size is 1 cm, then it was gradually increased to reduce the run time of the simulation. The total grid block size of the solvent zone is 4100. Figure 5.3 illustrates

the base case geometry and grid description. Several base cases were conducted at different temperature and pressure settings. The temperature setting ranges between 50 and 100 ^{o}C, and pressure ranges between 1600 and 3500 kPa.

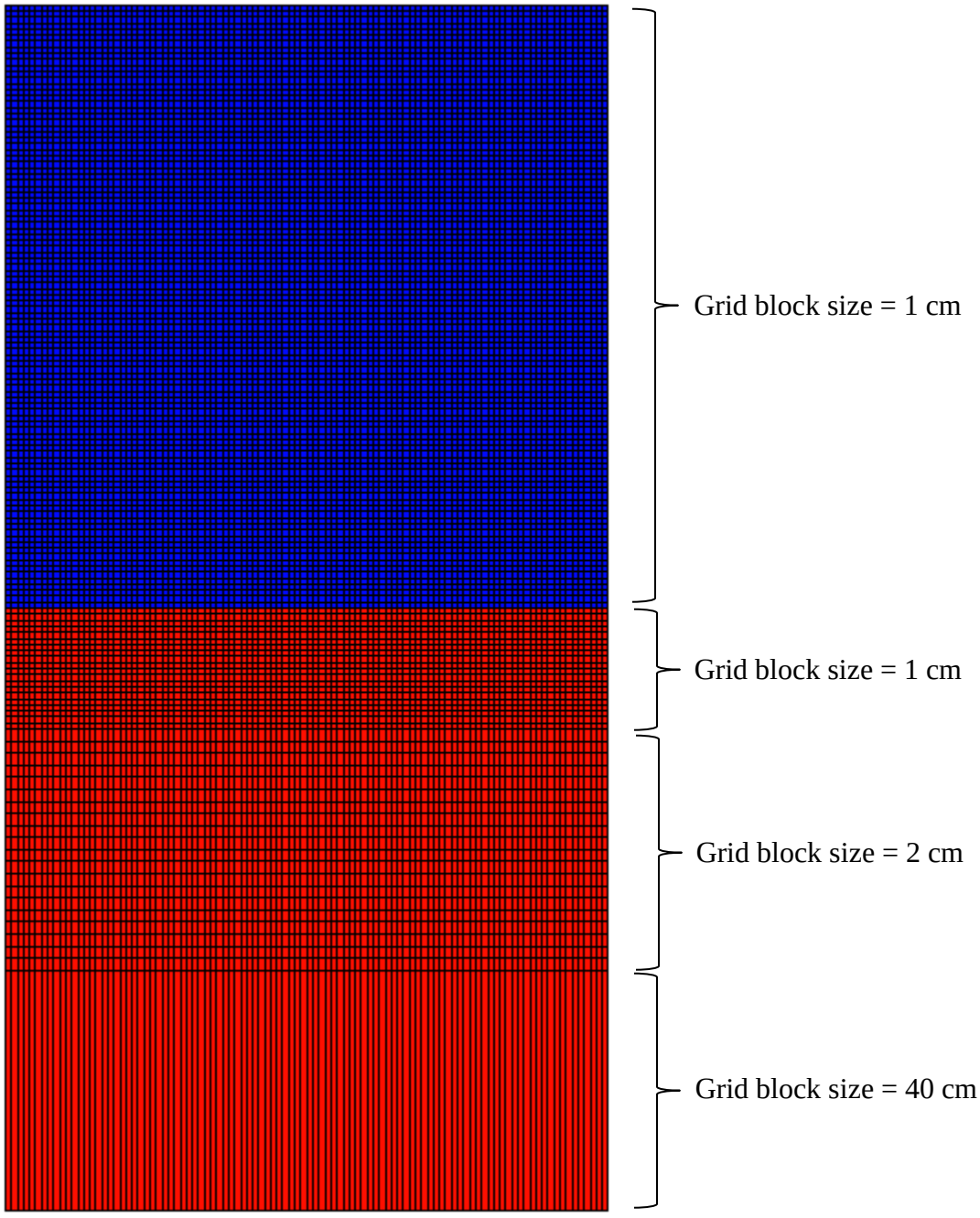

Figure 5.3: Simulation model base case – geometry and grid description.

Figure 5.4 shows oleic mole fraction of C_3 for one of the base cases of propane/bitumen system at 1600 kPa and 75 °C at different times during the gravity drainage process. The Results illustrate the diffusion of propane into bitumen as time progresses. As the base cases conducted using fine grid block size (1cm), the physics of diffusion, convective mixing, adverse mobility (gravity), and viscous fingering are deemed to be fully captured and observed as shown below.

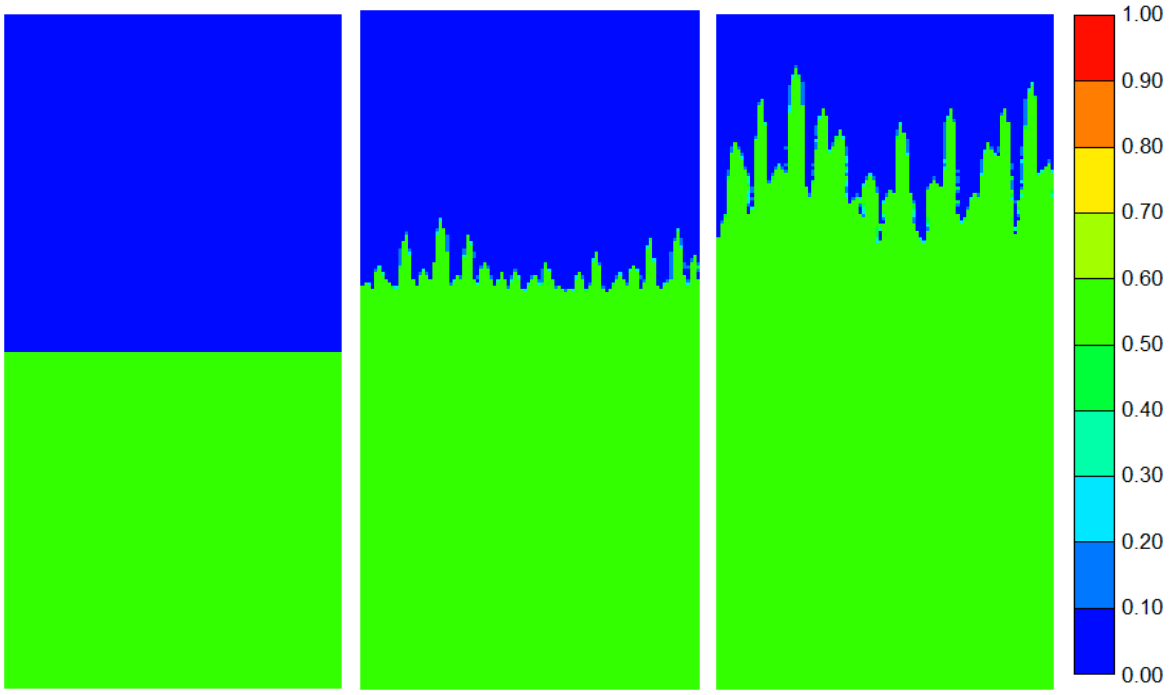

Figure 5.4: Propane/Bitumen system base case at 1600 kPa and 75 °C – oil mole fraction of propane (from left: t=0 days, t= 3 days, t = 5 days).

For illustration purposes, Figure 5.5 shows the cumulative drainage of oil for the base case (1 cm) of propane/bitumen system at 1600 kPa and 75^{o}C using equilibrium k-values. The results show that dissolution of solvent into bitumen results in mobilization and subsequent drainage of the bitumen. As mentioned before, all base cases are fine grids (1cm grid sizes) and modelled using equilibrium k-values where a grid block reach its equilibrium condition instantaneously. The

results for the 10 cm grid block size for the same temperature and pressure are also shown for comparison. As can be noted, the base case (1 cm) has a higher cumulative drainage compared to the 10 cm grid size case. This difference can be attributed to several reasons among which is the non-equilibrium interphase mass transfer phenomenon. In other words, the non-equilibrium phenomenon should be included in coarse grid simulation to achieve the fine grid simulation results. In this case the impact in oil drainage is about 8%. This shows the importance and necessity of including non-equilibrium interphase mass transfer phenomena when modelling field scale (coarse grid) solvent based EOR processes

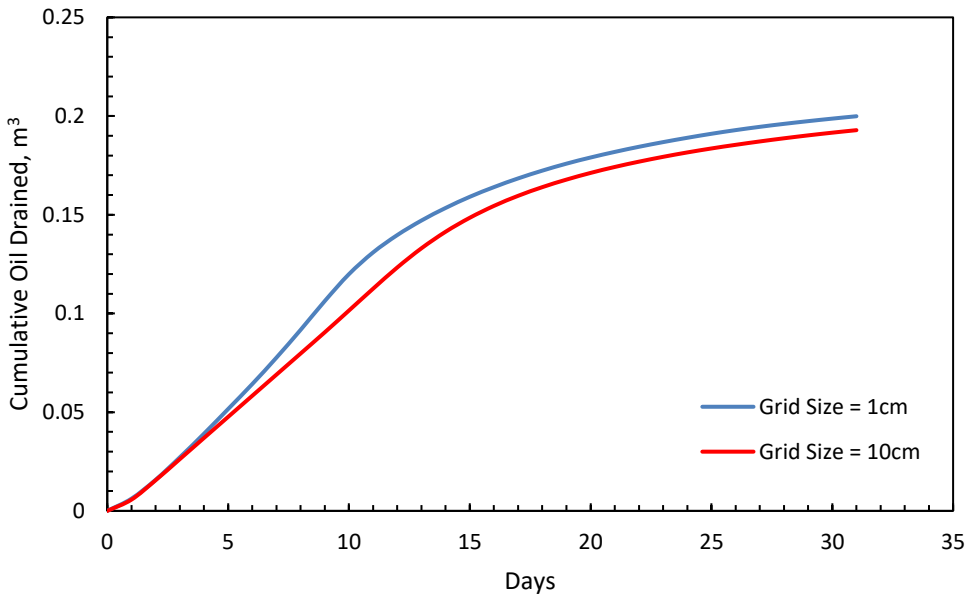

Figure 5.5: Cumulative oil drained for propane/bitumen system, blue line shows fine grid (1 cm) grid block size and red line shows 10cm grid block size both using equilibrium k-values.

Figure 5.6 shows a comparison between mole of propane in oil phase at different times for 1 cm grid block size as compared with 10 cm grid block size at T= 75 ºC and P=1600 kPa. The results show viscous/density- driven fingering is evident in the fine grid simulations. The results reveal that the coarse grid simulation is not able to capture the real physics of the problem. It is noted a common choice of grid block in field scale numerical simulation of thermal recovery processes is 1 m. However, it is impractical to model field scale cases with such high-resolution grid blocks and that is why inclusion of non-equilibrium interphase mass transfer aim at capturing the details of fine grid simulations.

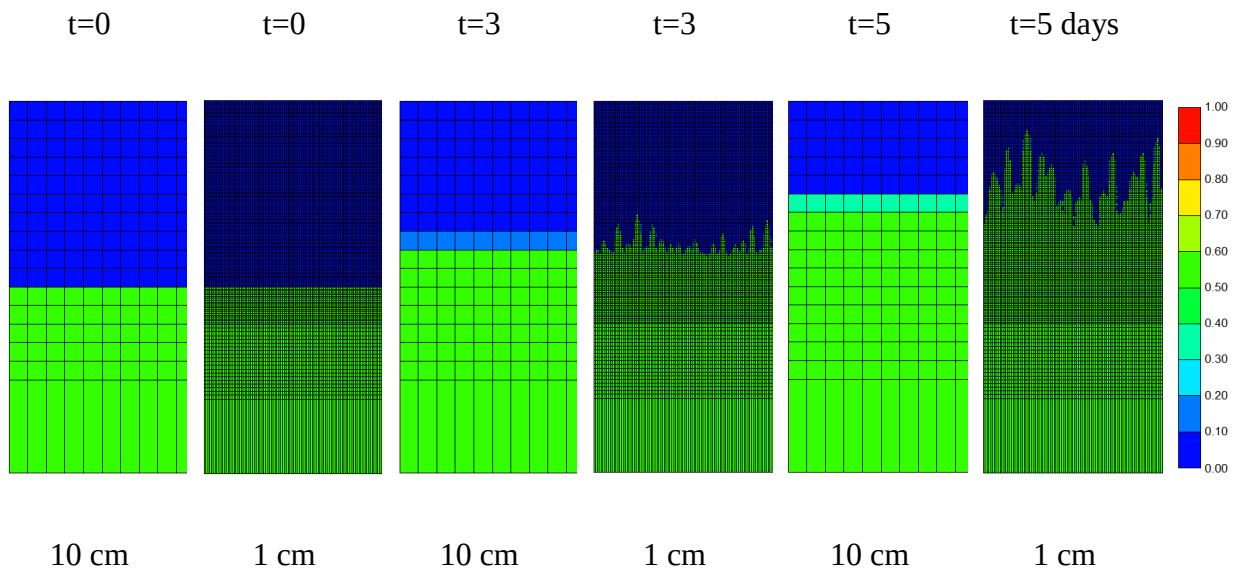

Figure 5.6: Mole of propane in oil phase at different times for 1 cm grid block size versus 10 cm grid block size at T= 75 °C and P=1600 kPa.

5.4 Numerical Determination of the Equilibrium Mass Transfer Coefficients for Propane/Bitumen System

Interphase mass transfer coefficient plays an important role in designing a successful solvent-based EOR processes. Therefore, the aim of this section is to present the typical results of interphase mass transfer coefficients for propane/bitumen mixture at different pressure and temperature conditions and for different grid size blocks.

2D numerical simulations were conducted at different pressure and temperatures by considering three grid block sizes of 1, 5, and 10 cm and the mass transfer coefficients of the propane/bitumen system were determined using:

$$j_i = k_{eff} A \rho \Delta \omega_i, \qquad \textbf{(5.10)}$$

where j_i is the mass flux of the component *i* [kg/s], k_{eff} is the effective mass transfer coefficient [m/s], A is the area normal to flow [m^2], and ρ is the density of the mixture [kg/m^3], and $\Delta\omega$ is the driving force mass fraction difference for component *i*. All parameters in equation (5.8) are known from the numerical simulation models using equilibrium k-values except for the effective mass transfer coefficients. The vertical black lines in Figures 5.7 to 5.9 describe the end of the process or when the solvent hit the top of the bitumen zone. Thus, any values for the mass transfer coefficients beyond the solid vertical black lines are meaningless. Also, it can be noted from Figures 5.7 to 5.9 that the mass transfer coefficients for propane/bitumen system at different temperature and pressure settings is in the range of 1×10^{-8} to 1×10^{-6} m/s. Mass transfer coefficient is inversely proportional to pressure and directly proportional to temperature. This also can be observed from Figures 5.7 to 5.9, as the temperature increases the solvent mass flux is reaching

the top of the bitumen zone faster. For 50 ^{o}C cases, the process ends, and solvent reaches the top of the bitumen zone in about 20 days, whereas in the case of 100 ^{o}C models the process ends in less than 3 days. In terms of sensitivity to grid block sizes, the above figures are inconclusive, and it is not possible to deduce a clear trend of mass transfer coefficient with grid block sizes. Therefore, the analysis of mass transfer coefficient sensitivity to grid block size is investigated in the next section of non-equilibrium interphase mass transfer modelling cases.

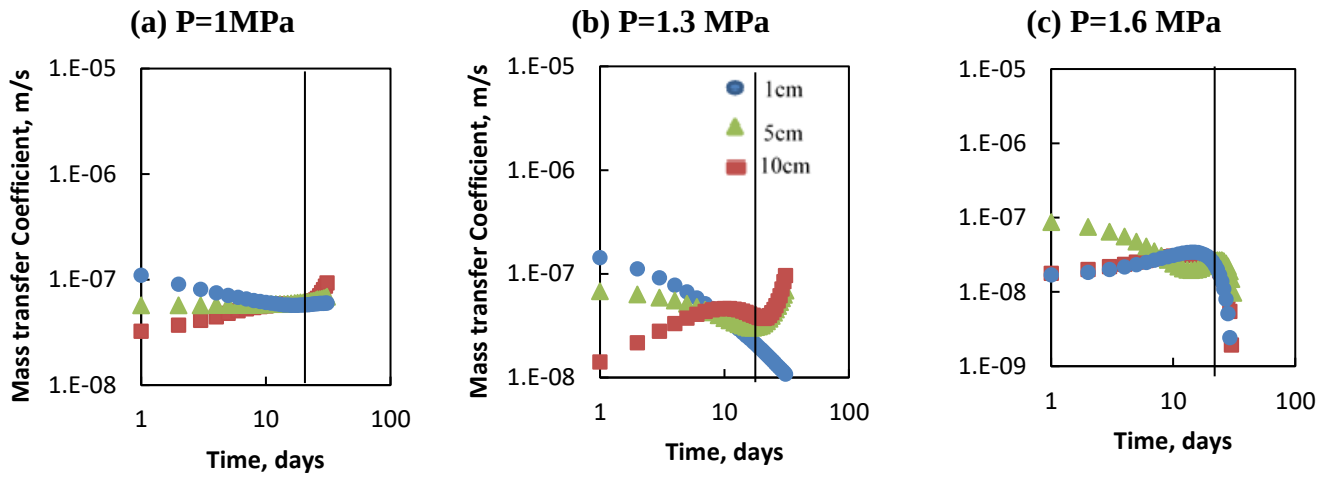

Figure 5.7: Mass transfer coefficients at 1MPa and 50 ^{o}C and different pressure.

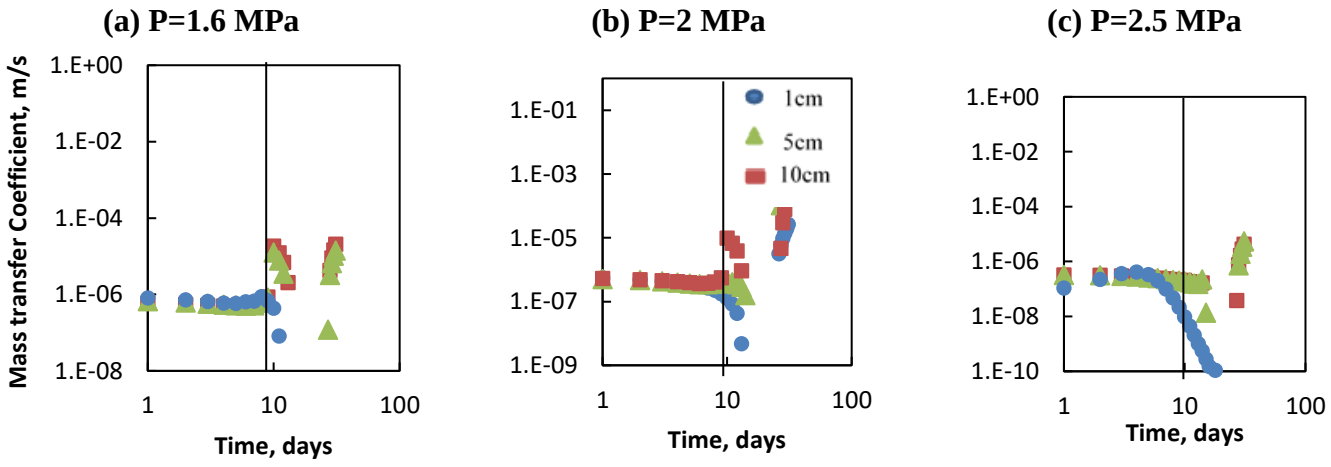

Figure 5.8: Mass transfer coefficients at 1MPa and 75 ^{o}C and different pressure.

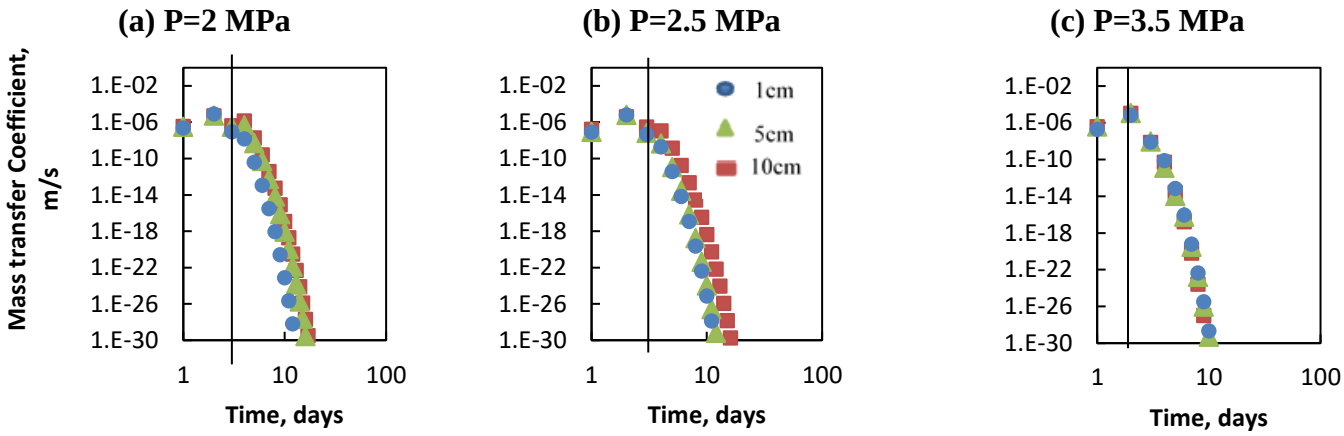

Figure 5.9: Mass transfer coefficients at 1MPa and 100 ºC and different pressure.

5.5 Numerical Results of Modelling Non-equilibrium Interphase Mass Transfer

As mentioned earlier, the assumption of instantaneous equilibrium may be valid in some cases. However, as the interphase mass transfer process is inherently a micro-scale process, it gives erroneous results when modelling field scale processes that involve slow mass transfer or heat source. Therefore, there is a need to properly model the non-equilibrium interphase mass transfer phenomenon to mitigate the erroneous modelling results. In this section non-equilibrium interphase mass transfer is included in the modelling cases as explained in Section 5.2. The non-equilibrium cases are then tuned to match the fine-grid equilibrium cases through adjusting the dissolution/exsolution frequency factors.

To achieve this, CMG CMOST (Computer Modelling Group, 2016) software was used. CMOST is CMG's history matching, optimization, sensitivity analysis, and uncertainty analysis tool. The

history matching and optimization aspects of this software was used in which the coarse grid non-equilibrium cases were optimized to match the respective fine grid equilibrium base cases through tuning two parameters only: dissolution frequency factor and exsolution frequency factor. The objective function of the CMOST is defined to minimize the difference in oil rates of the coarse grid non-equilibrium cases and fine grid base cases. In order to have a thorough design of experiment implemented, three temperature settings were selected: 50^{o}C, 75^{o}C, and 100^{o}C, and four pressure settings: 1600 kPa, 2000 kPa, 2500 kPa, and 3500 kPa. The levels of grid block size variables selected for the experiment are: 5 cm, 10 cm, 20 cm, and 1 m. In total, there were 50 experiments to be conducted for this design of experiment, 20 of which were conducted using CMOST software, the remaining were done manually as it was easy to achieve the match without the need to use CMOST software. It is worth noting that each CMOST study implemented required on average 100 simulation runs to be performed to get a decent match, and each simulation run takes approximately 30 mins of run time. Therefore, in total, ~1000 hours of simulation were done to complete the design of experiment.

The outcomes of this design of experiment are:

- Determining the impact of non-equilibrium interphase mass transfer phenomenon at different temperatures, pressures, and grid block sizes,
- Finding scaling relations for the non-equilibrium interphase mass transfer that can be employed in field scale modelling of solvent-based EOR processes,
- Determining the non-equilibrium interphase mass transfer coefficients at different temperatures, pressures, grid block sizes.

Further to the design of the experiment conducted and explained above, additional simulations were conducted to compare true field scale simulations. The fine grid (10 cm) and coarse grid (1 m, field scale) were both modeled using the equilibrium k-values. The difference between the fine and coarse grid reveals the inherent effect of non-equilibrium phenomenon associated with the coarse grid simulations, which need to be mitigated through inclusion of dissolution and exsolution rates into the coarse grid simulations. The numerical simulation models constructed for this study are 2D models, 10 m × 20 m. The number of the grid blocks in the 10 cm grid block case are 20,000 blocks whereas in the case of 1m grid block, the number of the grid blocks are 200 blocks. Figure 5.10 shows the geometry/size of the simulation models constructed for this case. Basically, three cases were performed at 100 °C for different pressures: 1600 kPa, 2000 kPa, and 3500 kPa.

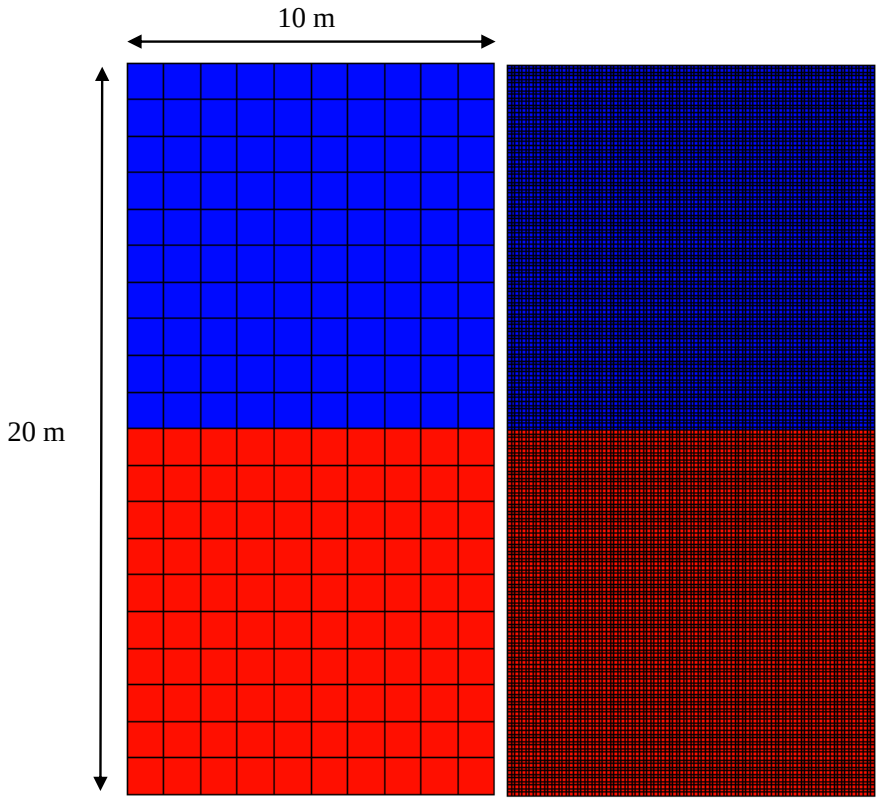

Figure 5.10: Field scale simulation models – geometry/size description (a) 1m grid size versus (b) 10cm grid size.

The results shown in Figures 5.11 to 5.13 demonstrate the impact of the absence of the non-equilibrium interphase mass transfer on oil recovery in coarse grid simulations at different conditions. These results compare the field scale models of 1 m grid block sizes with their respective base cases of 10 cm grid block sizes. In these simulations 10 cm grid block is considered as the fine scale since further refining of the model is prohibitive and computationally expensive.

As noted from for propane/bitumen system, the impact on oil recovery when upscaling simulation models from 10 cm to 1 m is ranging between 3% to 6%. In other cases, with lower temperatures, the impact could be as high as 10%. This difference can be partially mitigated through the inclusion

of the non-equilibrium interphase mass transfer terms. Also, it is worth noting from figures 5.11 to 5.13 that as pressure increases, the difference between equilibrium and non-equilibrium is mitigated. This can be due to the impact of pressure on the dissolution rate of propane into bitumen as observed from figures 5.7 to 5.9, higher pressure results in lower interphase mass transfer and therefore reducing the difference between equilibrium and non-equilibrium modelling results.

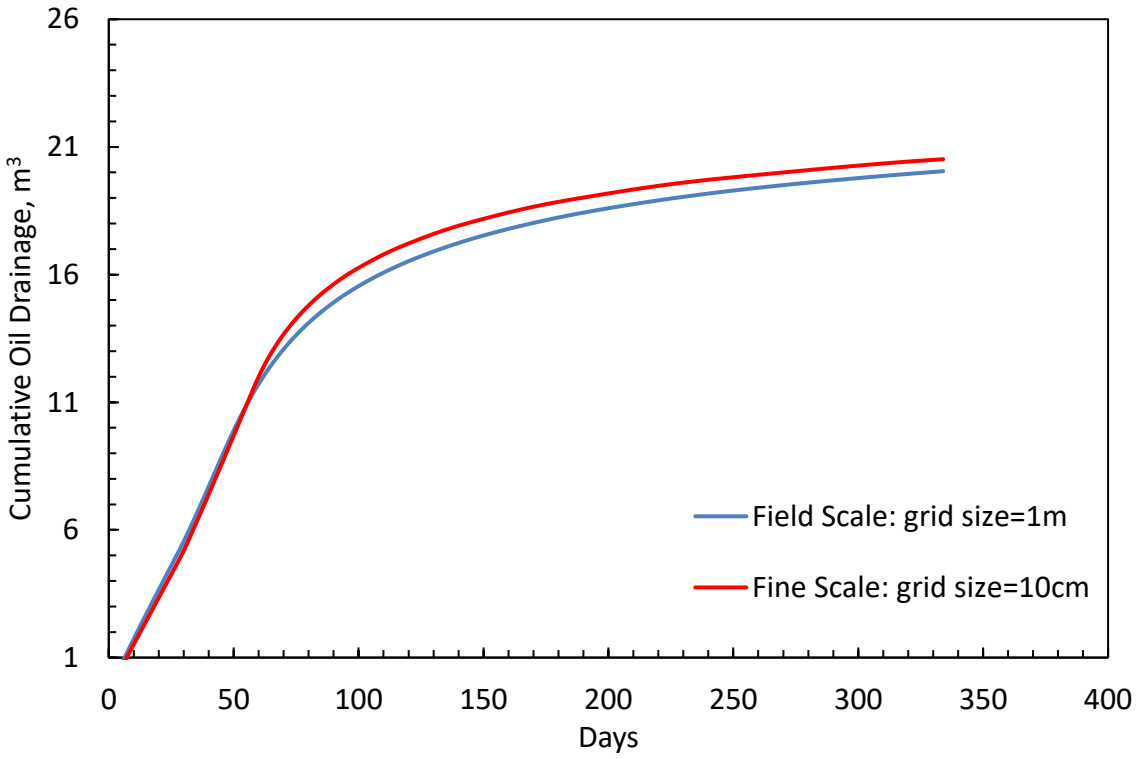

Figure 5.11: Cumulative oil drainage at 1.6 MPa and 100 °C.

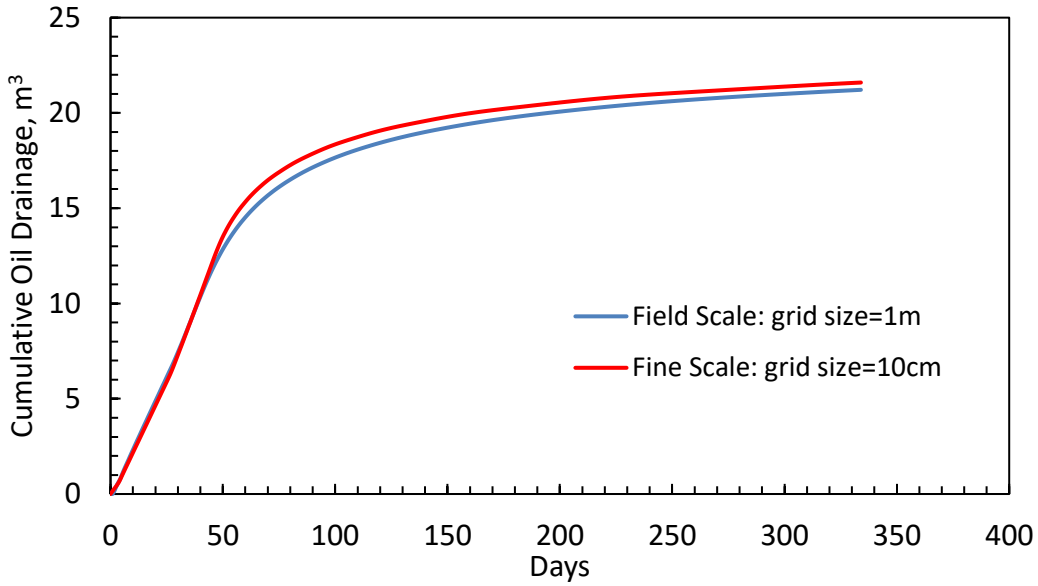

Figure 5.12: Cumulative oil drainage at 2 MPa and 100 ºC.

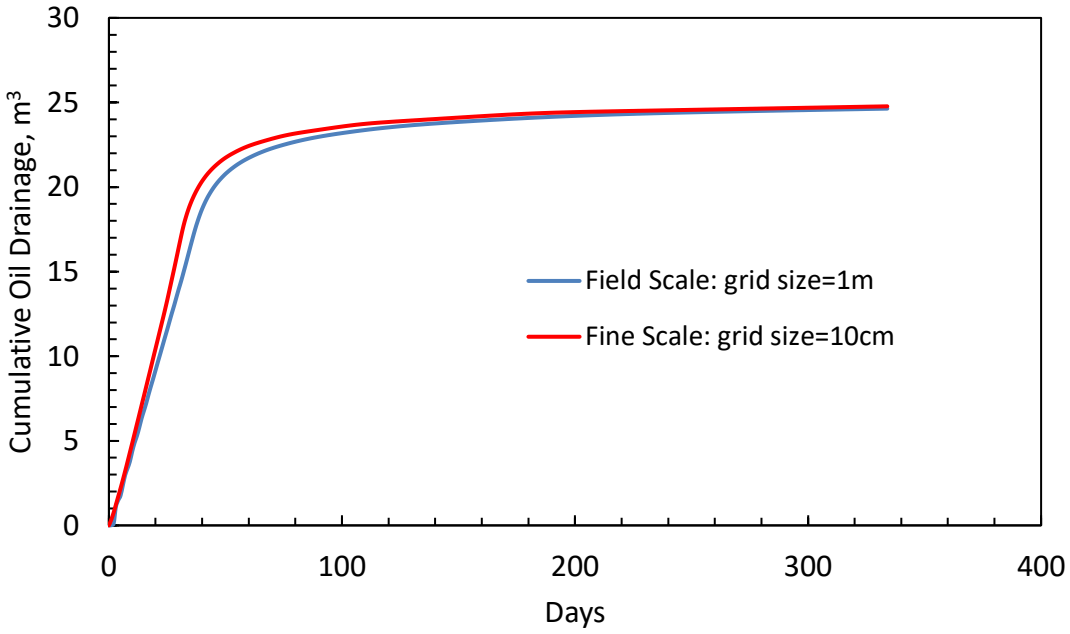

Figure 5.13: Cumulative oil drainage at 3.5 MPa and 100 ºC.

Proceeding to the design of the experiment explained at beginning of this section, when modelling the non-equilibrium interphase mass transfer through adding reaction terms, the oil recovery gap between field scale and fine scale is mitigated. The results shown in Figures 5.14 to 5.19 provides a comparison between the simulated volume of oil drained for equilibrium and non-equilibrium cases at different pressures and temperatures. The base case, which is modelled using fine grid block size, represents the ideal case that captures the physics of dissolution of solvent into bitumen, viscous/density-driven fingering effects, convective mixing, and dispersion. When using larger grid blocks, mechanisms that are inherently fine scale processes such as viscous/density-driven fingering effects are lost. Therefore, field scale modelling using the assumption of instant equilibrium will lead to erroneous results. The equilibrium cases presented in Figures 5.14 to 5.19 show the difference in oil recovery compared to the base cases. Finally, the non-equilibrium cases presented in these figures show the optimized results obtained using CMOST optimization software through tuning of dissolution/exsolution rate frequency parameters. It is noted that when adjusting the dissolution/exsolution rate frequency factors for the non-equilibrium cases, it is possible to mitigate the impact of non-equilibrium interphase mass transfer when modelling field scale cases. All the cases discussed here are for propane/bitumen mixtures at different pressures and temperatures. Two grid block sizes of 5 cm and 10 cm are presented in the examples shown in Figures 5.14 to 5.19. The remaining cases will be presented in subsequent section in tabulated format.

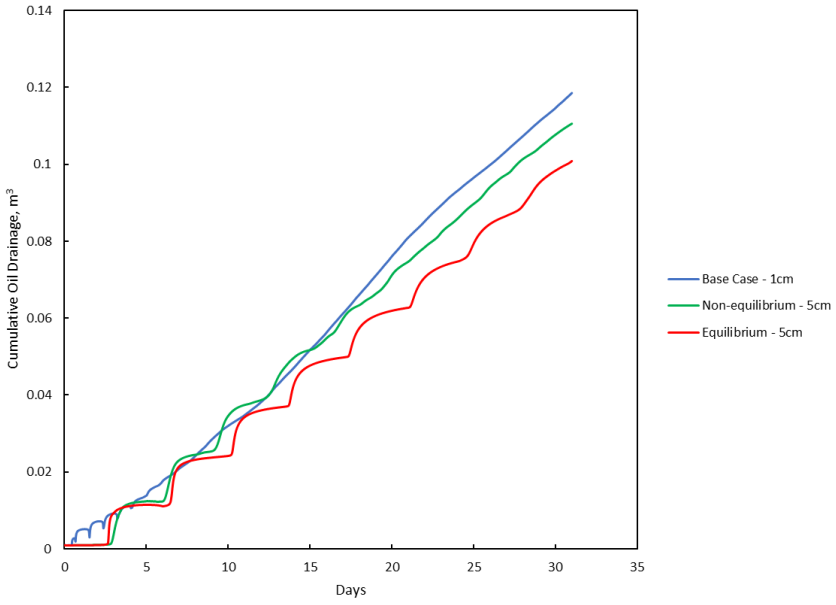

Figure 5.14: Cumulative oil drainage for Propane/Bitumen system at 1600 kPa and 50 °C - Equilibrium versus Non-equilibrium – 5 cm grid block size.

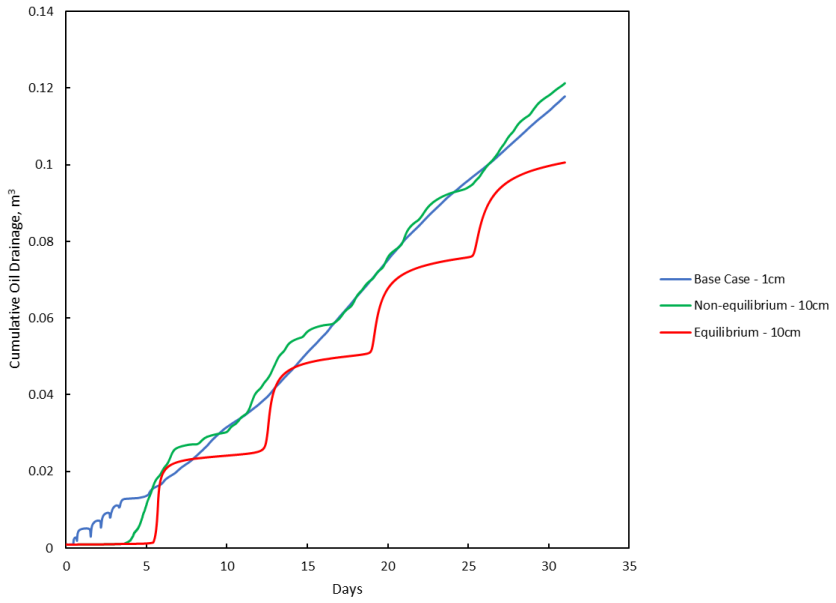

Figure 5.15: Cumulative oil drainage for Propane/Bitumen system at 1600 kPa and 50°C – 10 cm grid block size.

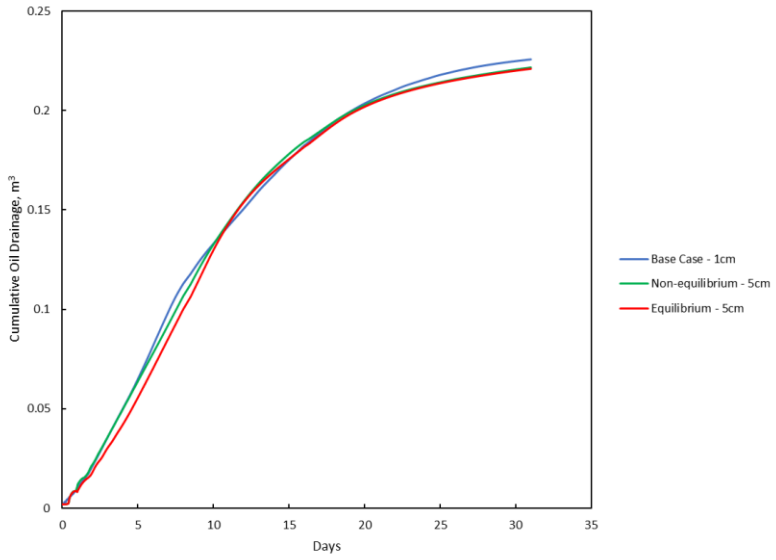

Figure 5.16: Cumulative oil drainage for Propane/Bitumen system at 2000 kPa and 75 °C – 5 cm grid block size.

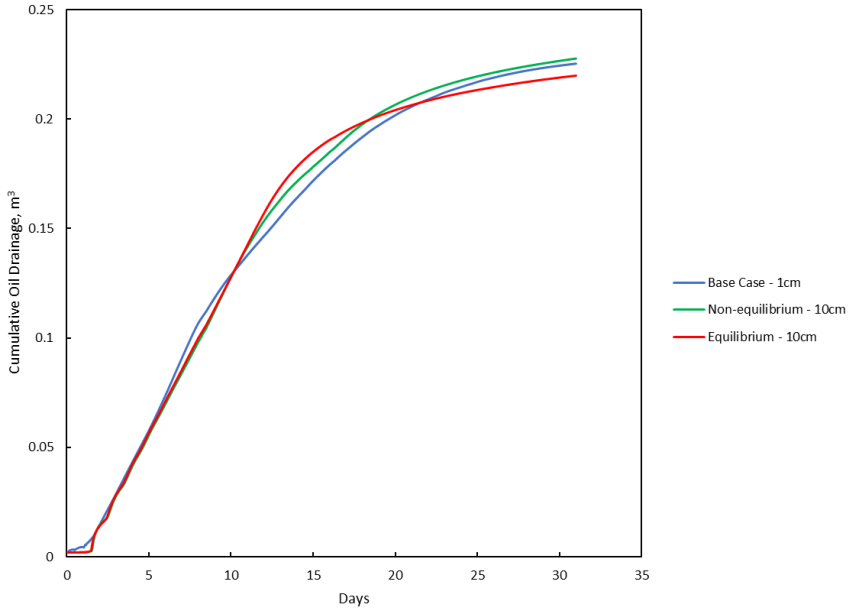

Figure 5.17: Cumulative oil drainage for Propane/Bitumen system at 2000 kPa and 75 °C – 10 cm grid block size.

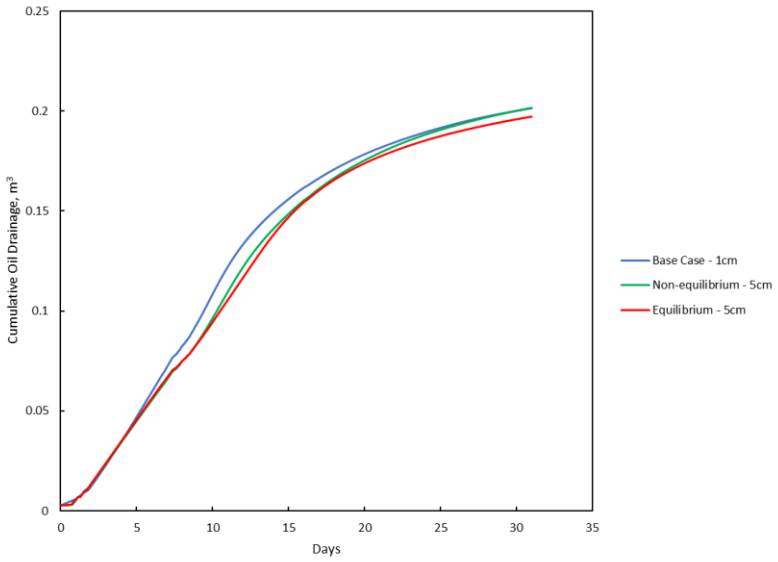

Figure 5.18: Cumulative oil drainage for Propane/Bitumen system at 1600 kPa and 75 °C - Equilibrium versus Non-equilibrium – 5 cm grid block size.

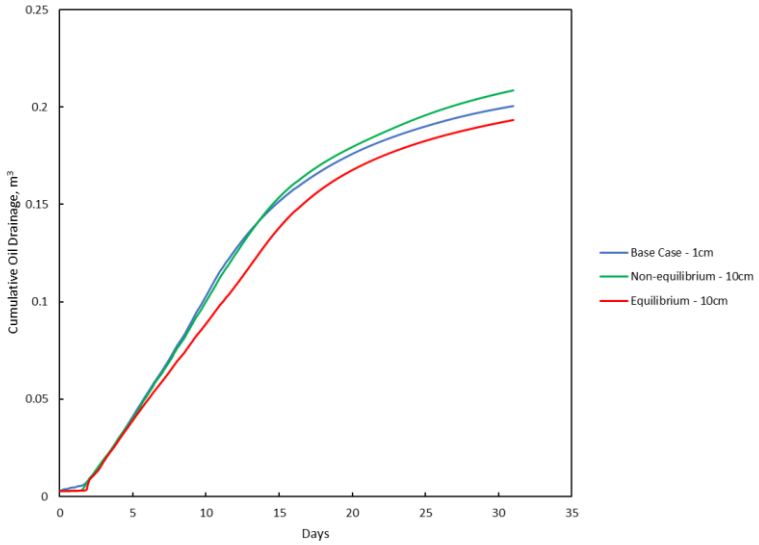

Figure 5.19: Cumulative oil drainage for Propane/Bitumen system at 1600 kPa and 75 °C – 10 cm grid block size.

Table 5.1 compares the % error in the cumulative oil drainage of the equilibrium and non-equilibrium cases against their respective base cases. It is calculated based on the final value of the cumulative oil drainage at the end of the simulation run. In almost all cases, it is possible to adjust the dissolution/exsolution frequency factors to obtain a good match to the base cases and reduce the error in oil recovery.

Table 5.1: Cumulative oil drainage % error – equilibrium versus non-equilibrium.

Case	Grid size (cm)	% error- Non-equilibrium	% error- Equilibrium
1600 kPa & 50°C	5	4.6	10.1
1600 kPa & 50°C	10	2.0	10.2
2000 kPa & 75°C	5	6.2	7.4
2000 kPa & 75°C	10	3.9	8.6
1600 kPa & 75°C	5	0.5	4.8
1600 kPa & 75°C	10	9.8	8.1

In general, the assumption of instant equilibrium modelling of field scale solvent-based EOR processes would results in error ranging between 4% to 10% in predicting oil recovery as shown in the Table 5.1 in the case of propane/bitumen system. This is for the case when grid blocks are upscaled 5 to 10 times. However, further upscaling of the model may result in higher discrepancy in predicting oil recovery. Also, using other solvents with bitumen would result into different range of errors in oil recovery. It is shown in Chapter 3 that the non-equilibrium interphase mass transfer phenomenon is strongly influenced by the pressure and temperature of the system, and composition of the diffusing component. It was shown that the non-equilibrium mass transfer phenomenon is more evident for gaseous solvents. However, liquid solvents have higher

diffusivities into bitumen. Therefore, each solvent is distinct and need to be investigated thoroughly to determine the impact of non-equilibrium interphase mass transfer phenomena on the performance of solvent-based EOR processes.

Through the analysis of 50 design experiments, and more than 1000 simulation hours for different pressures, temperatures, and grid block sizes, the scaling relations of dissolution rate frequency factors and interphase mass transfer coefficients were developed for propane/bitumen systems. The temperature setting ranges between 50 and 100 ^{o}C, pressure ranges between 1600 and 3500 kPa, and grid block sizes used in the development of the scaling relations are 5, 10, and 20 cm. Figure 5.20 shows the frequency factor for dissolution (K^{*}) versus grid block size. These scaling relations can be used in designing and modelling propane/bitumen EOR processes while capturing the impact of non-equilibrium interphase mass transfer phenomenon. The frequency factors for dissolution (K^{*}) for propane/bitumen system dissolution rate for various cases are provided in Table 5.2.

As observed from Figure 5.20, the dissolution rate of propane into bitumen increases with grid block size regardless of the temperature and pressure of the system. Typically, for very fine grid block sizes, the dissolution rate values are insignificant and in such cases the equilibrium and non-equilibrium modelling of mass transfer cases are similar. For large grid block sizes, the dissolution rate increases confirming the importance of the non-equilibrium interphase mass transfer when modelling field scale solvent based EOR processes. As the dissolution rate by definition is the product of the interphase mass transfer coefficient with specific interfacial area, i.e.: grid block dimension, non-equilibrium interphase mass transfer coefficient is directly proportional to dissolution rate frequency factor. Also, it can be observed from Figure 5.20 that for large gird

block sizes (1 m), the extrapolated dissolution rate tends to approach to a range of values between 8 and 10 (1/day) for the propane/bitumen system depending on the temperature and pressure condition of the system.

It is important to note that the exsolution frequency factors did not exhibit a consistent trend with varying grid block sizes and it takes large values ranging 5.5×10^{8} – 2.5×10^{18}. It is worth noting that the process studied here is governed by both dissolution and exsolution kinetics. However, simulation cases seem to be more sensitive to dissolution kinetics compared to exsolution, and therefore, it can be inferred that dissolution kinetics play a more important role compared to exsolution kinetics. This can be attributed to the fact that the simulation runs used in this study are dissolution dominant. However, in the presence of pressure variation and other dynamic mechanisms such as convective mixing, the exsolution kinetics may play a more important role. This will be explored further in this chapter when we apply the non-equilibrium approach to ES-SAGD process. Therefore, in this section the results for dissolution rate frequency factors are presented only. While the maximum grid block size used in our simulations is 20 cm, the trend of dissolution frequency factor suggests that a constant frequency factor range of 8 to 10 (1/day) will be able to capture the fine scale processes as the grid block approaches the typically used block size in field scale simulation of solvent-aided recovery processes. The results presented in Figure 5.20 serves as a guide line for history matching of field data by incorporation of dissolution kinetics into thermal simulations.

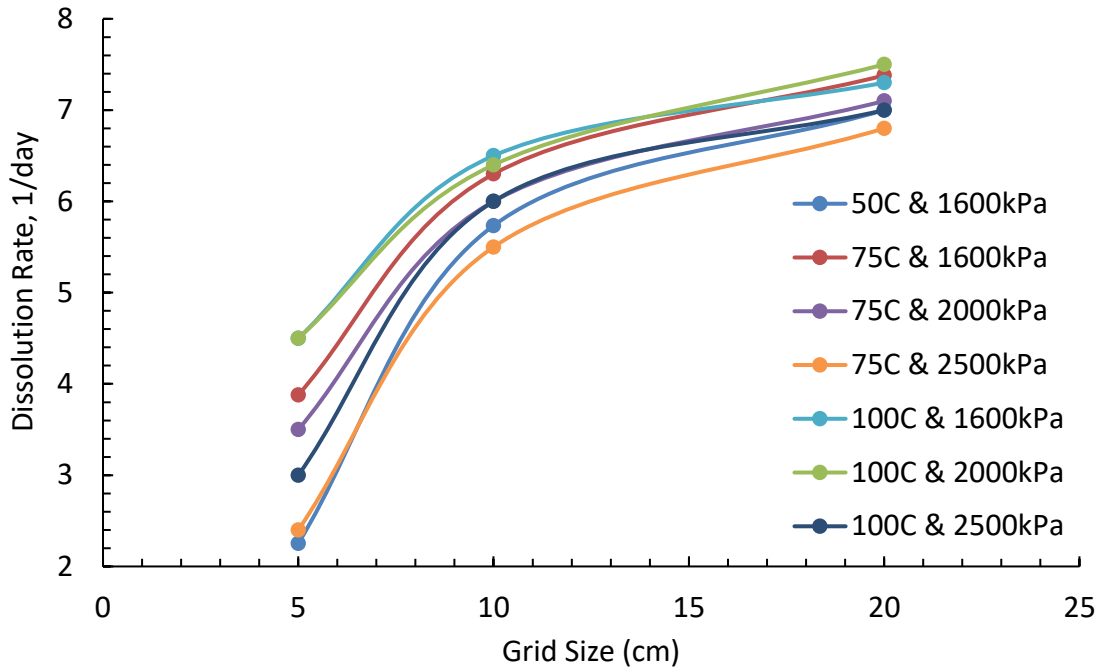

Figure 5.20: Propane/bitumen system dissolution rate versus grid size for different temperatures and pressures.

Table 5.2: Optimized dissolution rate frequency factors for propane/bitumen system as a function of temperature, pressure, and grid size.

Temperature,° C	Pressure, kPa	Grid block size, cm	Dissolution Rate, 1/day
50	1600	5	2.2535
50	1600	10	5.7345
50	1600	20	7
75	1600	5	3.88
75	1600	10	6.3
75	1600	20	7.38
100	2000	5	4.5
100	2000	10	6.4
100	2000	20	7.5
75	2000	5	3.5
75	2000	10	6
75	2000	20	7.1
100	1600	5	4.5
100	1600	10	6.5
100	1600	20	7.3
75	2500	5	2.4
75	2500	10	5.5
75	2500	20	6.8
100	2500	5	3
100	2500	10	6
100	2500	20	7

5.6 Statistical Analysis of the Results

A correlation for the dissolution rate frequency factor of the propane/bitumen system was developed based on the data presented in Table 5.2. First, the temperature, pressure, grid size variables were transformed and normalized to -1 and +1 range, and then a regression analysis was done using Essential Regression and Experimental Design for Chemist and Engineers (EREGRESS) tool to find a correlation model for the scaling relation of the dissolution rate frequency factor as a function of the temperature, pressure, and grid block size of the system. The correlation can be expressed as:

$$K^* = b_0 + b_1(\delta)^3 + b_2(\delta) + b_3\theta(\delta) + b_4\theta(\delta)^2 + b_5\eta + b_6\eta(\delta) + b_7\eta^3 + b_8\eta(\delta)^2,$$

where δ is for scaled grid block size, θ is for scaled temperature, and η is for scaled pressure, b_0 to b_8 are the correlation regressed coefficients. The summary results of the regression analysis are presented in the Table 5.3. As shown in Table 5.3, the predicted R-squared is 0.961, which shows how well the model can predict responses for new observations. The regressed scaling relation developed for the dissolution rate frequency factor is shown in Table 5.4 along with the coefficient test statistics. The correlation is valid for propane/bitumen system for the following range of temperature and pressure: 50 °C to 100 °C and 1600 kPa to 2500 kPa, respectively. The accuracy of the model is shown in Figure 5.21 where the actual dissolution rate values are compared against the predicted ones.

Table 5.3: Dissolution rate correlation – summary of the regression analysis.

|R|	**0.995**
R^2	0.989
R^2 adjusted	0.982
Standard Error	0.226
# Points	21
PRESS	2.22
R^2 for Prediction	0.961
Coefficient of Variation	4.074

Table 5.4: Dissolution rate correlation for propane/bitumen system.

$$K^* = b_0 + b_1(\delta)^3 + b_2(\delta) + b_3\theta(\delta) + b_4\theta(\delta)^2 + b_5\eta + b_6\eta(\delta) + b_7\eta^3 + b_8\eta(\delta)^2$$

		P value	Std Error	-95%	95%	t Stat	VIF
b_0	4.956	7.94537E-17	0.07384	4.795	5.117	67.12	
b_1	5.372	7.34684E-09	0.379	4.547	6.197	14.19	39.29
b_2	-3.339	1.18981E-06	0.374	-4.153	-2.525	-8.936	39.63
b_3	-0.459	0.000223	0.08828	-0.651	-0.266	-5.198	1.284
b_4	0.626	1.81949E-05	0.09160	0.426	0.825	6.831	1.182
b_5	-2.750	0.01945	1.020	-4.972	-0.528	-2.696	293.68
b_6	0.239	0.00859	0.07635	0.07310	0.406	3.136	1.209
b_7	2.588	0.02488	1.010	0.388	4.789	2.563	290.68
b_8	-0.286	0.07489	0.147	-0.605	0.03349	-1.950	4.114

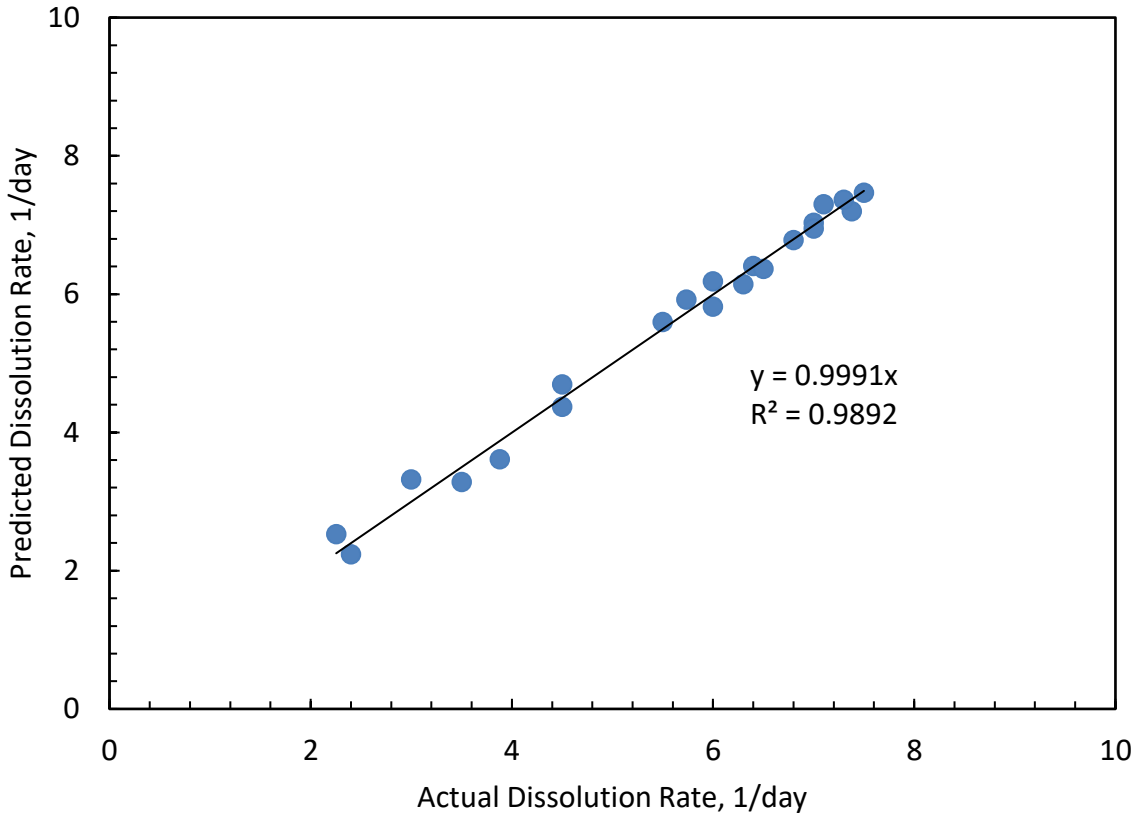

Figure 5.21: Predicted dissolution rate versus the actual dissolution rate.

As mentioned previously, the temperature, pressure, and grid size parameters were normalized before conducting the regression. Therefore, in order to use the scaling relation presented above with dimensional values for temperature, pressure, and grid size, the following normalization relations must be used:

$$\theta = 0.04 \times T - 3, \quad \textbf{(5.11)}$$

$$\eta = 0.002222 \times P - 4.555556, \quad \textbf{(5.12)}$$

$$(\delta) = 0.1333 \times (\Delta x) - 1.6667, \quad \textbf{(5.13)}$$

where θ, η, and δ are for dimensionless scaled temperature, pressure, and grid size. T is for temperature in ^{o}C, P is for pressure in kPa, and Δx is for grid size in cm.

The 3D surface plots presented below show the interactions between different variables and their effect on dissolution rate frequency factor. Figure 5.22 shows dissolution rate as a function of pressure and grid block size and Figure 5.23 shows dissolution rate as a function of temperature and grid block size. Both plots show that grid size block is the most influential variable impacting the dissolution rate.

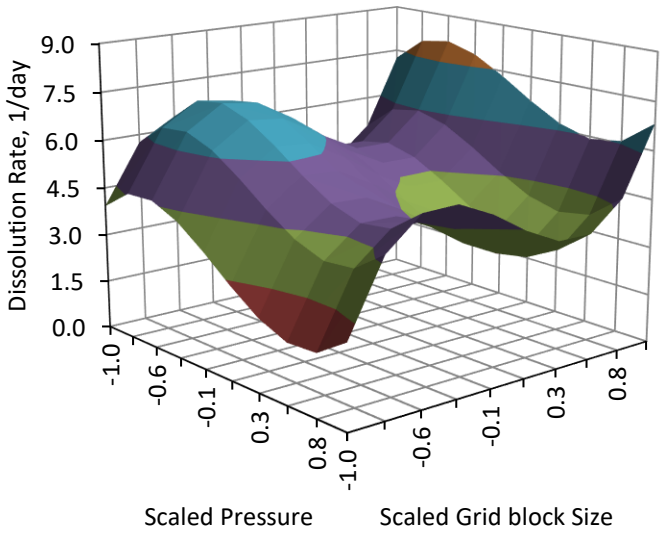

Figure 5.22: Dissolution rate as a function of pressure and grid block size.

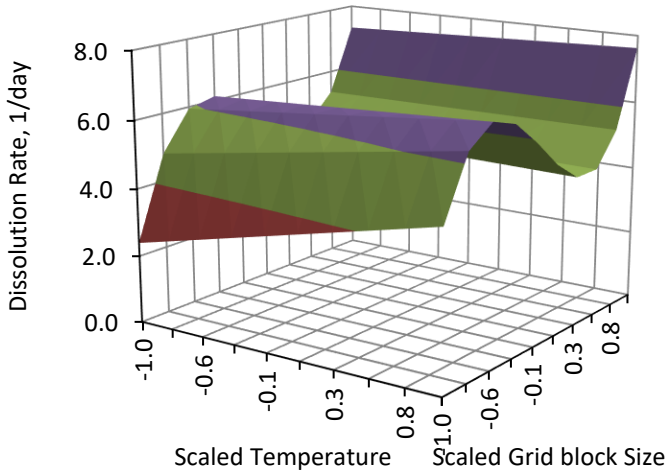

Figure 5.23: Dissolution rate as a function of temperature and grid block size.

The interphase mass transfer coefficient can be calculated from the dissolution frequency factor obtained above. The interphase mass transfer is the product of the dissolution rate with the grid size block dimension. The results for the interphase mass transfer coefficient for the propane/bitumen mixture at different temperatures, pressures, and grid block sizes are shown in Table 5.5. Figure 5.24 shows the interphase mass transfer coefficient in terms of grid block size.

Table 5.5: Non-equilibrium mass transfer coefficients for propane/bitumen system as a function of temperature, pressure, and grid size.

Temperature, C	Pressure, kPa	Grid block size, cm	Dissolution Rate, 1/day	Mass Transfer Coeff. m/s
50	1600	5	2.2535	1.30E-06
50	1600	10	5.7345	6.64E-06
50	1600	20	7	1.62E-05
75	1600	5	3.88	2.25E-06
75	1600	10	6.3	7.29E-06
75	1600	20	7.38	1.71E-05
100	2000	5	4.5	2.60E-06
100	2000	10	6.4	7.41E-06
100	2000	20	7.5	1.74E-05
75	2000	5	3.5	2.03E-06
75	2000	10	6	6.94E-06
75	2000	20	7.1	1.64E-05
100	1600	5	4.5	2.60E-06
100	1600	10	6.5	7.52E-06
100	1600	20	7.3	1.69E-05
75	2500	5	2.4	1.39E-06
75	2500	10	5.5	6.37E-06
75	2500	20	6.8	1.57E-05
100	2500	5	3	1.74E-06
100	2500	10	6	6.94E-06
100	2500	20	7	1.62E-05

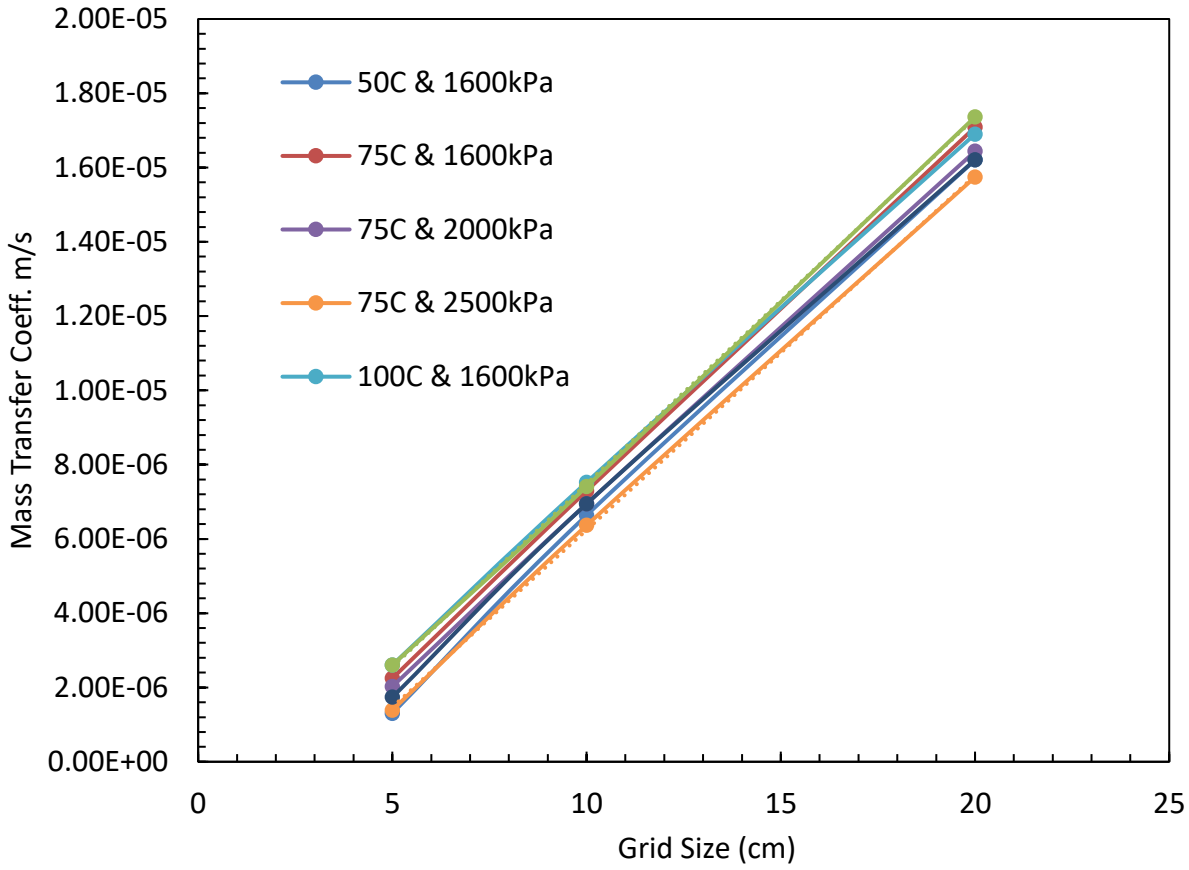

Figure 5.24: Mass transfer coefficient versus grid size for different temperatures and pressures.

As noted, the interphase mass transfer increases with increasing the grid block size. Since the grid size is the dominant parameter that affects the mass transfer coefficient the mass transfer coefficient versus the grid block size results in a linear relationship. Similar to the dissolution rate behaviour, the importance of the interphase mass transfer is quite prominent at field scale models, which proves the necessity of including non-equilibrium mass transfer when modelling field scale solvent-based EOR processes.

5.7 Applications of the Non-equilibrium Approach to ES-SAGD

CMG-STARS was used to simulate the expanding solvent steam assisted gravity drainage (ES-SAGD) process. The reservoir modeled is a cross section of 30 meter thickness, 50 meter width, and 1 km length. The reservoir model constructed is a 2D cartesian system with injector and producer horizontal wells located at the far-right end of the model simulating half well geometry only. Figure 5.25 illustrates the numerical simulation model geometry and well locations.

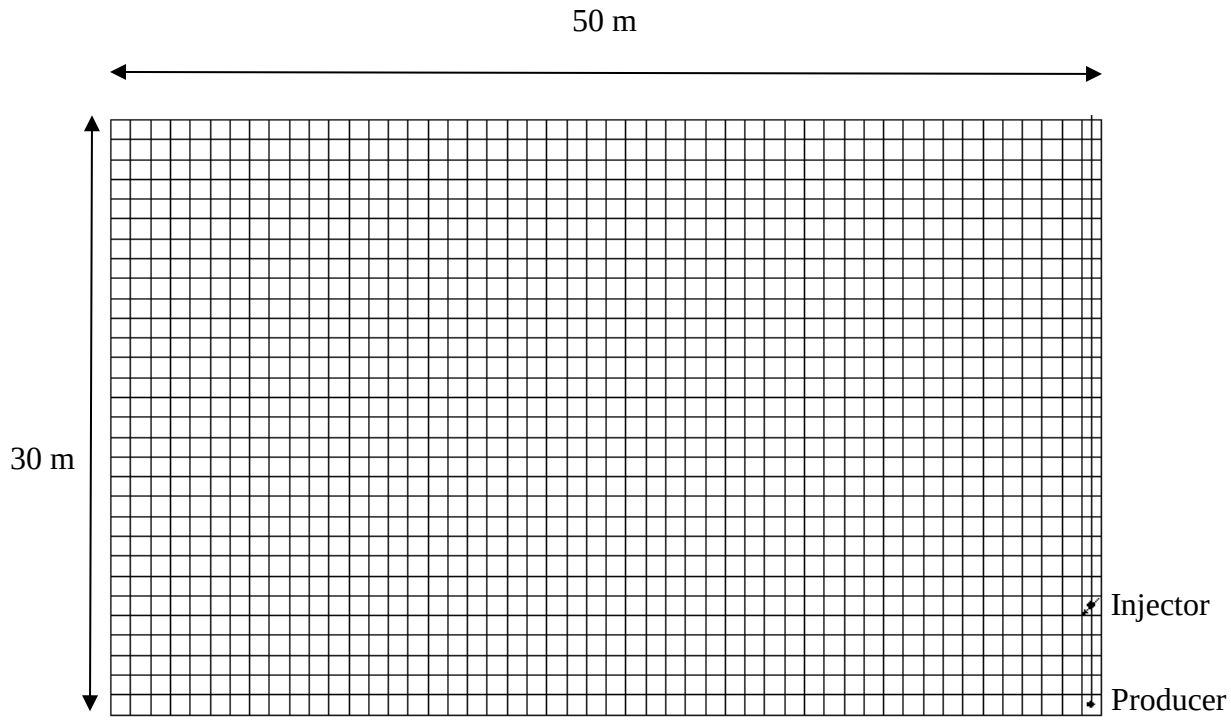

Figure 5.25: ES-SAGD model geometry and well locations.

Two grid size numerical models were constructed, the first one is 25 cm grid block size model representing the fine scale base case, the second model is constructed using the typical grid block size of 1 m representing the field scale cases. Both models were uniformly discretized into 200×1×120 grid blocks and 50×1×30 grid blocks for the 25 cm and 1 m grid block size cases, respectively. Two parallel horizontal wells positioned 5 m apart were defined. The upper well is the injector and the lower well is the producer. The reservoir was assumed homogenous with constant properties. Table 5.6 summarizes the reservoir and rock properties used in the model.

Table 5.6: Summary of reservoir and thermal properties used in the numerical model.

	Parameters	**Value**	**Unit**
Reservoir properties	Porosity	0.3	-
	Permeability	1000	mD
	Initial water saturation	0.15	-
	Mole fraction of Solvent	0	-
	Reference Pressure	3000	kPa
Thermal Properties	Thermal Conductivity-Rock	2.47×10^{5}	J/m/day/C
	Thermal Conductivity-Water	5.35×10^{4}	J/m/day/C
	Thermal Conductivity-Oil	1.15×10^{4}	J/m/day/C
	Thermal Conductivity-Gas	4500	J/m/day/C
	Volumetric Heat Capacity	1.2×10^{6}	J/m^3
	Formation Compressibility	7×10^{-6}	1/kPa
	Over/Under burden capacity	2.74×10^{6}	J/m^3/day
	Over/Under burden compressibility	2.47×10^{5}	J/m/day/C

The initial reservoir temperature was assumed to be 10 °C. Steam was injected during circulation phase and assisted with two heaters defined in each of the horizontal wells with constant temperature supply of 240 °C. The relative permeability curves used in the numerical models are the same as the Underground Test Facility (UTF) curves presented by Good, Rezk and Felty (1997), and defined in Chapter 4.

The fluid model for the equilibrium cases consist of three components: water, bitumen, and gaseous propane, and for the non-equilibrium cases, the fluid model has an additional component which enables the definition of another form of propane. So, propane is defined as solution gas (dissolved in oil) and as free gas, as explained previously in Section 5.2. The fluid models were created through matching the experimental PVT data for the propane/bitumen mixture that were explained thoroughly in Chapter 4 of this thesis. The viscosity and density models used in this numerical study were also explained in Chapter 4 of this thesis. The base and equilibrium field scale cases use equilibrium K-values for species in gas/bitumen mixture whereas the non-equilibrium cases use the reaction-based approach explained in Chapter 5, Section 5.2.

Similar to SAGD process, in the simulation of ES-SAGD process, producer and injector are put on steam circulation for 3 months. Steam is injected at a rate of 100 m^3/day or maximum bottom hole pressure of 4000kPa whichever target hits first. To assist steam injection during circulation stage, two heaters were defined as well along the wellbores with constant heat temperature of 240 ^oC. Once communication is established, the wells are put into production stage though which

gaseous solvent (propane in this case) is co-injected with steam for the whole period of production (10 years). Constant steam injection of 100 m^3/day was set for this study. The numerical simulations models performed for this study can be categorized into the following categories:

Base Equilibrium Cases

The base equilibrium cases are 25 cm grid block size and use the typical equilibrium K-values approach for the species in the gas/bitumen mixture. The base case represents the fine grid model.

Field Scale Equilibrium Cases

In this category, all models are 1m grid size blocks and they use the typical equilibrium K-values approach for the species in gas/bitumen mixture. A comparison will be drawn between the equilibrium cases and their respective base cases to examine the impact on oil rate.

Field Scale Non-equilibrium Cases

The last category herein is for the field non-equilibrium cases in which rate-based reaction approach is employed to simulate the delay of dissolution/exsolution of solvent into bitumen. Through tuning of the dissolution/exsolution frequency factors, the difference between field equilibrium cases and their respective base cases' performance is mitigated.

To examine the impact of solvent concentration on the performance of ES-SAGD, four scenarios were also developed for each of the categories explained above: 20/80, 40/60, 60/40, and 80/20 solvent-to-steam split by volume.

5.7.1 Results of Numerical Simulations

The first scenario that will be presented is for 80/20 solvent to steam split by volume. As mentioned previously steam injection rate is constant in all cases at 100 m^3/day and therefore the amount of propane injected in 80/20 split is 400 standard m^3/day. Figure 5.26 shows the performance of the ES-SAGD in terms of oil production. Three cases are presented in the figure: the base case which has the fine grid block size (25 cm), the equilibrium field scale case (1 m), and non-equilibrium field scale case (1 m). All reservoir conditions and operating parameter are exact in the three cases. The only difference is the inclusion of non-equilibrium effects in the non-equilibrium field scale case. The fine-grid base case shows the best performance in terms of oil rate. The equilibrium field scale case presented in the figure shows a lower oil performance compared to the base case and that is mainly attributed to the inter-related mechanisms of solvent dissolution into bitumen that are lost when upscaling the simulation models. To capture the physics and mechanisms of interphase mass transfer and solvent dissolution into bitumen, inclusion of non-equilibrium mass transfer effects is implemented. The green curve presented in the figure represents the non-equilibrium case which shows a better overall performance compared to the typical K-value instantaneous equilibrium approach. The results show that inclusion of the non-equilibrium was able to improve the prediction of oil rate. The optimized dissolution/exsolution frequency factors obtained for the non-equilibrium field scale case are 14.9 1/day and 18 1/day, respectively.

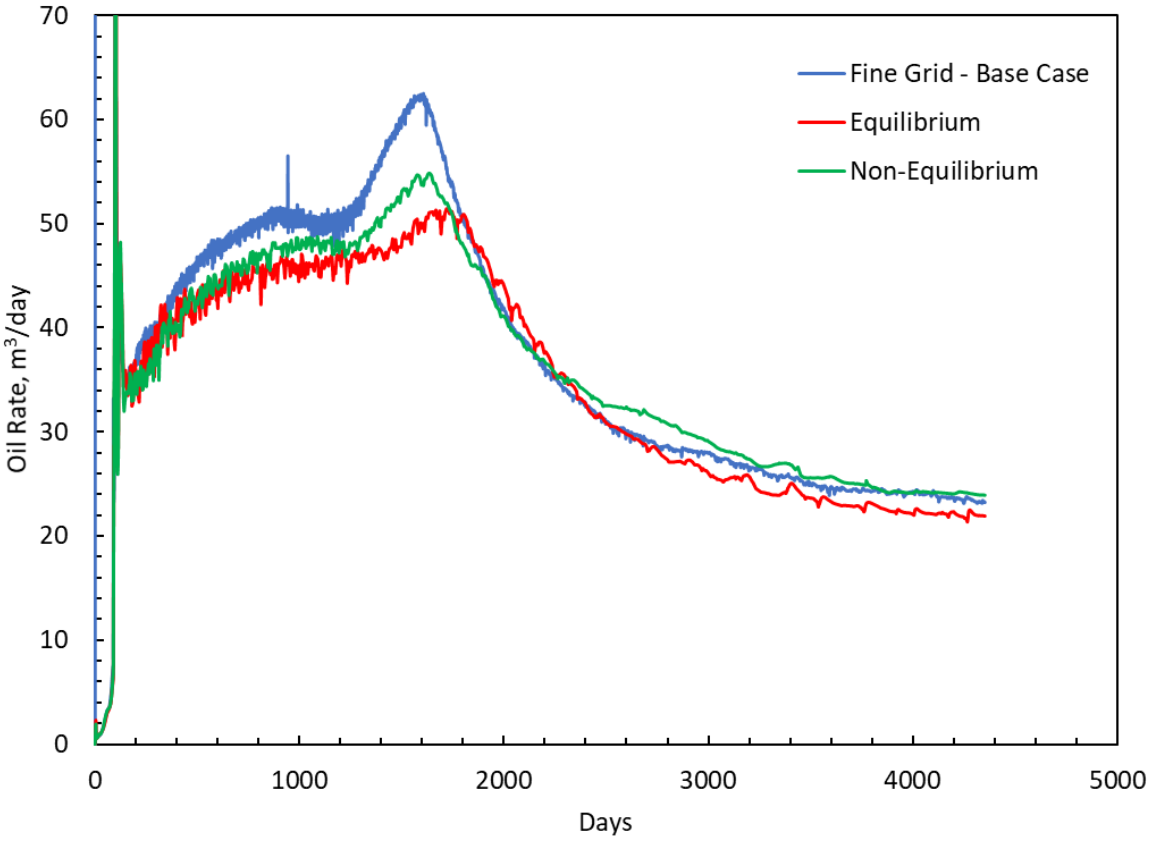

Figure 5.26: Oil production rate – equilibrium versus non-equilibrium for 80/20 solvent-to bitumen split scenario.

In terms of cumulative oil, Figure 5.27 shows the results for the 80/20 solvent-to-steam split scenario. As noted, the equilibrium field scale case shows a lower oil recovery compared to the fine grid base case. The non-equilibrium field case mitigated the overall difference in oil recovery. The percent error between base case and equilibrium case is 6.3% whereas the error between base case and non-equilibrium case is merely a 2.5%. Another important economic factor to analyze the performance of ES-SAGD process is the cumulative steam oil ratio (cSOR), which measures the average volume of steam input required to producer one barrel of bitumen. Figure 5.28 presents the cSOR for the three cases for the 80/20 solvent-to-steam split scenario. As can be observed, the

fine grid base case presents the most economic performance in terms of cSOR whereas the typical field scale equilibrium case shows a ~6.7% increase in cSOR compared to the base case. Through inclusion of non-equilibrium mass transfer effects, the error difference was mitigated to 2.6%.

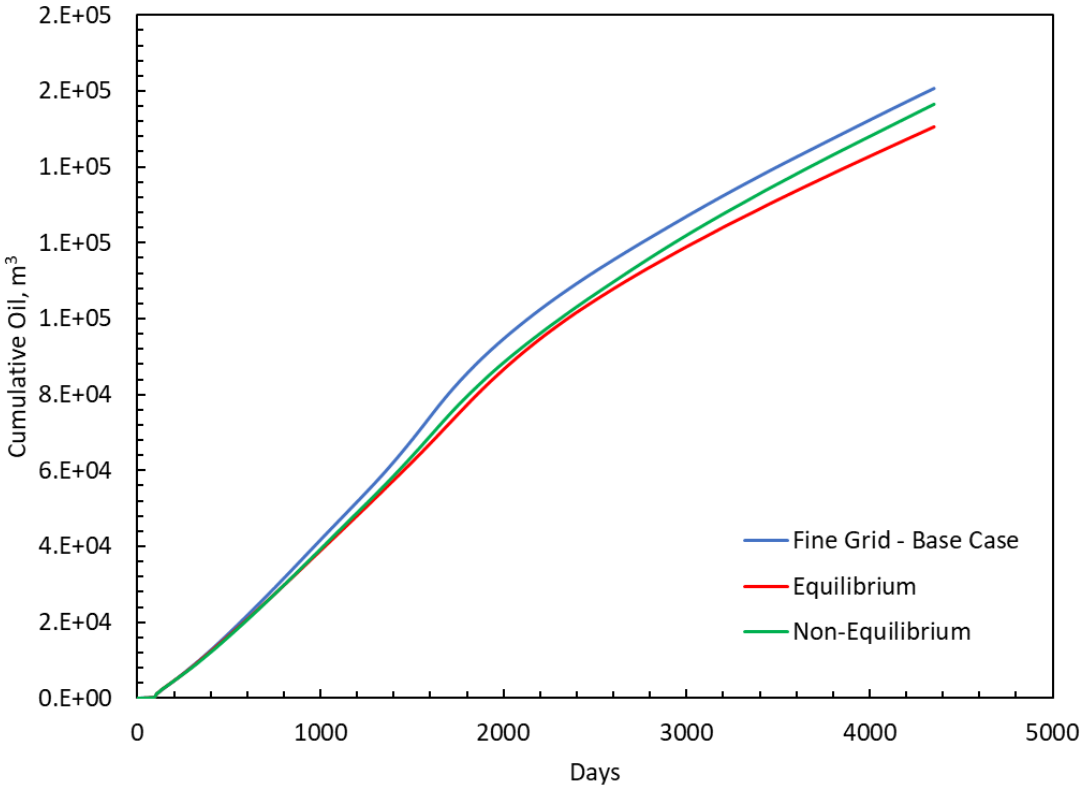

Figure 5.27: Cumulative oil – equilibrium versus non-equilibrium for 80/20 solvent-to bitumen split scenario.

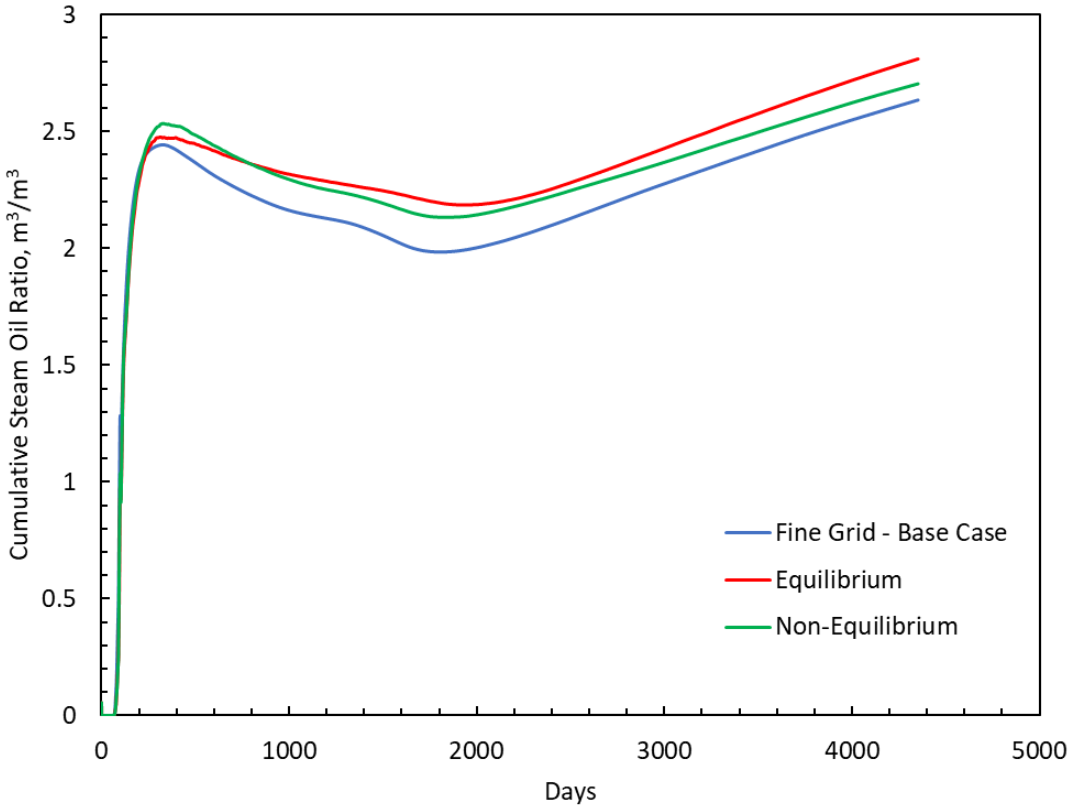

Figure 5.28: Cumulative SOR – equilibrium versus non-equilibrium for 80/20 solvent-to bitumen split scenario.

One of the main advantages of modelling non-equilibrium interphase mass transfer in solvent-aided thermal recovery processes such as ES-SAGD is the ability to history match field gas production rates. When using the typical K-value instantaneous equilibrium approach to model solvent-aided processes, solvent injected tend to dissolve instantaneously into bitumen without allowing any sufficient time for the solvent dissolution/exsolution from bitumen to happen. Therefore, the modeled gas production rates tend to be lower than what is observed in the field trials. Knorr et al., (2008) conducted several lab experiments on solvent vapor extraction (SVX) process in which they also modelled, and history matched their results using equilibrium approach

simulation models. They found that simulated cumulative gas production rates history match is poor near the beginning of the experiment when high gas production rates were recorded. They attributed their findings to liberation of gas from oil is more rapid compared to simulation results. They indicated that equilibrium simulation approach does not consider foamy oil phenomenon of which there should be two phases of the gas present: dispersed gas and free gas. Therefore, they concluded that gas production behaviour was not modelled well using equilibrium simulation approach.

Knorr et al., (2008) conclusions are in agreement to the gas production rates obtained in this study. By including non-equilibrium mass transfer effects into the modelling of solvent-aided processes, solvent dissolution/exsolution from bitumen mechanism is delayed as it becomes rate and time dependent. Therefore, the inclusion of non-equilibrium proves to be a useful tool to match the field gas production data. Figure 5.29 shows the difference in produced gas rates when modelling instantaneous equilibrium versus non-equilibrium approach. As can be observed, in the case of instantaneous K-value equilibrium approach, the propane injected is instantly dissolved in bitumen and therefore is produced with oil in oleic form (blue curve). The rate of propane produced in the gaseous form is close to zero in the case equilibrium. On the other hand, in the non-equilibrium mass transfer case, the rate of propane produced in the gaseous form (yellow curve) is substantial and remarkably close to the oleic propane production rates in the case of equilibrium K-value model. Only small amounts of the injected gaseous propane dissolves into oil in the case of non-equilibrium modelling of mass transfer (orange curve) and that can be attributed to the delay of solvent dissolution into bitumen modeled through the use of non-equilibrium reaction terms.

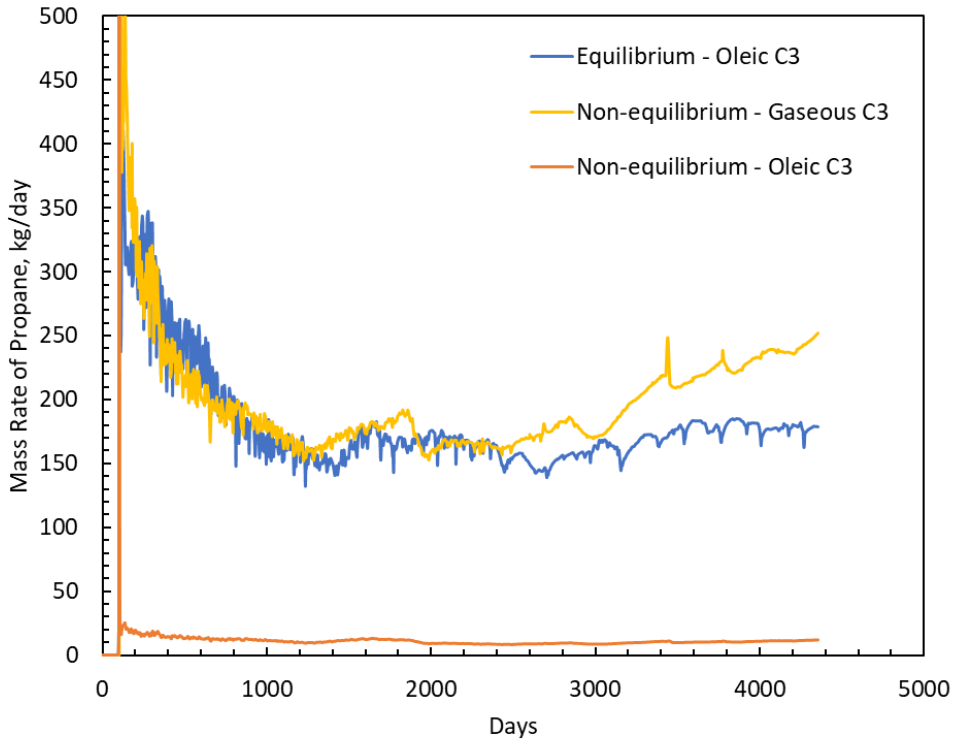

Figure 5.29: Gas production rates – equilibrium versus non-equilibrium for 80/20 solvent-to bitumen split scenario.

To examine the impact of solvent concentration on the performance of ES-SAGD, other scenarios were conducted where the solvent-to-steam injection split varied. Figure 5.30 shows the performance of ES-SAGD in terms of oil production rate for propane/bitumen mixture. The higher the solvent injection ratio, the better the oil rate performance during early SAGD time. However, it seems that higher concentration of propane hinders the steam chamber development at the later stages of the SAGD life. This can be due to accumulation of gaseous solvent in the ceiling of the steam chamber hindering steam condensation and latent heat delivery to the bitumen formation.

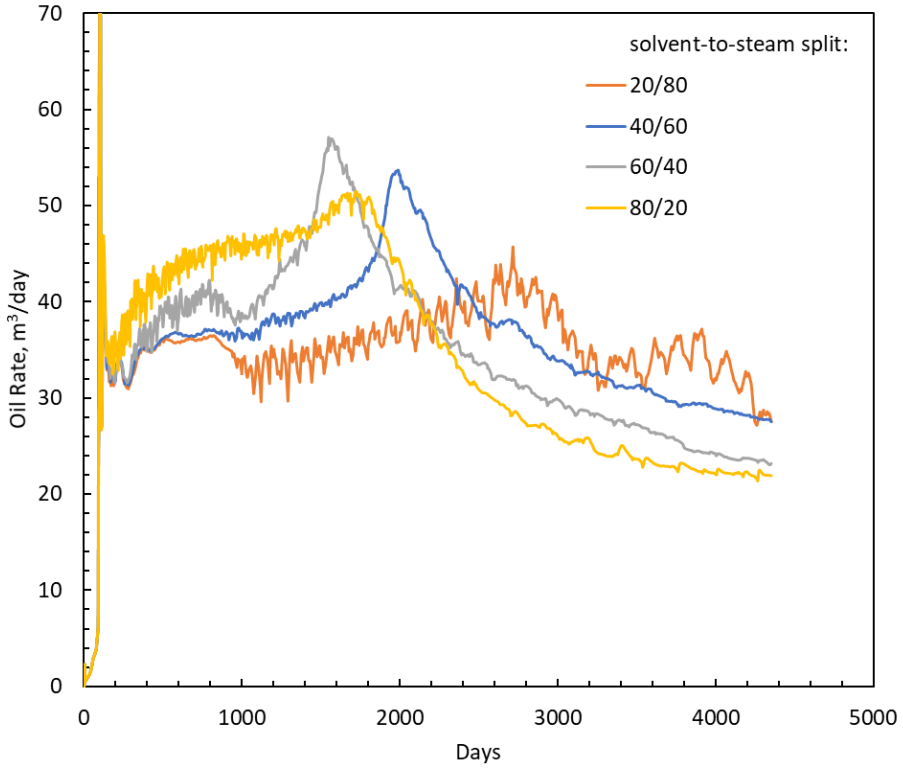

Figure 5.30: Oil production rates for different solvent-to-steam split scenarios.

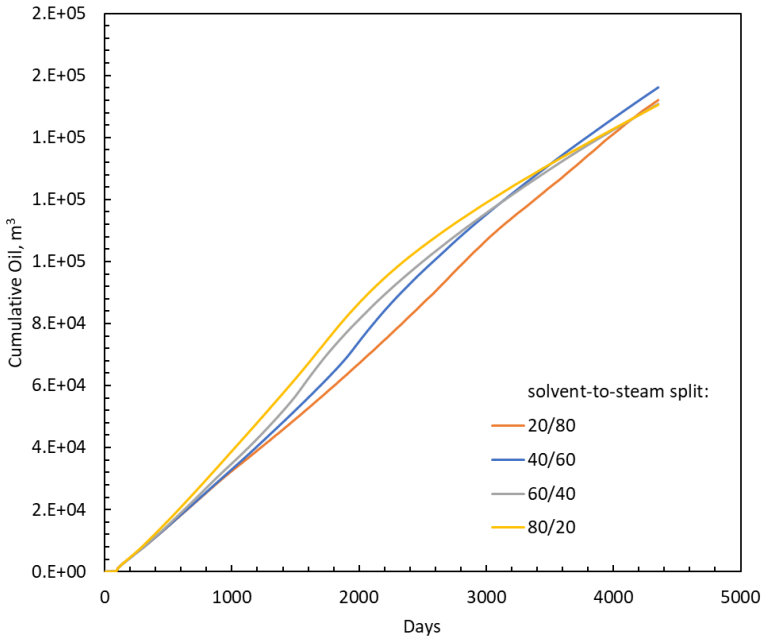

Figure 5.31: Cumulative oil production for different solvent-to-steam split scenarios.

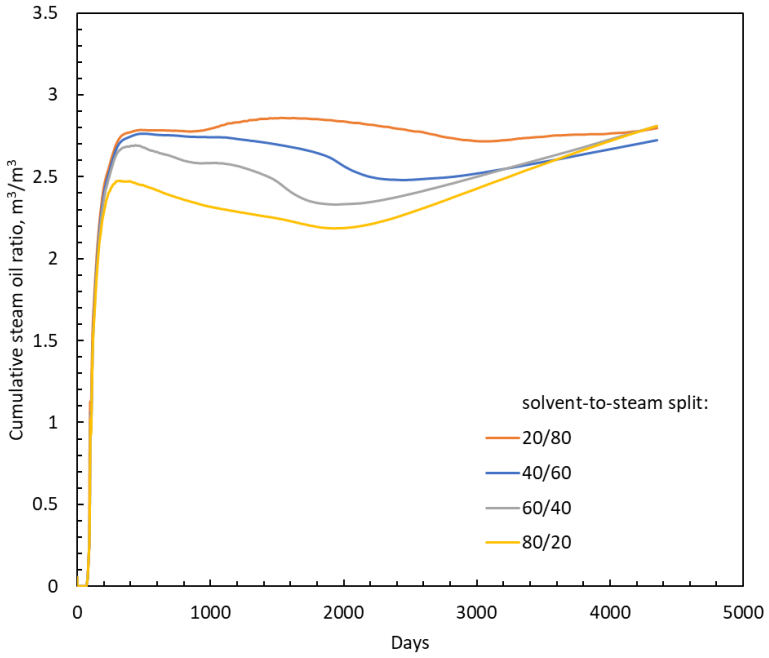

Figure 5.32: Cumulative steam oil ratio for different solvent-to-steam split scenarios.

Figures 5.31 and 5.32 show the cumulative oil production and steam oil ratio for the different solvent-to-steam split scenarios, respectively. As can be observed, the last case of 80/20 solvent-to-steam split shows the highest oil recovery early time of the ES-SAGD process. As more solvent accumulates in the steam chamber, the oil recovery starts to decline. Since steam injection rate is constant in all scenarios presented herein, cSOR is a direct function of only oil production rate and solvent injected, and hence it is predictable to see the last scenario of 80/20 solvent-to-steam split performs the best in terms of cSOR.

5.8 Summary and Conclusion

In this chapter, a kinetic approach was incorporated into a 2D multiphase thermal simulation model in order to quantify the impact of the non-equilibrium mass transfer and analyze the performance of solvent-aided thermal recovery processes for the propane/bitumen system. Also, one of the main purposes of incorporating the non-equilibrium interphase mass transfer terms into simulation models is to find correlation or a guideline that can be used for field scale modelling of solvent aided thermal recovery processes. The incorporation of the non-equilibrium interphase mass transfer into simulation models was accomplished through the use of reaction terms. The mechanistic studies were carried out using commercial thermal reservoir simulator (STARS). Primarily, the cumulative oil drainage was used as the objective function to find the non-equilibrium interphase mass transfer coefficients.

First, typical range of interphase mass transfer coefficients for propane/bitumen mixture were determined for different pressure and temperature settings and for different grid size blocks. It was found that the interphase mass transfer coefficients for propane/bitumen system at different

temperature and pressure settings is in the range of 1×10^{-8} to 1×10^{-6} m/s. Also, it was observed that mass transfer coefficient is in general inversely proportional to pressure and directly proportional to temperature.

In the next section, the non-equilibrium interphase mass transfer is included in the numerical simulations. The non-equilibrium cases are tuned to match the fine-grid equilibrium cases through adjusting the dissolution/exsolution frequency factors. It was noted that for propane/bitumen system, the impact on oil recovery when upscaling simulation models from 10 cm to 1m is in the range of 3% to 6%. In other cases, with lower temperatures, the impact could be as high as 10%. This large difference was simply mitigated through the inclusion of the non-equilibrium interphase mass transfer terms.

Dissolution rate frequency factor was obtained for propane/bitumen systems. The temperature setting ranges between 50 and 100 ^{o}C, pressure ranges between 1600 and 3500 kPa, and grid block sizes used in the development of the scaling relations are 5, 10, and 20 cm. The range of dissolution rate frequency factors obtained for the propane/bitumen system is 2.5 to 7.5 1/day which is directly proportional to the grid block size used in the study. For the typical 1m grid block size simulations, extrapolation of the results suggests that the dissolution frequency factors for the propane/bitumen system were found to be in the range of 8 to 10 1/day. It was observed that the dissolution rate of propane into bitumen increases with grid block size regardless of the temperature and pressure of the system. Typically, for very fine grid block sizes, the dissolution rate values are insignificant

and in such cases the equilibrium and non-equilibrium modelling of mass transfer cases are identical. For large grid block sizes, the dissolution rate increases confirming the importance of non-equilibrium interphase mass transfer when modelling field scale solvent based EOR processes.

Finally, non-equilibrium modelling of mass transfer was applied on an ES-SAGD process to investigate its applicability and significance. It was found that through inclusion of non-equilibrium interphase mass transfer in field scale simulations yield better match to their respective fine-scale simulation models when compared to the K-value equilibrium approach models. It was found that the non-equilibrium field case mitigated the overall difference in both oil recovery and cSOR in which the percent error was reduced more than 4%.

Chapter Six: **Conclusions and Recommendations**

6.1 Conclusions

This dissertation presented the analysis of non-equilibrium interphase mass transfer phenomenon with applications to solvent-based enhance oil recovery processes. The contributions of the presented work can be categorized into the following: estimation of interphase mass transfer coefficient for propane/bitumen system, quantifying the impact of the non-equilibrium interphase mass transfer on the performance of solvent-based EOR processes, and finally presenting a correlation that will be used as a guideline for modelling the non-equilibrium interphase mass transfer for field scale simulations of solvent-based EOR processes. The contributions of the presented work is described in further details in the subsequent sections.

6.1.1 Theoretical Analysis

Interphase mass transfer is a fundamental process in multiphase flow as it is encountered in numerous applications ranging from enhanced oil recovery, NAPL contamination/remediation, and carbon capture/storage, drying of porous media, and fuel cell technology. An analytical model was used in Chapter 3 to find the pure diffusive interphase mass transfer for several solvents at different pressure and temperature settings.

It is imperative to note that the obtained interphase mass transfer coefficient using the analytical solution is for pure diffusion. Therefore, the values obtained are the low limiting values for mass transfer. Therefore, when comparing the analytical solution of the interphase mass transfer coefficients with the numerical simulation counterparts, that latter is much higher as it considers other mechanisms influencing mass transfer such as convective mixing, viscous/density-driven fingering, and numerical dispersion. It was shown that the analytical solution of the pure interphase

mass transfer coefficients is in the range of 1×10^{-11} to 1×10^{-8} m/s whereas the numerical results shown to be in the range of 1×10^{-8} to 1×10^{-6} m/s.

Figure 6.1 shows a comparison of the interphase mass transfer between the analytical solution, which is a pure diffusion only, and the numerical solution, which considers other important mechanisms such as convective mixing, numerical dispersion, and viscous/density-driven fingering. This figure is for propane diffusing into bitumen as a function of bitumen viscosity. The scaling relations shown in Figure 6.1 finds applications in numerical simulations of field scale solvent-aided recovery processes when propane is utilized as a solvent.

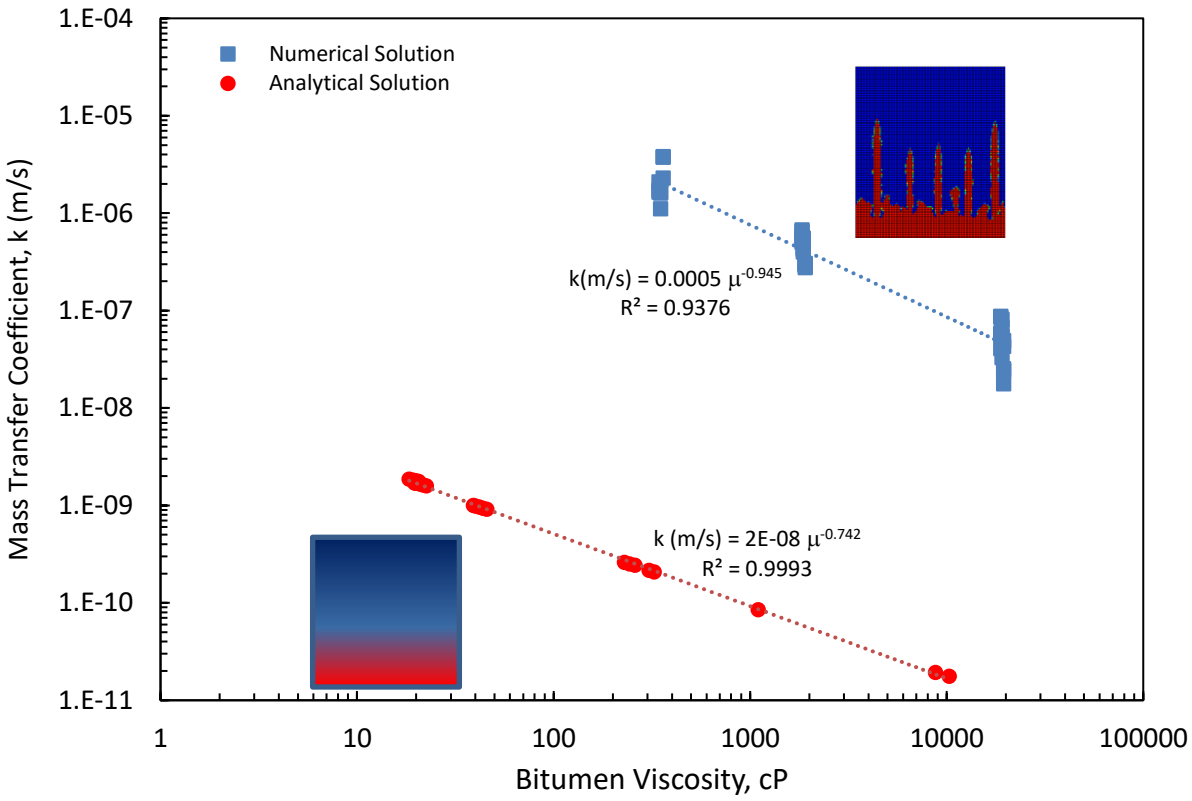

Figure 6.1: Interphase mass transfer coefficient for propane/bitumen mixture – pure diffusion versus full numerical solution.

6.1.2 Numerical Modelling of Non-equilibrium Interphase Mass Transfer and its Applications

A good understanding of the interphase mass transfer is necessary for field scale simulation of solvent-aided processes. Conventional thermal simulators assume instantaneous thermodynamic equilibrium is achieved in the grid blocks. In reality, the local equilibrium assumption often fails at larger scales or in situations where flow velocities are large compared to that of mass or heat transfer (Niessner and Hassanizadeh, 2009). Therefore, the non-equilibrium modelling of phase behavior in multiphase systems should be considered. The non-equilibrium interphase mass

transfer was incorporated into multiphase thermal simulation model using a kinetic approach in order to quantify the impact of non-equilibrium mass transfer on the performance of solvent-aided thermal recovery processes through the use of reaction terms.

Mechanistic studies were conducted using commercial thermal reservoir simulator (STARS) for the propane/bitumen mixture to determine scaling relations for the non-equilibrium interphase mass transfer coefficients. The purpose of the scaling relations is for field scale simulation modelling. As shown in Chapter 5, in the case of propane/bitumen systems, there is about 4 to 10% error in oil recovery when upscaling the models 5 to 10 times only. Therefore, such scaling relations can be used in commercial field scale modelling of solvent-aided thermal recovery processes for properly designing and predicting the process performance.

6.2 Recommendations for Future Research

The presented work improved our understanding on the importance of modelling non-equilibrium for proper design, implementation, and prediction of solvent-based EOR processes. Although the presented work provides a useful tool for quantifying the impact of non-equilibrium interphase mass transfer and scaling relations for field simulations of solvent-based EOR processes, it is mainly done for propane/bitumen systems. Therefore, further analysis and investigation is required to study the impact of other solvents.

Interphase mass transfer coefficient was shown to be relatively higher for lighter solvents such as methane, ethane, and propane and specially when a heat source is present. Therefore, proper modelling of the non-equilibrium interphase mass transfer phenomena is relatively more important for gaseous solvents when designing and implementing a successful solvent-aided thermal recovery process.

The assumption of instant equilibrium modelling of field scale solvent-based EOR processes would results in error ranging between 4% to 10% in predicting oil recovery as shown in the case of propane/bitumen system. Using other solvents with bitumen would result into different range of errors in predicting oil recovery. As shown in Chapter 3, the non-equilibrium interphase mass transfer phenomenon is strongly influenced by the pressure and temperature of the system, and composition of the diffusing component. For gaseous solvents a higher mass transfer coefficient is required to capture the non-equilibrium process. However, liquid solvents have higher diffusivities into bitumen and more pronounced dilution effect. Therefore, each solvent is distinct and need to be investigated thoroughly to determine the impact of non-equilibrium interphase mass transfer phenomena on the performance of solvent-based EOR processes. Also, it is worthwhile to validate results of numerical simulations described herein using experimental data on solvent-based processes. This may provide more confidence on the results obtained from numerical simulations.

References

Acedemies, C. of C. (2015) *Technological Prospects for Reducing the Environmental Footprint of Canadian Oil Sands*.

Azinfar, B. *et al.* (2018) A thermodynamic model to predict propane solubility in bitumen and heavy oil based on experimental fractionation and characterization, *Journal of Petroleum Science and Engineering*, 168(April), pp. 156–177.

Bayestehparvin, B., Abedi, J. and Farouq Ali, S. M. (2017) Development of a non-equilibrium pore scale reservoir simulator, *SPE Canada Heavy Oil Technical Conference*, (February), pp. 15–16.

Butler, M. (1991) Thermal recovery of oil and bitumen, pp. 30–37.

Canadian Association of Petroleum Producers (2017) Crude oil forecast, market and transportation, p. 54.

Chang, J. and Ivory, J. (2013) Field-scale simulation of cyclic solvent injection (CSI), *Journal of Canadian Petroleum Technology*, 52(4), pp. 251–265.

Civan, F. and Rasmussen, M. L. (2006) Determination of gas-diffusion and interface-mass-transfer coefficients for quiescent reservoir liquids, *Spe Journal*, 11(1), pp. 71–79.

Computer Modelling Group (2016) 'STARS User Guide', *Computer Modelling Group Ltd.* Calgary, p. 1511.

Computer Modelling Group (2016) 'CMOST User Guide', *Computer Modelling Group Ltd.* Calgary, p. 351.

Etminan, S. R., Maini, B. B. and Chen, Z. (2014) Determination of mass transfer parameters in solvent-based oil recovery techniques using a non-equilibrium boundary condition at the interface, *Fuel*, 120, pp. 218–232.

Faradonbeh, M. R. (2013) *Mathematical Modeling of Steam-Solvent Gravity Drainage of Heavy Oil and Bitumen in Porous Media*.

Good, W. K., Rezk, C. and Felty, B. D. (1997) *Other Criteria Affecting SAGD Performance in the Athabasca McMurray Formation, S.I., Alberta Energy*.

H. Zhang and F.W. Schwartz (2000) Simulating the oxidative treatment of chlorinated compounds by potassium permanganate, *Water Resources Research*, 36(10), pp. 3031–3042.

Hassanzadeh, H. and Harding, T. (2016) Analysis of conductive heat transfer during in-situ electrical heating of oil sands, *FUEL*, 178, pp. 290–299.

Hassanzadeh, H., Pooladi-Darvish, M. and Keith, D. W. (2005) Modelling of convective mixing in CO2 storage, *Journal of Canadian Petroleum Technology*, 44(10), pp. 43–50.

Hunt, J. R., Sitar, N. and Udell, K. S. (1988) Nonaqueous phase liquid transport and cleanup: 1. Analysis of mechanisms, *Water Resources Research*, 24(8), pp. 1247–1258.

IEA (2017) World Energy Outlook 2017, *International Energy Agency*.

Imhoff, P. T., Jaffe, P. R. and Pinder, G. F. (1993) An experimental study of complete dissolution of a nonaqueous phase liquid in saturated porous media, *Water Resources Research*, 30(2), pp. 307–320.

Indrupskiy, I. M. and Lobanova, O. A. (2015) Modelling non-equilibrium phase behavior of hydrocarbon mixtures, *Society of Petroleum Engineers*, 463(1), pp. 695–698.

International Energy Agency (2015) Energy policies of IEA countries, *Canada 2015*.

Israel, B. (2017) *Using solvents in the oilsands*, *Pembina Institute*. Available at: http://www.pembina.org/blog/using-solvents-oilsands (Accessed: 12 March 2018).

Jia, P., Knorr, K. D. and Imran, M. (2013) Advanced numerical simulation of solvent vapour extraction (SVX) processes, *SPE Heavy Oil Conference - Canada, 2013*, (June), pp. 1–20.

Lu, X. H., Ji, Y. H. and Liu, H. L. (2011) Non-equilibrium thermodynamics analysis and its application in interfacial mass transfer, *Science China Chemistry*, 54(10), pp. 1659–1666.

Mayer, A. S. *et al.* (2005) *Soil And Groundwater Contamination: Nonaqueous Phase Liquids - Principles And Observations*. Washington, DC: American Geophysical Union.

Mehrotra, A. K. and Svrcek, W. Y. (1986) Viscosity of compressed Athabasca bitumen, *The Canadian Journal of Chemical Engineering*, 64(5), pp. 844–847.

Miller, C. T., Poirier-McNeil, M. M. and Mayer, A. S. (1990) Dissolution of trapped nonaqueous phase liquids: mass transfer characteristics, *Water Resources Research*, 26(11), pp. 2783–2796.

Nambi, I. M. and Powers, S. E. (2003) Mass transfer correlations for nonaqueous phase liquid dissolution from regions with high initial saturations, 39(2).

Nasr, T. N. and Isaacs, E. E. (2002) Process for enhancing hydrocarbon mobility using a steam additive, US Patent No. US 6,230,814 B1

Nduagu, E. *et al.* (2017) *Economic Potentials and Efficiencies of Oil Sands Operations: Processes and Technologies, Calgary, Canadian Energy Research Institue* .

Nghiem, L. X. and Sammon, P. H. (1997) A non-equilibrium equation-of-state compositional simulator, *SPE Reservoir Simulation Symposium*.

Niessner, J. and Hassanizadeh, S. M. (2009a) Modeling kinetic interphase mass transfer for two-phase flow in porous media including fluid-fluid interfacial area, *Transport in Porous Media*, 80(2), pp. 329–344.

Niessner, J. and Hassanizadeh, S. M. (2009b) Non-equilibrium interphase heat and mass transfer during two-phase flow in porous media-Theoretical considerations and modeling, *Advances in Water Resources*, 32(12), pp. 1756–1766.

Niessner, J. and Hassanizadeh, S. M. (2011) Mass and heat transfer during two-phase flow in porous media - theory and modeling, *Mass Transfer in Multiphase Systems and its Applications*

Prof. Mohamed El-Amin (Ed.), InTech, Available from: http://www.intechopen.com/books/mass-transfer-in-multiphase-systems-and-its-applications/mass-and-heattransfer-during-two-phase-flow-in-porous-media-theory-and-modeling.

Nourozieh, H., (2013) Phase partitioning and thermo-physical properties of Athabasca bitumen/solvent mixtures (Doctoral dissertation, University of Calgary). Available at https://prism.ucalgary.ca/handle/11023/1022.

Nourozieh, H., Ranjbar, E. and Kumar, A. (2015) Modelling of non-condensable gas injection in sagd process - important mechanisms and their impact on field scale simulation models, *SPE Heavy Oil Conference - Canada 2015*, pp. 1–15.

Nuske, P., Joekar-Niasar, V. and Helmig, R. (2014) Non-equilibrium in multiphase multicomponent flow in porous media: An evaporation example, *International Journal of Heat and Mass Transfer*, 74, pp. 128–142.

Oil Sands Extraction and Processing | Natural Resources Canada (no date). Available at: http://www.nrcan.gc.ca/energy/oil-sands/18094 (Accessed: 8 March 2018).

Oil Sands Processes | Natural Resources Canada (no date). Available at: https://www.nrcan.gc.ca/energy/oil-sands/5853 (Accessed: 8 March 2018).

Pacheco Roman, F. J. and Hejazi, S. H. (2016) Graphical estimation of interface mass-transfer coefficient (k) using pressure-decay data, *Chemical Engineering Science*, 146, pp. 35–43.

Peng, S. S. D. (1992) A non-equilibrium phase behaviour model for compositional reservoir simulation, *Petroleum Society of Canada*.

Poling, B. E., Prausnitz, J. M. and O'Connell, J. P. (2001) *The properties of gases and liquids*, *McGraw-Hill*. New York.

Powers, S. E., Abriola, L. M. and Weber, W. J. (1992) An experimental investigation of nonaqueous phase liquid dissolution in saturated subsurface systems - steady-state mass-transfer rates, *Water Resources Research*, 28(10), pp. 2691–2705.

Riazi, M. R. (2001) *Characterization and Properties of Petroleum Fractions*, West Conshohocken, Pa: ASTM International.

Riazi, M. R. and Whitson, C. H. (1993) Estimating diffusion coefficients of dense fluids, *Industrial and Engineering Chemistry Research*, 32(12), pp. 3081–3088.

Sheikha, H., Pooladi-Darvish, M. and Mehrotra, A. K. (2005) Development of graphical methods for estimating the diffusivity coefficient of gases in bitumen from pressure-decay data, *Energy and Fuels*, 19(5), pp. 2041–2049.

Sheng, J. (2013) *Enhanced Oil Recovery - Field Case Studies* -. Available at: https://app.knovel.com/web/view/khtml/show.v/rcid:kpEORFCS01/cid:kt00U16AL2/viewerType:khtml/root_slug:17-sagd-for-heavy-oil-recovery/url_slug:sagd-heavy-oil-recovery?b-toc-cid=kpEORFCS01&b-toc-root-slug=&b-toc-url-slug=sagd-heavy-oil-recovery&b-toc-title (Accessed: 10 April 2018).

Soh, Y., Rangriz-Shokri, A. and Babadagli, T. (2018) Optimization of methane use in cyclic solvent injection for heavy-oil recovery after primary production through experimental and numerical studies, *Fuel.*, 214(November 2017), pp. 457–470.

Wilkins, M. D., Abriola, L. M. and Pennell, K. D. (1995) An experimental investigation of rate-limited nonaqueous phase liquid volatilization in unsaturated porous media: steady state mass transfer, *Water Resources Research*, 31(9), pp. 2159–2172.

Wu, W. *et al.* (1998) Modeling non-equilibrium mass transfer effects for a gas condensate field, *Spe*, (1985).

Zirrahi, M., Hassanzadeh, H. and Abedi, J. (2017) Experimental and modelling studies of MacKay River bitumen and light n-alkane binaries, *Canadian Journal of Chemical Engineering*, 95(7), pp. 1417–1427.

Knorr, K. K. D., Wilton, R. R. and Zeng, F. B. (2008) Evaluation of solvent vapour extraction (svx) processes using a 3d physical model - year 3, *Petroleum Technology Research Centre*. Saskatchewan.